UNIVERSITE DE PARIS-SUD

CENTRE D'ORSAY

THESE

présentée
pour obtenir

Le grade de DOCTEUR EN SCIENCE
Spécialité Physique des Solides

par

Pierre-Marie Billangeon

SUJET :

Détection de bruit quantique mésoscopique
à très haute-fréquence

Soutenue le 1er février 2008 devant la commission d'examen :

MM.	H. Bouchiat	Directrice de thèse
	R. Deblock	Invité
	C. Glattli	
	P. Hakonen	Rapporteur
	F. Hekking	Rapporteur
	T. Martin	

Contents

Part I

Introduction

Chapter 1

Aperçu des résultats obtenus

I Détection de bruit haute-fréquence par un détecteur quantique

1 Introduction

De manière générale, le courant électrique à travers un élément conducteur n'est jamais une constante dans le temps: c'est en particulier le cas dans un système mésoscopique. Imaginons un circuit idéal: un élément résistif, polarisé par un générateur de tension idéal, dont on lit le courant qui passe au travers d'un ampèremètre idéal. Un enregistrement montrerait que le courant fluctue au cours du temps, autour d'une valeur moyenne $\langle \mathrm{I}(t) \rangle$. L'amplitude des ces fluctuations est mieux représentée par la fonction $\delta \mathrm{I}(t) = \mathrm{I}(t) - \langle \mathrm{I}(t) \rangle$. On quantifie l'amplitude de ces fluctuations par un corrélateur temporel

$$\mathrm{C}(\tau) = \langle \delta \mathrm{I}(t+\tau) \delta \mathrm{I}(t) \rangle$$

Pour un système stationnaire, le corrélateur temporel ne dépend que de τ. En pratique, on préfère travailler avec la densité spectrale de bruit $\mathrm{S_I}(\omega)$ (la densité spectrale de puissance du processus stochastique mis en jeu est le carré de la transformée de Fourier du signal considéré): le théorème de Wiener-Khintchine permet d'identifier la densité spectrale de bruit à la transformée de Fourier du corrélateur temporel, sous une hypothèse d'ergodicité. On distingue différents types de bruit: le bruit thermique, le bruit de grenaille, le bruit en $1/f$... Par la suite, il sera surtout question de bruit thermique, ainsi que de bruit de grenaille. On sera amené à voir que dans des systèmes mésoscopiques, différentes échelles d'énergie se dégagent: la température $k\mathrm{T}$, la fréquence $\hbar\omega$ ainsi que la tension $e\mathrm{V}$. Selon le rapport entre ces différentes grandeurs, on verra que l'on peut explorer différents régimes: la frontière classique/quantique par exemple, selon que $\hbar\omega \lessgtr k\mathrm{T}$. On peut s'interroger aussi sur ce que deviennent les différentes composantes du bruit (bruit à l'équilibre/hors-équilibre) pour $\hbar\omega \lessgtr e\mathrm{V}$: quelles informations peut-on retirer sur un système mésoscopique à partir de la dépendance en fréquence de sa densité spectrale de bruit?

2 Bruit thermique (Johnson-Nyquist)

En 1928, Johnson [1] établit expérimentalement l'existence d'un bruit à l'équilibre, gouverné par les fluctuations thermiques. Subséquamment, Nyquist publia une interprétation en terme d'échange d'énergie rayonnée qui permettait de comprendre quantitativement ces fluctuations [2]: le bruit Johnson-Nyquist se présentait alors comme un analogue pour les systèmes électroniques du rayonnement du corps noir. La démonstration de Nyquist en terme d'échange de photons est d'ailleurs étonnamment proche de l'interprétation qui est

faite du bruit quantique en physique mésoscopique: ce point sera précisé ultérieurement, car il joue un rôle assez essentiel dans la compréhension du sens que l'on donne à un corrélateur non symétrisé des fluctuations de courant. On trouve fréquemment l'expression de la densité spectrale de bruit à fréquence nulle sous la forme $S(\omega = 0) = 4\,k\mathrm{TG}$, où G est la conductance du système (cette expression dépend malgré tout de la convention prise pour définir la transformée de Fourier du corrélateur temporel, ainsi que de la symétrisation). On comprend dès lors que mesurer le bruit Johnson-Nyquist n'apporte en général pas plus d'information qu'une mesure de conductance: ce n'est donc pas cette source de bruit qui nous intéressera par la suite. Il est néanmoins possible que le théorème fluctuation-dissipation ne soit pas respecté dans un système fortement désordonné (régime non-ergodique): dans ce cas alors, la mesure de bruit à l'équilibre apporte des informations sur la nature du transport électronique.

A fréquence finie, on observe une transition entre le régime de bruit thermique ($\hbar\omega \ll k\mathrm{T}$), et le régime de bruit quantique à proprement parler ($\hbar\omega \gg k\mathrm{T}$): de manière générale, le terme de bruit quantique est employé pour désigner les fluctuations de courant à haute fréquence ($ie.\hbar\omega \gg k\mathrm{T}$), et englobe parfois aussi le bruit hors-équilibre.

3   Bruit hors-équilibre

Tubes à vide: 'Wärmeeffekt' et 'Schroeteffekt'

En 1918, Schottky compris l'origine des fluctuations de courant observées dans les tubes à vide: il les décomposa sous deux appellations différentes, 'Wärmeeffekt' et 'Schroeteffekt'. Le 'Wärmeeffekt' n'est rien d'autre que le bruit thermique (bruit à l'équilibre), alors que le 'Schroeteffekt' semble être à première vue le bruit de grenaille. Sa densité spectrale à fréquence nulle est égale à $2e\mathrm{I}$, comme pour le bruit de grenaille dans les systèmes mésoscopiques (processus poissonien). En réalité, cette similitude est trompeuse car l'origine du bruit de grenaille dans les tubes à vide est classique, alors que dans les systèmes mésoscopiques elle est quantique. En effet, dans un tube à vide, la transmission des électrons est idéale (T = 1), et les fluctuations de courant sont liées aux fluctuations de la statistique des porteurs dans la cathode [3][4]. Etant donné les températures mises en jeu, il n'y a d'ailleurs rien de très étonnant à ce que l'origine du bruit de grenaille soit classique dans ces systèmes. Malgré tout, ces prédictions présageaient que la granularité de la charge pouvait être une source de bruit, en plus des fluctuations thermiques.

Bruit de grenaille

Lorsqu'un conducteur est mis hors équilibre, il apparaît en plus du bruit Johnson-Nyquist un bruit supplémentaire, associé à la granularité de la charge. Ce bruit est dénommé bruit de grenaille. On donne souvent l'expression de la densité spectrale qui lui est associée à fréquence nulle (formule de Schottky)

$$S(\omega = 0) = 2e\mathrm{I}$$

Cette prédiction faite par Schottky a été vérifiée expérimentalement dans les tubes à vide dès 1925 [5]. Pour un système mésoscopique, la situation est un peu différente: on peut montrer n'importe quel conducteur peut être décrit comme un ensemble de N canaux de transmission, avec chacun un coefficient de transmission $\mathrm{T_i}$. On peut caractériser la plupart de ces propriétés de transport par l'ensemble de ces paramètres $\{\mathrm{T_i}\}_{i\in[1:N]}$, et c'est en particulier le cas pour le bruit. Pour un canal de transmission T, on peut montrer que

$$S(\omega = 0) = 2e\mathrm{I}\,(1 - \mathrm{T})$$

On comprend tout de suite qu'il y a, malgré les apparences, une différence fondamentale entre le tube à vide, et un système mésoscopique: dans la limite de transmission idéale (système balistique), il n'y a pas de bruit de grenaille, alors que le tube à vide présente un bruit lié à la granularité de la charge, bien que $T = 1$. Ceci tient à ce que, dans le cas d'un système mésoscopique, le bruit de grenaille est un effet quantique: un électron a une probabilité T de traverser par effet tunnel, et $(1 - T)$ d'être réfléchi. C'est ce caractère aléatoire du transfert de la charge à travers un conducteur, propre à la mécanique quantique, qui est à l'origine du bruit hors équilibre. Pour être encore plus général, on devrait écrire que $S(\omega = 0) = 2q\mathrm{I}(1 - T)$, où q est la charge des porteurs mis en jeu dans le processus de transport considéré. On entrevoit alors l'intérêt du bruit de grenaille: en le mesurant, on peut par exemple déterminer cette charge q, typiquement dans des systèmes présentant de fortes corrélations électroniques. Ceci a permis de mettre en évidence expérimentalement l'existence de la charge fractionnaire des quasiparticules de Laughlin dans le régime d'effet Hall quantique fractionnaire [6][7], ainsi que la charge $2e$ des paires de Cooper [8][9]. Le bruit de grenaille apporte aussi un certain nombre d'informations sur la statistique des porteurs: en particulier, il est clair que pour des fermions sans interactions, le bruit ne peut être que sub-poissonien (à cause du principe de Pauli). On caractérise le caractère sub-poissonien du bruit par le facteur de Fano, défini comme

$$\mathcal{F} = \frac{\mathrm{S_I}(f = 0)}{2q\mathrm{I}} = \frac{\mathrm{S_I}(\omega = 0)}{\pi^{-1}q\mathrm{I}}$$

4 Bruit quantique: corrélateur non-symétrisé *vs.* symétrisé

Le corrélateur temporel des fluctuations de courant est souvent déterminé comme étant une grandeur symétrisée, ce qui se traduit pour la densité spectrale par

$$\mathrm{S_I}(\omega) = \frac{1}{2\pi} \int_{-\infty}^{+\infty} \mathrm{d}\tau \mathrm{e}^{\mathrm{i}\,\omega\tau} \left\langle \frac{1}{2} \left[\delta\mathrm{I}(t + \tau)\delta\mathrm{I}(t) + \delta\mathrm{I}(t)\delta\mathrm{I}(t + \tau) \right] \right\rangle$$

Ceci n'a pas posé de problème jusqu'à maintenant, car on n'a considéré que des fréquences nulles. Mais que passe-t-il à haute-fréquence, typiquement lorsque $\hbar\omega \gg k\mathrm{T}$? Dans ce cas, on doit regarder le courant comme un opérateur: c'est alors que la question de la symétrisation intervient, les opérateurs courant pris à des temps différents ne commutant pas. Ainsi, bien que les opérateurs $\widehat{\mathrm{I}}(t)$ et $\widehat{\mathrm{I}}(t + \tau)$ soient hermitiques, le produit $\widehat{\mathrm{I}}(t + \tau)\widehat{\mathrm{I}}(t)$ ne l'est pas: par contre, si l'on symétrise cette expression, on retrouve une matrice hermitique [10]. C'est cette convention qui semble avoir été suivie dans de nombreux ouvrages et publications. Ce choix n'est pas justifié, car il n'est pas nécessaire que $\widehat{\mathrm{I}}(t + \tau)\widehat{\mathrm{I}}(t)$ soit hermitique pour que sa transformée de Fourier $S(\omega)$ soit réelle. La symétrisation est un choix d'autant plus surprenant, qu'à première vue, elle ne respecte pas la causalité. Pourquoi alors cette convention a-t-elle subsisté aussi longtemps?

Bruit à l'équilibre

L'expresion de la densité spectrale de bruit à l'équilibre (non-symétrisée) est donnée par

$$\mathrm{S_I}(\omega) = \frac{\mathrm{G}}{\pi} \frac{\hbar\omega}{1 - \mathrm{e}^{-\beta\,\hbar\omega}}$$

Cette expression est une illustration du théorème fluctuation-dissipation quantique (QFDT) [11]: on constate donc que le bruit à l'équilibre est non-symétrique (cf. figure 1.1). En réalité, on peut décomposer cette expression en deux termes: le premier étant le bruit thermique proprement dit, et le second les fluctuations de point-zéro (manifestation du principe d'incertitude d'Heisenberg). Ce sont les fluctuations de point-zéro qui brisent la

symétrie entre fréquences négatives et fréquences positives: il est clair qu'un système dans son état fondamental ne peut pas émettre d'énergie, mais il peut être excité par son environnement. On pourrait donc penser que les fluctuations de courant à l'équilibre permettent d'apporter une réponse à la question concernant la pertinence de la symétrisation: on verra que ce point est en réalité plus délicat qu'il n'y paraît car les schémas de détection utilisés expérimentalement qui permettent *a priori* d'accéder au bruit à l'équilibre ne sont pas sensibles aux fréquences négatives/positives, et réciproquement les schémas de détection qui sont sensibles au caractère non-symétrisé du corrélateur ne détectent pas le bruit à l'équilibre.
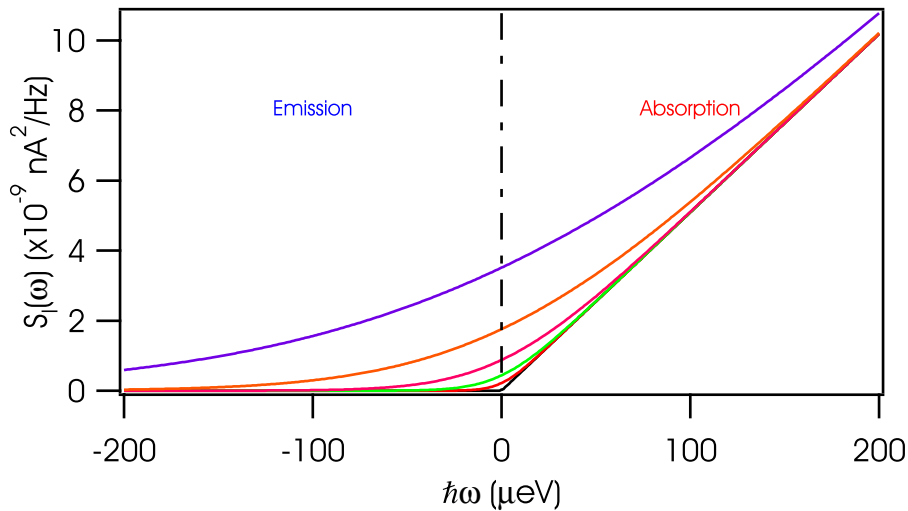
Figure 1.1: Densité spectrale non-symétrisée du bruit à l'équilibre thermique d'une résistance (R = 1 kΩ) en fonction de la fréquence, pour différentes températures (T = 0 mK, 50 mK, 100 mK, 200 mK, 400 mK et 800 mK).

Bruit hors-équilibre

Un des problèmes qui se pose est que la plupart des sytèmes mésoscopiques ont un bruit en excès[1] qui est naturellement symétrique ($S(\omega) = S(-\omega)$): il est par conséquent assez difficile de discriminer expérimentalement la pertinence de l'une ou l'autre convention. D'autre part, la réponse à cette question dépend très vraisemblablement du mode de détection: il semblerait par exemple, que si le courant qui passe à travers l'échantillon est mesuré avec un amplificateur, ce soit le corrélateur symétrisé que l'on mesure [12]. Par contre, si l'on utilise un détecteur quantique, on devrait mesurer le corrélateur non symétrisé. Mais qu'entend-on alors par détecteur quantique? Il faut revenir sur la signification de la densité spectrale: la différence entre fréquences négatives et positives repose sur la possibilité de distinguer les photons qui sont émis de ceux qui sont absorbés. On peut définir un bon détecteur quantique par sa capacité à distinguer les photons émis des photons absorbés.

5   Détection de bruit quantique

La détection de bruit quantique dans les conducteurs mésoscopiques est une tâche délicate, et les expériences s'y rapportant sont paradoxalement assez peu nombreuses comparé à

---

[1]On entend par bruit en excès le bruit qui apparaît en plus lorsque le conducteur est mis hors-équilibre
$$S_{I,exc}(\omega) = S_I(\omega, V) - S_I(\omega, V = 0)$$

l'essor du sujet sur le plan théorique. La première expérience remonte à 1981: Koch *et al.* ont montré que le bruit à fréquence nulle aux bornes d'une jonction Josephson shuntée par une résistance R polarisée en tension sous le gap ($eV < 2\Delta$) permet de remonter au bruit quantique de cette dernière [13][14][15]. En fait, la composante haute-fréquence de la résistance est mixée avec l'effet Josephson AC de la jonction Josephson: cette expérience a permis de mettre en évidence la transition entre régime classique et quantique (autour de $\hbar\omega \approx k$T, cf. figure 1.2), et reste une des rares à ce jour à avoir mis en évidence les fluctuations de point zéro (S($\omega > 0$) $\propto \hbar\omega/2$) dans un système électronique. Par contre, elle n'apporte pas de réponse sur la pertinence de la symétrisation: en effet, les fréquences positives de l'effet Josephson AC sont redressées par les fréquences négatives du bruit quantique de la résistance de shunt, et réciproquement les fréquences négatives de l'effet Josephson AC sont redressées par les fréquences positives du bruit quantique de la résistance. On comprend donc très intuitivement que cette expérience donne accès à un corrélateur symétrisé.
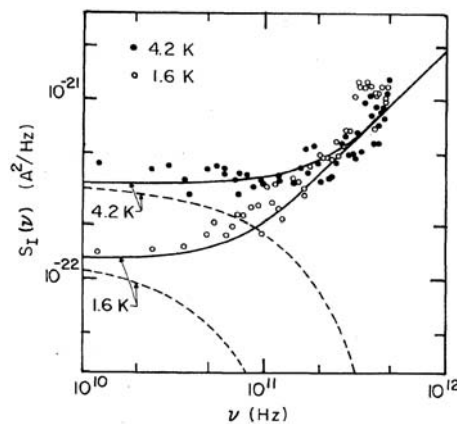
Figure 1.2: Densité spectrale de bruit en courant dans la résistance de shunt en fonction de la fréquence, pour deux valeurs distinctes de la température (T = 1, 6 K et 4, 2 K) dans l'expérience de Koch *et al.* [14].

Viennent ensuite les expériences de Yale: Schoelkopf *et al.* ont exploré la dépendance en fréquence du bruit de grenaille dans un fil diffusif court (régime *a priori* sans interactions) [16]. Ils ont confirmé la coupure à $\hbar\omega = e$V de la densité spectrale du bruit de grenaille (cf. figure 1.3) prédite par la théorie, et ont confirmé qu'ils étaient bien dans un régime sans interactions. Le dispositif de mesure s'appuyait sur de l'électronique haute-fréquence: les fluctuations de tension aux bornes de l'échantillon sont amplifiées par un amplificateur à froid (à base de transistors de type HEMT[2], qui présentent d'excellentes caractéristiques en matière de bruit). Le signal en sortie de l'amplificateur est ensuite redressé par une diode PIN. Malgré les bonnes performances des HEMT, le niveau de bruit d'un tel amplificateur est bien trop élevé comparé au signal recherché: il est donc nécessaire de travailler en modulation d'amplitude. La question de la symétrisation ici aussi ne peut pas être tranchée: d'une part, parce que le bruit en excès d'un fil diffusif est symétrique, et d'autre part parce que l'utilisation d'un amplificateur semble compromettre la possibilité de détecter un corrélateur non-symétrisé. L'autre contrainte de cette technique est qu'elle impose de travailler avec des échantillons d'impédance 50 Ω, à moins d'utiliser une ligne quart d'onde pour procéder à une adaptation d'impédance [17].

---

[2]HEMT est l'acronyme de High Electron Mobility Transistor.
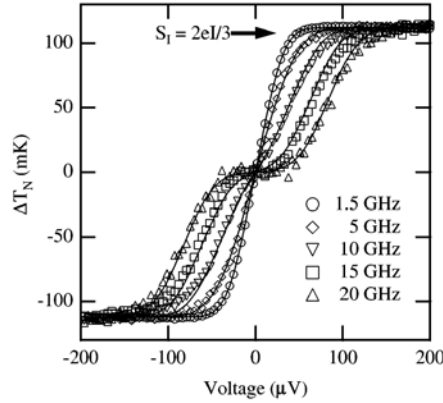
Figure 1.3: Détermination expérimentale de la variation de la température de bruit dans un fil diffusif en fonction de la tension continue aux bornes de l'échantillon (mesure en modulation), pour différentes fréquences [16]. On distingue l'effet de la coupure à eV: lorsque $\hbar\omega > eV$, la densité spectrale ne dépend plus de la tension de polarisation (et donc $\partial S_I(\omega)/\partial V = 0$).

Citons aussi deux expériences du groupe de NEC (Tsukuba, Japon). En 1997, Nakamura *et al.* ont réalisé la spectroscopie des états cohérents d'une boîte à une paire de Cooper (SCPB) [18], en détectant le courant photo-assisté sur le cycle Josephson-quasiparticule: Nakamura *et al.* ont détecté deux marches photo-assistées lorsque $n_g = 1 \mp \varepsilon$, devant correspondre respectivement à l'absorption/émission de photons par la SCPB. Néanmoins, cette expérience ne permet pas de trancher clairement la question de la symétrisation, étant donnée la symétrie entre les processus d'émission/absorption dans la boîte. Puis en 2004, Astafiev *et al.* ont mesuré la relaxation dans le même système, qui est reliée au spectre d'absorption de l'environnement [19]: cependant, ces mesures ont révélé un excès de bruit comparé à ce qui était attendu théoriquement. Il semble que le couplage du qubit à des systèmes à deux niveaux (fluctuateurs dans la barrière tunnel des jonctions ou dans le substrat, cette question est vivement débattue) qui est responsable du déphasage de ces sytèmes, puisse aussi expliquer la relaxation de ces systèmes [20]. La possibilité d'utiliser des qubits à base de circuits supraconducteurs comme spectromètre semble donc pour l'instant limitée par le couplage à ces systèmes parasites.
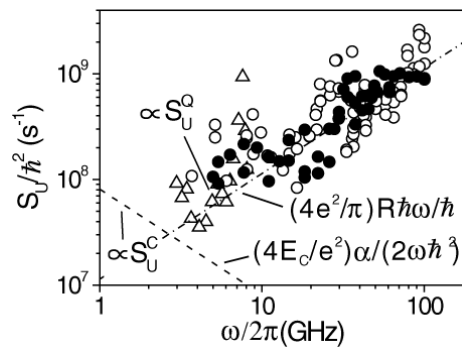
Figure 1.4: Densité spectrale du bruit en tension de l'environnement (absorption), déduite de la mesure du temps de relaxation du qubit T_1 [19].

Enfin, venons en à l'expérience de Delft en 2003 [21], dont nos expériences sont une suite logique. Deblock *et al.* ont utilisé une jonction supraconducteur-isolant-supraconducteur (SIS) comme détecteur de bruit haute-fréquence: la détection repose sur la mesure du courant photoassisté (courant de quasiparticules induit par une irradiation haute-fréquence). Les avantages de cette méthode sont nombreux: ils permettent une mesure résolue en fréquence, dans une large gamme de fréquences (entre 0 et $2\Delta/h$). La gamme de fréquences accessibles est donc fixée par la nature du matériau supraconducteur qui constitue les électrodes: pour des raisons pratiques liées à la nanofabrication, on utilise souvent l'aluminium. Son gap supraconducteur étant de l'ordre de 250 μeV, on peut ainsi mener des expériences entre 0 et 100 GHz: ce type de mesures serait beaucoup plus difficile à mettre en oeuvre en utilisant des techniques à base d'électronique haute-fréquence (à cause des contraintes imposées par le travail en milieu cryogénique). Dans ces expériences, l'ensemble du processus de détection haute-fréquence est assuré au niveau de la jonction SIS, à proximité de l'échantillon à étudier, et la lecture de l'information se réduit à une mesure de transport DC des propriétés du détecteur. Le détecteur est couplé capacitivement à l'échantillon, dans un environnement "on-chip" bien contrôlé à haute-fréquence, selon le schéma proposé par Aguado *et al.* [22]: ces derniers ont établi une expression reliant l'amplitude du courant photo-assisté à la densité spectrale de bruit du système couplé au détecteur, à partir de la théorie du blocage de Coulomb dynamique. Ce mode de détection présente donc comme autre avantage d'être quantitatif, ce qui est plus délicat à partir de mesures à base d'électronique haute-fréquence (la calibration de ces dernières est relativement imprécise, selon le montage utilisé, à cause des dérives de certains éléments du circuit d'amplification). Enfin, un autre point qui doit être souligné, est la possibilité de pouvoir séparer les processus d'émission des processus d'absorption: on en revient au point délicat de la définition d'un détecteur quantique. On avait discuté précédemment de la pertinence d'un corrélateur non-symétrisé *vs.* symétrisé: Aguado *et al.* avaient imaginé pouvoir distinguer les processus d'émission de ceux d'absorption en utilisant les différents processus inélastiques dans un double puits quantique. Deblock *et al.* ont utilisé le gap du supraconducteur des électrodes de la jonction SIS (détecteur) pour séparer les fréquences négatives des fréquences positives: tout se passe comme si les fréquences négatives (émission haute-fréquence) de la source étaient redressées par les fréquences positives (absorption haute-fréquence) du détecteur, et réciproquement. C'est cet effet de redressement qui donne lieu au courant photo-assisté (blocage de Coulomb dynamique).

Depuis que nous avons réalisé nos mesures, d'autres expériences de mesure de bruit haute-fréquence ont été réalisées dans de nouveaux systèmes. Zakka-Bajjani *et al.* ont mesuré la suppression du bruit à haute-fréquence dans un point de contact quantique (QPC) avec un dispositif à base d'électronique haute-fréquence [17], les problèmes d'adaptation d'impédance étant surmontés par l'utilisation d'une ligne quart d'onde. Gustavsson *et al.* ont réalisé le schéma proposé par Aguado *et al.*, en couplant un point de contact quantique à un double puits quantique (tous deux réalisés dans un gaz bidimensionnel d'électrons, par lithographie AFM) [23]: cette mesure résolue en fréquence a permis de confirmer quantitativement la valeur de la densité spectrale de bruit dans un QPC, par la mesure du courant photo-assisté dans le double puits quantique.

II   Détection du bruit quantique d'une jonction Josephson

1   Principe de détection: effet photo-assisté

On peut essayer de comprendre de manière intuitive pourquoi une jonction SIS semble *a priori* un bon candidat pour la détection de corrélateur non symétrisé. Pour cela, précisons le sens que l'on donne à la distinction entre fréquences négatives/positives dans ce manuscrit: les fréquences négatives correspondent au flux d'énergie qui s'échappe du système étudié (photons émis par la source), alors que les fréquences positives matérialisent le flux d'énergie allant vers la source (photons absorbés par la source).
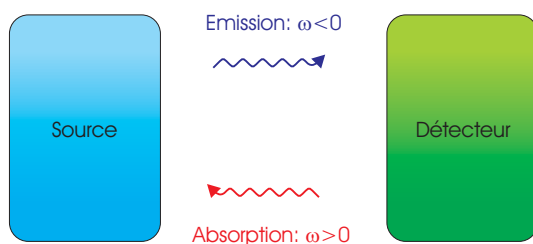
Figure 1.5: Schématisation de la notion de fréquences négatives/positives en fonction des flux d'énergie entre la source et le détecteur.

Schématisons maintenant les états électroniques dans les électrodes d'une jonction SIS (détecteur), en tenant compte de la densité d'états BCS. On suppose que l'on se place à température nulle pour simplifier: une température finie ne fait que créer des états vacants en dessous du 'niveau de Fermi' et occupés au-dessus, sans changer fondamentalement les processus inélastiques qui nous intéressent (dans la limite de très basses températures, ce qui sera bien évidemment le cas dans nos expériences). On comprend que selon que l'on polarise la jonction en-dessous ou au-dessus du gap, on peut détecter réciproquement les photons émis par l'environnement (cf. figure 1.6-a: les photons émis par la source, sont absorbés par le détecteur, induisant un courant photo-assisté) ou les photons absorbés par l'environnement (cf. figure 1.6-b: les photons absorbés par la source, permettent aux quasiparticules de relaxer en cédant de l'énergie, entraînant une réduction du courant de quasiparticules).
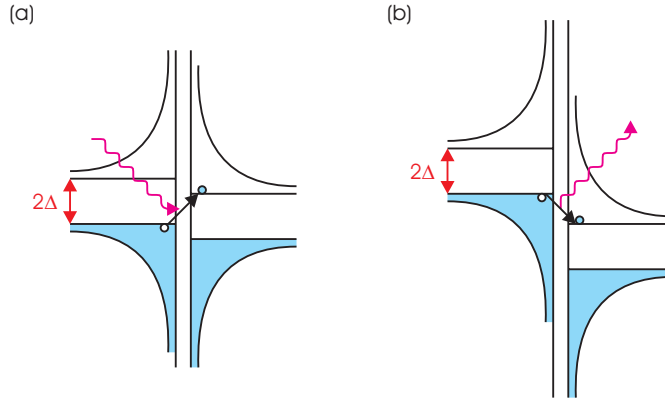
Figure 1.6: Processus inélastiques entrant en jeu dans la détection, et responsables du courant photo-assisté. (a) - Processus permettant de détecter les photons émis par la source. (b) - Processus permettant de détecter les photons absorbés par la source.

On peut donc remonter à l'énergie des photons détectés *via* la largeur des marches de courant photo-assisté (mesure résolue en fréquence), mais plus intéressant, on devrait pouvoir *a priori* distinguer les processus d'émission de ceux d'absorption. Un exemple de courbes typiques de courant photo-assisté sont représentées sur la figure 1.7. Au vu des processus mis en jeu, on voit aussi que la détection est restreinte à une gamme de fréquence comprise entre 0 et $2\Delta/h$ (soit entre 0 et 100 GHz pour des jonctions en aluminium).
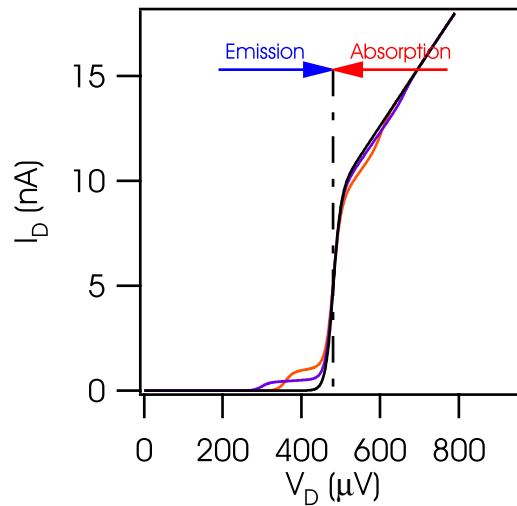
Figure 1.7: Effet de l'irradiation haute-fréquence sur la caractéristique $I(V)$ de notre détecteur, pour deux fréquences différentes (29 GHz and 44 GHz).

2   Schéma de détection

Comme dans le schéma proposé par Aguado *et al.* [22], la détection repose sur un couplage capacitif (cf. figure 1.8-a) entre le système à étudier et la jonction SIS (détecteur): ce dispositif présente le double avantage de présenter un bon couplage à haute fréquence, tout

en permettant de polariser indépendamment la source et le détecteur en DC. Les résistances on-chip en platine définissent le couplage entre la source et le détecteur. Qualitativement, on comprend qu'en leur absence, tout le signal HF généré par la source partirait vers la masse: plus quantitativement, un schéma équivalent HF permet de réaliser que les fluctuations de courant au travers de la source sont reliées aux fluctuations de tension aux bornes du détecteur, par une fonction de transfert $Z(\omega)$ (dite 'transimpédance'), qui correspond à la valeur de la résistance de ces fils de platine (coupés à basse fréquence par les capacités de couplage, et à haute fréquence par la capacité géométrique de la jonction SIS). Les capacités de shunt quant à elles définissent un point d'arrêt à notre environnement haute-fréquence: elles n'étaient pas dans le montage de Delft, qui utilisait la capacité entre les plots de contact.
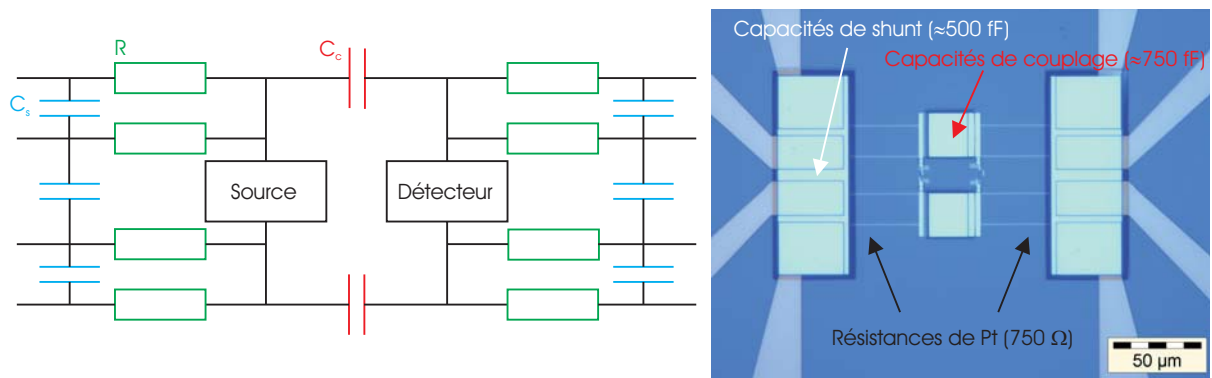
Figure 1.8: (a) - Schéma de couplage, utilisé dans le cadre de cette thèse, entre le système à étudier (source) et le détecteur. (b) - Cliché en microscopie optique de l'échantillon qui nous a permis d'étudier les propriétés d'émission/absorption HF d'une jonction Josephson.

L'ensemble du circuit doit être réalisé dans des dimensions les plus réduites possibles afin d'éviter d'être sensible à d'éventuels effets de propagation, d'où la nécessité d'un couplage 'on-chip': on se fixe comme critère $\ell_{\text{carac}} < \lambda$, où ℓ_{carac} est une dimension caractéristique du circuit, et λ la longueur d'onde typique des signaux radiofréquences étudiés. A 100 GHz, on a $\lambda \approx 3$ mm: notre circuit remplit largement cette condition (cf. figure 1.8-b).

3   Problématique et résultats obtenus

L'expérience de Delft avait permis de valider la possibilité d'utiliser une jonction SIS comme détecteur haute-fréquence, sans pour autant trancher clairement sur sa capacité à détecter un corrélateur nonsymétrisé/symétrisé: seules des mesures en émission ($e\text{V}_{\text{D}} < 2\Delta$) avaient été réalisées. Nous avons progressé dans la compréhension de la détection par

- d'une part une meilleure compréhension des propriétés d'émission/absorption d'une jonction Josephson (bruit de quasiparticules)

- d'autre part des mesures en absorption ($e\text{V}_{\text{D}} > 2\Delta$)

Le premier point s'est révélé assez essentiel: en effet la plupart des systèmes mésoscopiques ont naturellement un spectre de bruit (en excès) symétrique (jonctions tunnels, fil diffusif, point de contact quantique). Or la densité spectrale du bruit de quasiparticules (en excès)

dans une jonction Josephson est asymétrique (cf. calcul en appendice). Cette asymétrie s'interprète de façon assez intuitive en terme de processus inélastiques: à cause du gap dans la densité d'états du supraconducteur qui constitue les électrodes, on a une asymétrie entre les processus d'émission/absorption qui n'existe pas par exemple dans une jonction tunnel en métal normal (NIN).

Bruit en émission

On observe dans le signal mesuré deux contributions différentes, la première est liée à l'effet Josephson AC, et la seconde au bruit de quasiparticules lorsque la jonction Josephson (source) est polarisée sur la branche quasiparticules (cf. figure 1.9).
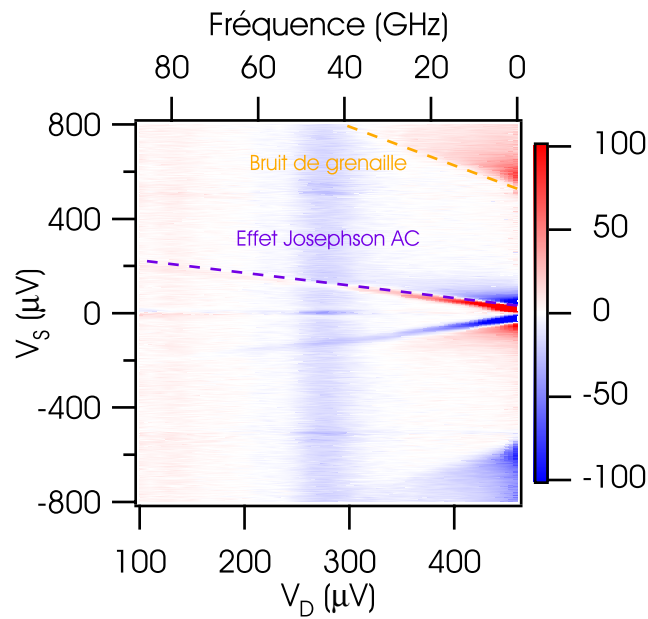
Figure 1.9: Dérivée du courant photo-assisté par rapport à la tension de polarisation sur la source $\partial I_{PAT}/\partial V_S$ en fonction des tensions de polarisation DC sur la source (V_S) et le détecteur (V_D): on distingue deux singularités, l'une correspondant à l'effet Josephson AC de la jonction Josephson ($\hbar\omega = 2eV_S$), et l'autre au bruit de quasiparticules ($\hbar\omega = (eV_S - 2\Delta)$ si $eV_S > 2\Delta$).

Effet Josephson AC. Lorsque la jonction Josephson est polarisée en tension sous le gap ($eV_S < 2\Delta$), elle émet un rayonnement monochromatique à la fréquence $\omega = 2eV_S/\hbar$: c'est l'effet Josephson AC, que l'on peut interpréter comme l'émission/absorption d'un photon associée au transfert cohérent d'une paire de Cooper. Cet effet est bien connu: c'est l'analogue hors-équilibre de l'effet Josephson DC. On peut l'observer de manière indirecte par exemple, en détectant le redressement d'une irradiation haute-fréquence sur une jonction Josephson (pas de Shapiro [24]). Dans nos mesures, nous avons détecté l'effet Josephson AC de la jonction source *via* une marche de courant photo-assisté, dont la largeur varie selon la loi précédemment énoncée (cf. figure 1.9). Dans notre cas, l'effet Josephson AC sert à calibrer le couplage entre la source et le détecteur: on peut en effet à partir d'une théorie qui quantifie les échanges d'énergie entre les deux systèmes (dite de blocage de Coulomb dynamique - BCD), relier l'amplitude du courant photo-assisté dans

le détecteur à la densité spectrale de bruit de la source. La quantité qui détermine la force de ce couplage est la transimpédance $Z(\omega)$, introduite précédemment: l'émission HF associée à l'effet Josephson AC étant monochromatique, elle permet la détermination de la transimpédance (en réalité, cette émission est légèrement élargie par des effets thermiques, ainsi que par des effets d'environnement, mais nous n'en tiendrons pas compte). Il s'est avéré que la transimpédance déterminée à partir de l'effet Josephson AC est moindre que la valeur prédite à partir d'un calcul simple assimilant la transimpédance à une fonction de transfert, et les valeurs des résistances de platine mesurées en continu: ce point avait déjà été observé dans les expériences de Delft [21]. Cette valeur réelle de la transimpédance permettra dans un second temps de comparer les prédictions théoriques s'appuyant sur la théorie du blocage de Coulomb dynamique pour l'amplitude du courant photo-assisté dans le régime de bruit de grenaille (en émission et en absorption) avec nos mesures.

Bruit de grenaille. Précédemment, nous avons vu comment nous nous étions assurés du bon fonctionnement de notre détecteur, ainsi que du schéma de couplage, en regardant un processus d'émission bien connu. On peut donc désormais s'intéresser à des processus d'émission haute-fréquence plus originaux, et essayer par exemple de répondre à la question de la symétrisation: pour cela, regardons l'émission HF d'une jonction Josephson dans le régime du bruit de grenaille. Comme cela a été dit précédemment, la plupart des systèmes mésoscopiques ont naturellement un spectre de bruit en excès symétrique, mais un calcul simple du spectre de bruit de quasiparticules d'une jonction SIS dans le cadre de la réponse linéaire prédit pour cette dernière un spectre de bruit en excès asymétrique (cf. appendice)

$$S_I(\omega, V) = \frac{e}{2\pi} \left[\frac{I_{qp}(\hbar\omega/e + V)}{1 - e^{-\beta(\hbar\omega + eV)}} + \frac{I_{qp}(\hbar\omega/e - V)}{1 - e^{-\beta(\hbar\omega - eV)}} \right]$$

Pour clarifier la discussion, on peut représenter le spectre de bruit en excès, dans le cas non-symétrisé (cf. figure 1.10): on distingue d'abord une singularité en absorption à $\hbar\omega = 2\Delta + eV_S$, quelle que soit la tension de polarisation sur la source. Il n'est pas possible de détecter ce processus car notre détecteur n'est sensible qu'aux fréquences comprises entre 0 et $2\Delta/\hbar$ (en émission comme en absorption). Il reste l'autre singularité qui évolue en absorption comme $\hbar\omega = 2\Delta - eV_S$ lorsque $eV_S < 2\Delta$, et en émission comme $\hbar\omega = (eV_S - 2\Delta)$ lorsque $eV_S > 2\Delta$. Cette singularité est accessible à notre système de détection, et permet de déterminer si la symétrisation est pertinente ici. En effet, la seule mesure en émission doit suffire à trancher entre les deux scénarios:

- si on est sensible au corrélateur non-symétrisé, on doit détecter une singularité en émission à $\hbar\omega = eV_S - 2\Delta$ uniquement lorsque $eV_S > 2\Delta$

- si on est sensible au corrélateur symétrisé, on aura alors une singularité à $|eV_S - 2\Delta|$, que la jonction soit polarisée en-dessous ($eV_S < 2\Delta$), ou au-dessus du gap ($eV_S > 2\Delta$)
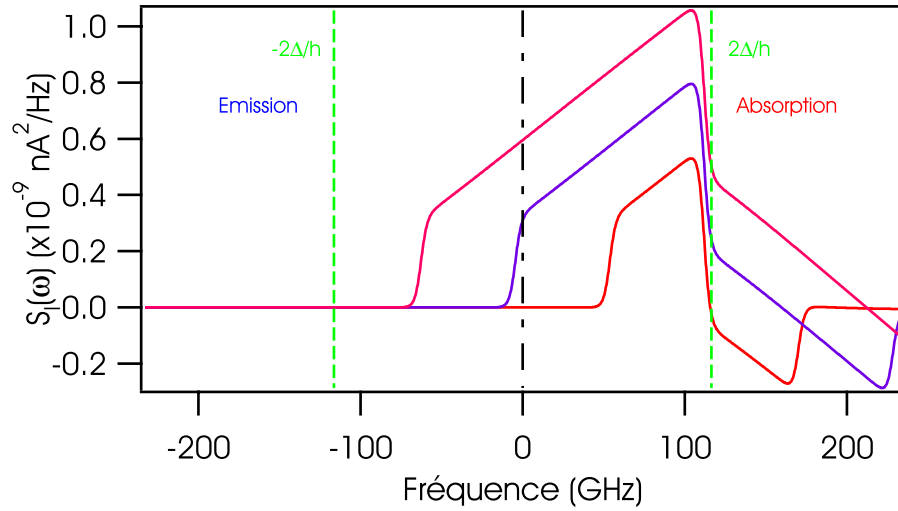
Figure 1.10: Densité spectrale du bruit de quasiparticules (en excès) non-symétrisée pour une jonction Josephson, pour différentes tensions de polarisation (V $=$ $\Delta/e, 2\Delta/e$ and $3\Delta/e$).

L'asymétrie dans le spectre de bruit de la jonction SIS peut s'interpréter de façon assez intuitive en la reliant aux processus inélastiques mis en jeu (cf. figure 1.11):

- Si $eV_S < 2\Delta$: on retrouve deux singularités en absorption, pour $\hbar\omega = (2\Delta \pm eV_S)$, et aucun processus d'émission.

- Si $eV_S > 2\Delta$: on distingue aussi deux singularités, une en émission à $\hbar\omega = (eV_S - 2\Delta)$, et une en absorption à $\hbar\omega = (2\Delta + eV_S)$.
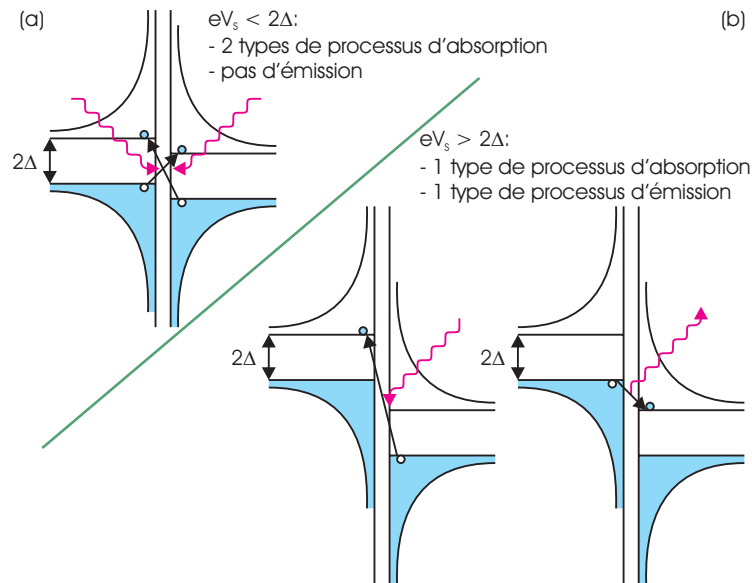
Figure 1.11: Processus inélastiques associé au courant de quasiparticules d'une jonction Josephson.

Si on se réfère à la figure 1.9, on constate que l'on observe une singularité à $\hbar\omega = (eV_S - 2\Delta)$, **uniquement lorsque $eV_S > 2\Delta$**: notre détecteur quantique est donc sensible au corrélateur non-symétrisé. La jonction semble donc être un détecteur quantique, dans le sens où il paraît capable de distinguer les processus d'émission de ceux d'absorption. Des calculs numériques s'appuyant sur la théorie du blocage de Coulomb dynamique, et intégrant la valeur de la transimpédance déterminée précédemment à partir de l'effet Josephson AC, confirment la pertinence de l'expression du spectre de bruit non-symétrisé d'une jonction Josephson (courant de quasiparticules) donnée précédemment.

On a montré que la détection de bruit utilisant une jonction SIS est sensible au corrélateur non-symétrisé, par une mesure d'émission: néanmoins pour être complet une mesure d'absorption s'impose.

Bruit en absorption

De façon assez similaire à ce qui a été fait pour le régime d'émission, nous avons mesuré le courant photo-assisté dans le régime d'absorption ($eV_D > 2\Delta$): les résultats sont présentés sur la figure 1.12. On distingue à nouveau une contribution liée à l'effet Josephson AC, ainsi que deux singularités qui semblent associées au régime de bruit de quasiparticules. Ceci est *a priori* surprenant car d'après ce qui a été dit précédemment, on n'en attend qu'une. Quelle est l'origine de cette singularité supplémentaire?
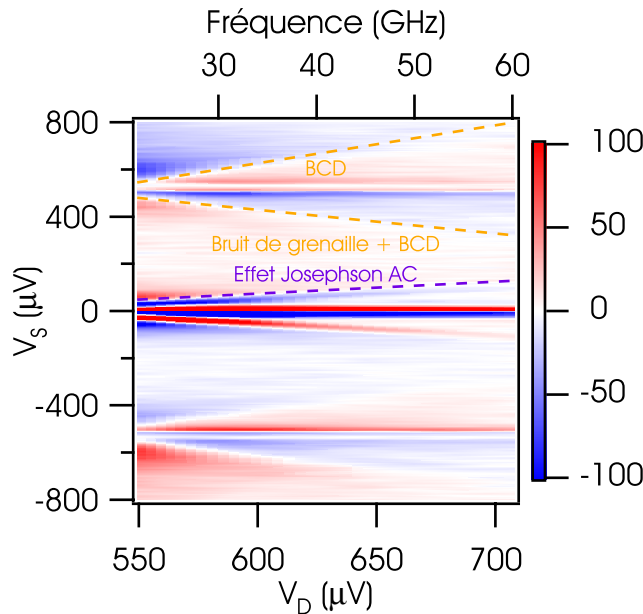
Figure 1.12: Dérivée du courant photo-assisté par rapport à la tension de polarisation sur la source $\partial I_{PAT}/\partial V_S$ pour différentes tensions de polarisation DC sur la source: comme pour l'émission, on a une singularité à $\hbar\omega = 2eV_S$ qui correspond à l'effet Josephson AC, ainsi que deux singularités à $\hbar\omega = (2\Delta - eV_S)$ (si $eV_S < 2\Delta$) et $\hbar\omega = (eV_S - 2\Delta)$ (si $eV_S > 2\Delta$).

Effet Josephson AC   Comme pour l'émission, on détecte un processus d'absorption de la jonction Josephson (source) lorsqu'elle est polarisée sous le gap ($eV_S < 2\Delta$), qui varie selon $\omega = 2eV_S/\hbar$ (cf. figure 1.12). Nous avons comparé les prédictions théoriques faites à partir du blocage de Coulomb dynamique, et la transimpédance extraite à partir des

données en émission: l'accord avec nos données est bon. On a donc déjà un premier signe que notre détecteur fonctionne bien dans le régime de détection des processus d'absorption.

Bruit de grenaille   Le régime du bruit de quasiparticules révèle une surprise inattendue, car on détecte deux singularités à $\hbar\omega = |eV_S - 2\Delta|$, quel que soit le régime de polarisation sur la source. Ce résultat est en contadiction avec l'expérience faite dans le régime d'émission, car il correspond au corrélateur symétrisé. Quelle est donc l'origine de cette seconde singularité, qui remet en question les résultats précédents? La réponse semble venir de l'environnement: en effet, lorsque l'on polarise la source autour de $eV_S = 2\Delta$, son impédance est fortement modifiée, non seulement à basse-fréquence, mais aussi à haute-fréquence. Ces effets de la conductance dynamique de la source sont plus sensibles dans le régime d'absorption car dans ce cas de figure, le détecteur a dans une impédance finie, alors que dans le régime d'émission, son impédance est infinie: un calcul numérique toujours basé sur la théorie du blocage de Coulomb dynamique appuie cette hypothèse. Par conséquent

- **$eV_S < 2\Delta$** on observe une singularité dans le courant photo-assisté à $(2\Delta - eV_S)$, qui est due à un effet d'environnement

- **$eV_S > 2\Delta$** on observe une singularité dans le courant photo-assisté à $(eV_S - 2\Delta)$, qui est la somme d'un effet d'environnement, et d'un processus d'absorption à cette même fréquence

Nous avons donc confirmé dans le régime d'absorption que notre schéma de détection est sensible au corrélateur non-symétrisé, mais le gain haute-fréquence de ce dernier étant dépendant de la dynamique des différents éléments du circuit de polarisation, l'interprétation des données lorsque l'impédance du détecteur est finie doit être menée avec précaution.

4   Conclusion

Cette première partie permet de conclure de façon définitive sur la pertinence de la symétrisation: il existe des détecteurs (comme la jonction SIS de ces expériences), capables de distinguer les photons émis des photons absorbés par le système étudié. C'est donc le corrélateur non-symétrisé qui est pertinent: il peut être compris en terme de processus inélastiques. Ce dernier point est important car il permet d'intuiter quels seraient les autres sytèmes présentant une telle disymétrie de leur bruit en excès.

Peut-on trouver d'autres systèmes présentant des propriétés d'émission/absorption originales? Enfin, notre schéma de détection est bien adapté pour des échantillons d'assez haute impédance: mais comment l'adapter à des échantillons de basse impédance?

III   Le transistor à une paire de Cooper

1   Motivations

On a vu dans la partie concernant la jonction Josephson qu'il était pertinent d'utiliser un détecteur quantique, directement couplé au système à étudier, dans un environnement électromagnétique bien contrôlé, pour mesurer les propriétés d'émission/absorption à haute-fréquence d'un système mésoscopique. On peut donc penser étendre ce mode de détection à d'autres systèmes plus complexes maintenant que l'on s'est assuré de son bon fonctionnement sur un système *a priori* bien connu. On a vu en particulier que l'on était en mesure

de détecter les photons émis/absorbés lors du transfert cohérent de paires de Cooper au travers d'une jonction Josephson (effet Josephson AC). On peut se demander s'il est possible d'avoir un système dont l'émission haute-fréquence est modulable par un paramètre extérieur, autre que la tension appliquée. On peut penser à un système qui serait accordable par une tension de grille: ces systèmes sont rassemblés sous le terme générique de 'transistor', bien que les effets qui sont à l'origine de l'effet de la grille soient de nature différente. Le transistor qui valut le prix Nobel à Bardeen, Brattain et Shockley en 1956, utilise la possibilité de moduler la densité électronique d'un semi-conducteur, alors que le transistor à un électron [25][26] repose sur la manipulation des effets de charge dans des systèmes métalliques, et requiert de très basses températures ($k\mathrm{T} \ll \mathrm{E_c}$)[3].

Le transistor à un électron (SET) est constitué d'une île métallique, reliées à deux contacts eux-aussi métalliques, via deux barrières tunnels: suite à l'amélioration des procédés de nanofabrication, les jonctions tunnels peuvent être réduites de telle manière que les effets de charge peuvent être sondées (à condition que $k\mathrm{T} \ll \mathrm{E_c}$). Pour des conditions d'oxydation typiques, on a pour une jonction de 100 nm × 100 nm, une capacité de l'ordre de 1 fF , soit une énergie de charge de l'ordre de 100 μeV.
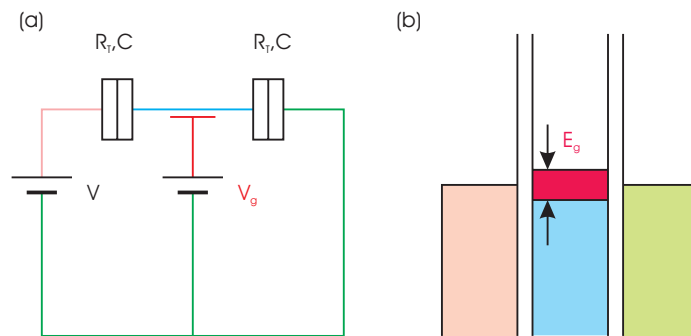
Figure 1.13: (a) - Schematic representation of a SET. (b) - Illustration of the Coulomb blockade effect in a SET.

---

[3]Il a cependant été démontré que ces effets de charge peuvent être observés à température ambiante dans des systèmes tels que des nanotubes de carbone [27], ou des nanocristaux de silicium [28].
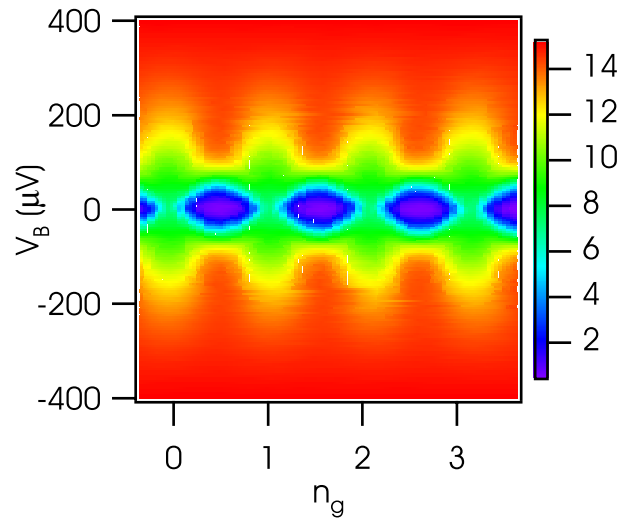
Figure 1.14: Conductance G (en μS) du transistor à une paire de Cooper étudié dans cette thèse, dans l'état normal (*ie.* un SET) en fonction de la tension de polarisation V_B et de la tension de grille ($n_g = C_g V_g/e$): on voit clairement que la conductance à basse tension est modulée par la grille, ouvrant la possibilité d'avoir soit des états passants, soit des états bloqués de Coulomb. Dans cet échantillon, les effets de blocage de Coulomb sont relativement faibles, étant donné la valeur l'énergie de charge: cependant pour des valeurs plus élevées de E_c, les effets de charge peuvent être bien plus importants, permettant alors l'observation de "diamants de Coulomb".

La situation devient un peu plus complexe lorsque l'on introduit de la supraconductivité dans ce système: en effet, en plus des effets de charge, on doit aussi prendre en compte des effets de parité imposés par le gap supraconducteur. En effet, les états à une quasiparticule sont interdits, disons plus exactement qu'ils ont un coût énergétique de l'ordre du gap Δ, qui les rend en théorie hautement improbables aux températures mises en jeu habituellement dans ce type d'expérience. On verra qu'en pratique, ces états à une quasiparticule existent bel et bien, et que leur effet sur les propriétés de transport, et de cohérence de ces systèmes n'est pas à négliger. En première approximation donc, le transistor à une paire de Cooper (SCPT) se comporte comme un SET, dont les propriétés de transport ne sont plus $e-$ périodiques, mais $2e-$ périodiques: à cela s'ajoute la possibilité d'observer des effets cohérents. En effet, comme pour la jonction Josephson précédemment étudiée, on peut observer un courant non dissipatif (effet Josephson DC) associé au transfert cohérent de paires de Cooper au travers de l'îlot, dont l'amplitude est modulable par la grille [29][30] (cf. figure 1.15).
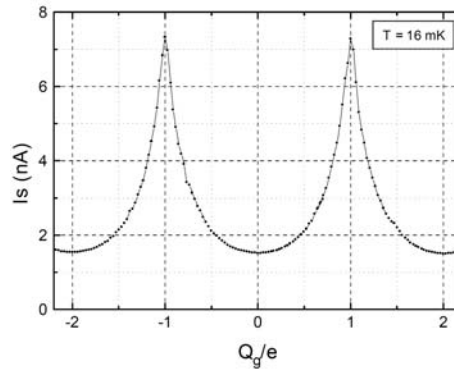
Figure 1.15: Exemple de modulation de l'amplitude du supercourant d'un transistor à une paire de Cooper, en fonction de $Q_g = C_g V_g$ [30].

En effet, pour certaines valeurs de tension de grille, les états de charge $|n = 0\rangle$ et $|n = 2\rangle$ du SCPT sont proches énergétiquement: la dégénérescence est alors levée par le couplage Josephson. Il en découle une certaine dispersion des nivaux d'énergie par rapport à la phase, que l'on peut associer à un couplage Josephson effectif: ce dernier est alors maximal lorsque les états de charge $|n = 0\rangle$ et $|n = 2\rangle$ sont dégénérés, ie. lorsque $n_g = 1$[2]. On parle alors d'état passant (réminiscent de ce qui se passe pour les états à un électron dans le SET): la délocalisation de la charge est alors maximale, ainsi que l'amplitude du supercourant. A l'opposé, lorsque $E_{|2\rangle} - E_{|0\rangle}$ est maximum, le couplage Josephson effectif est minimum, et le transfert de paires de Cooper est bloqué. Ce raisonnement explique parfaitement la modulation du supercourant observée expérimentalement. Partant de cet exemple assez simple, on peut explorer des cas de figure un peu plus compliquées: on peut se demander en particulier ce qui se passe à haute-fréquence. Comment l'amplitude, ainsi que la fréquence de l'effet Josephson AC sont-ils modulés par la grille? Existe-t-il d'autres processus d'émission/absorption haute-fréquence associés au transfert cohérent de paires de Cooper à travers le transistor?

2   Emission haute-fréquence d'un transistor à une paire de Cooper: effet Josephson AC généralisé

Pour cette étude, on reprend le même mode de détection que celui décrit dans la première partie concernant l'étude du bruit haute-fréquence d'une jonction Josephson. Néanmoins, pour des raisons liées à la sensibilité de la mesure, on se restreint au régime d'émission. On mesure le courant photo-assisté dans une jonction SIS couplée capacitivement au SCPT: pour améliorer la précision, on travaille en modulation.

Effet Zener

Nous avons essayé de comprendre comment l'émission haute-fréquence d'un SCPT était modulée par la grille, tant sur le plan de l'amplitude que du contenu en fréquence. A voir la relation énergie-phase d'un SCPT (déduite de la diagonalisation numérique de son hamiltonien), on s'attend à une émission haute-fréquence monochromatique (effets thermiques et d'environnement mis à part) lorsque $n_g = 0$, et fortement anharmonique lorsque $n_g = 1$ (cf. figure 1.16).
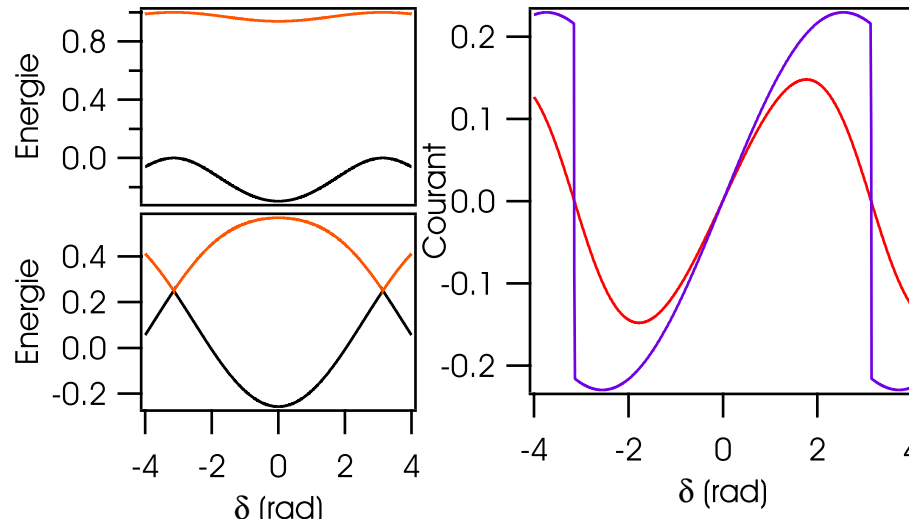
Figure 1.16: (a) - Energie des deux premiers états de charge $|n = 0\rangle$ et $|n = 2\rangle$, en fonction de la différence de phase supraconductrice δ à $n_{\mathrm{g}} = 0$. (b) - Idem à $n_{\mathrm{g}} = 1$. (c) - Relation courant-phase associée à ces deux mêmes niveaux à $n_{\mathrm{g}} = 0, 1$.

On s'attend donc à ce que le contenu en fréquence de l'émission haute-fréquence du transistor autour de $n_{\mathrm{g}} = 1$ soit riche en harmoniques: une des difficultés possibles pour les observer est qu'elles ont une amplitude significative dans une gamme assez restreinte de tensions de grille. Nous avons donc détecté dans le régime probable d'effet Josephson AC (basse tension), l'émission haute-fréquence ($e\mathrm{V_D} < 2\Delta$) du SCPT à $n_{\mathrm{g}} = 0, 1$ (cf. figure 1.17). On voit qu'à $n_{\mathrm{g}} = 0$, on détecte une raie d'émission Josephson AC qui suit la relation Josephson $\omega = 2e\mathrm{V_S}/\hbar$ conformément à ce que laissait présager la relation énergie-phase, alors qu'à $n_{\mathrm{g}} = 1$ on a non pas un jeu d'harmoniques, mais une sous-harmonique à $\omega = e\mathrm{V_S}/\hbar$. Cette observation s'explique si l'on tient compte de la dynamique de la phase: comme on peut le voir sur la figure 1.16, lorsque $n_{\mathrm{g}} = 1[2]$ la relation énergie-phase présente des points de dégénérescence entre les niveaux $|n = 0\rangle$ et $|n = 2\rangle$, à $\delta = \pi[2\pi]$. En pratique, ces dégénérescences sont levées par la dissymétrie des jonctions du transistor (cette dissymétrie est d'autant plus importante que l'on travaille avec de petites jonctions). Dans un régime adiabatique, on s'attend à ce que le système reste dans son état fondamental: par contre, si l'évolution de la phase (fixée par la tension continue aux bornes du transistor) est très rapide, le système peut transiter du fondamental vers le premier état excité, et réciproquement (effet Landau-Zener [31]). On comprend alors que l'on rétablit une relation énergie phase harmonique, avec un doublement de la période (en accord avec une émission à $\omega = e\mathrm{V_S}/\hbar$). Cet effet avait déjà été observé de manière indirecte, *via* des pas de Shapiro [30].
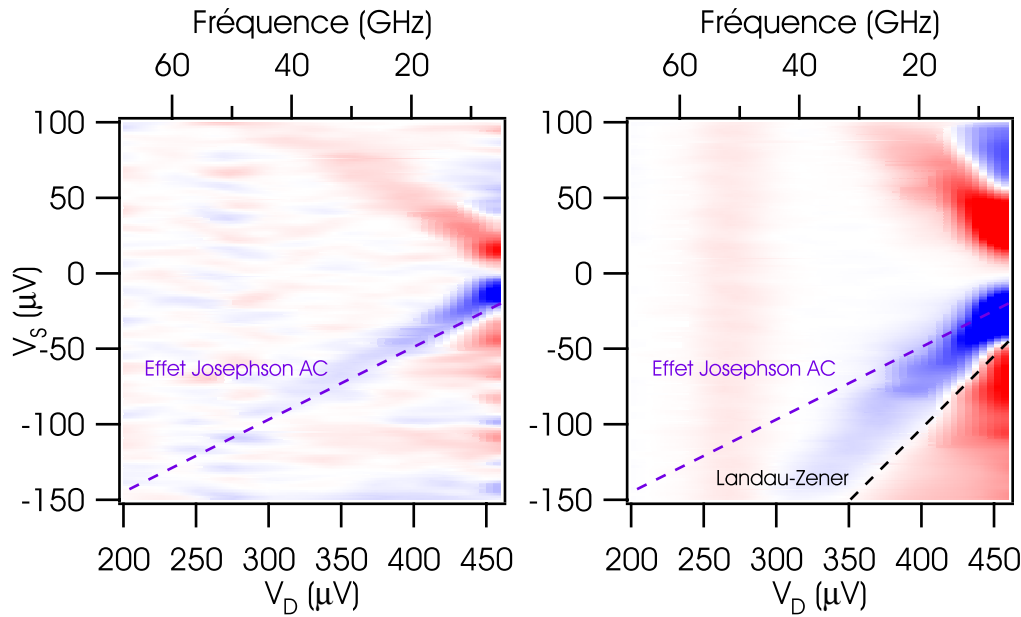
Figure 1.17: Dérivée du courant photo-assisté par rapport à la tension de polarisation sur le SCPT $\partial I_{PAT}/\partial V_S$ pour différentes tensions DC. (a) Lorsque $n_g = 0$, on observe une singularité en émission à $\hbar\omega = 2eV_S$. (b) Lorsque $n_g = 1$, on observe une singularité en émission à $\hbar\omega = eV_S$.

Contrairement au régime continu, où le SCPT se comporte à l'équilibre comme une jonction Josephson dont le couplage Josephson est ajustable par la grille, la situation est un peu plus compliquée dans le régime d'effet Josephson AC. Dans un régime où la phase évolue de manière non-adiabatique, l'émission HF est monochromatique, mais la fréquence comme l'amplitude sont ajustables par la grille. Néanmoins, on s'est restreint jusqu'ici à un régime de polarisation à basse tension, mais que se passe-t-il à plus haute tension (tout en restant dans un régime où les propriétés de transport du SCPT sont $2e-$périodiques)?

Régime d'émission HF associée au régime de transfert résonant de paires de Cooper (RCPT).

L'application d'une tension tend à stabiliser des états un peu plus originaux du transistor: en effet, la passage d'une paire de Cooper au travers du transistor apporte au système un gain d'énergie électrostatique dont on peut tenir compte dans l'hamiltonien de façon heuristique *via* un terme $\mathcal{H}_{él} = -2eV_S$ [32]. On peut alors raisonner avec un nouveau jeu d'états du système: $|n, k\rangle$ où n correspond à l'état de charge de l'îlôt, et k au nombre de paires de Cooper qui sont passées au travers du transistor. Pour certaines valeurs de la tension appliquée sur le SCPT, ces états peuvent entrer en résonance: on peut observer des signatures très claires de ces résonances en transport DC [33][34][30]. On parle plus couramment de transfert résonnant de paires de Cooper (RCPT). Quelles sont les signatures de ces transitions à haute-fréquence? Ce régime de transfert de charges s'apparente à une forme d'effet Josephson AC, dans un régime plus complexe lié à la présence d'états intermédiaires: nous avons montré qu'à haute-fréquence, le comportement du SCPT est plus complexe que ce qui est observé en transport continu. Le contenu en

fréquence est plus riche, et dans ce régime, le transistor ne se ramène plus à une jonction Josephson dont le couplage Josephson est ajustable par la grille.

3   Spectroscopie très haute fréquence des niveaux d'énergie du SCPT

Problématique

L'existence d'états à une quasiparticule a été évoquée précédemment: ces effets, appelés plus généralement effets "d'empoisonnement", constituent un réel frein au développement de ce type de circuit, notamment dans le domaine de l'information quantique. En effet, ces circuits supraconducteurs constituent l'élément de base idéal (un système à deux niveaux cohérent, ou "qubit") pour le calcul quantique. Une bonne compréhension de la façon dont ces niveaux dits "impairs" interviennent dans les processus de transport du transistor est donc importante, si l'on veut améliorer les propriétés de cohérence de ces systèmes: un certain nombre d'expériences récentes se sont intéressées à cette problématique sous différents angles. L'approche développée ici vise à réaliser une mesure de spectroscopie des niveaux d'énergie du transistor. Un certain nombre d'expériences de spectroscopie ont déjà été réalisées par le passé sur ce type de systèmes: il s'agit plus souvent de boîtes à paires de Cooper (un îlot supraconducteur relié à un seul réservoir *via* une barrière tunnel, dont le potentiel électrostatique est lui aussi contrôlé par une grille). Ces expériences courantes dans la communauté des "qubits" se concentrent sur les deux premiers niveaux "pairs", car ce sont ces états quantiques qui permettent de définir un système à deux niveaux cohérent. En adaptant la taille des jonctions, on peut choisir une valeur de l'énergie de charge qui ramène la mesure de spectroscopie dans des gammes de fréquence accessibles habituellement en milieu cryogénique. Les niveaux impairs sont plus délicats à étudier car ils nécessitent des fréquences de l'ordre du gap du supraconducteur qui constitue le SCPT, soit 100 GHz dans le cas de l'aluminium: ce type d'expérience pose des problèmes à basse température. Une alternative serait donc d'utliser un dispositif de mesure "on-chip". Comment réaliser une telle expérience?

Dispositif de couplage "on-chip"

Pour cette expérience, nous avons inversé les rôles entre le SQUID et le SCPT: en maximisant son couplage Josephson avec le flux, nous avons transformé le SQUID en jonction Josephson. L'effet Josephson AC en fait un générateur HF "on-chip", qui permet d'irradier le SCPT de façon bien contrôlé: la puissance d'irradiation est contrôlée par le flux, et sa fréquence d'irradiation par la tension de polarisation. Nous avons supposé que cette source est presque monochromatique (en pratique, l'émission Josephson AC a une largeur d'émission finie à cause d'effets thermiques et de l'environnement). Le transistor devient en quelque sorte le détecteur, l'idée étant de voir comment ses propriétés de transport sont modifiées par les transitions entre niveaux induites par l'irradiation.

Mesure du supercourant du SCPT en fonction de l'irradiation

La première idée était de mesurer l'effet de l'irradiation HF associée à l'effet Josephson AC de la jonction Josephson sur le supercourant du SCPT (cf. figure 1.18). On peut d'abord se concentrer sur les deux cas opposés ($n_{\mathrm{g}} = 0, 1$), représentés sur la figure 1.18-a:

- **Pour $n_{\mathbf{g}} = 1$:** A l'équilibre, cet état dit "passant" correspond à un maximum du supercourant: or on s'aperçoit que selon la fréquence d'irradiation, l'amplitude de ce supercourant peut être soit diminuée (de manière très significative), soit augmentée.

Cet effet est assez surprenant, surtout si l'on tient compte du fait que la puissance d'irradiation est relativement faible (de l'ordre de la dizaine de femtowatts).

- **Pour $n_g = 0$:** *A contrario*, cet état correspond à l'équilibre à un minimum du supercourant: l'irradiation permet de rehausser l'amplitude du supercourant.
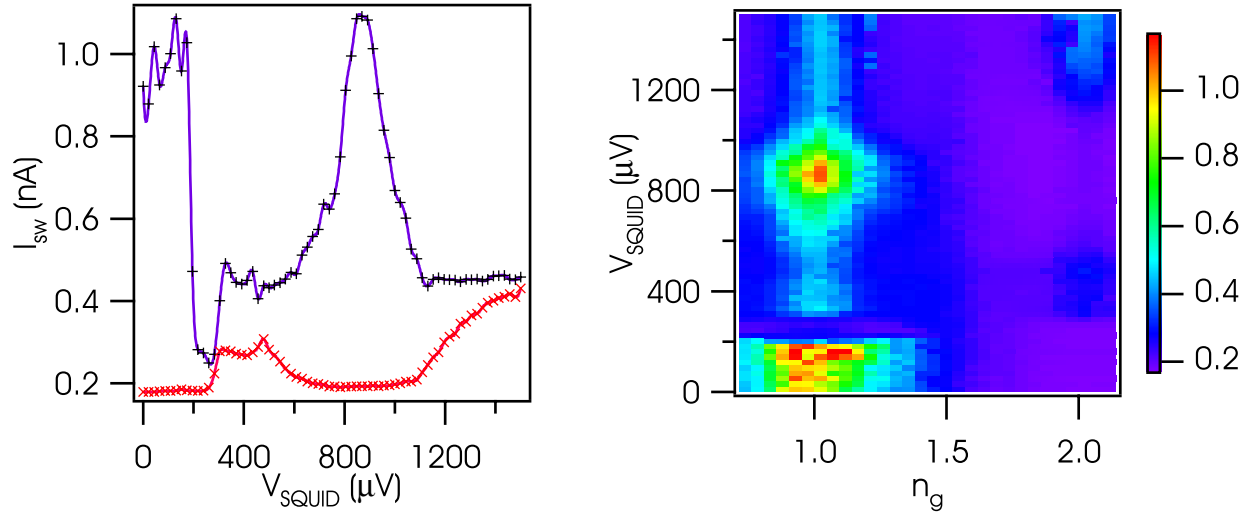
Figure 1.18: Effet de l'irradiation HF générée par l'effet Josephson AC de la source sur le courant de switching du SCPT à T = 90 mK. (a) - Courant de switching du SCPT en fonction de la tension de polarisation du SQUID, pour deux valeurs différentes de la tension de grille ($n_g = 0$ et $n_g = 1$). (b) - Idem pour différentes valeurs de la tension de grille.

On peut réaliser cette mesure pour différentes valeurs de tension de grille (cf. figure 1.18): on s'aperçoit entre autres choses, que l'on est en mesure d'atteindre un régime $e-$périodique à très haute-fréquence. Pourtant, il est difficile d'identifier clairement les transitions qui expliquent ces fortes variations du courant de switching au vu de ces données, peut-être à cause d'un défaut de moyennage.

Ces mesures sont effectivement assez contraignantes: le principal problème concerne la rapidité d'acquisition des données. La forte impédance de notre échantillon (48.5 kΩ), conjuguée à la capacité des câbles de mesure, donnent un temps $\tau = RC$ assez élevé qui nous oblige à répéter ces mesures de switching relativement lentement (trop lentement pour réaliser une bonne statistique). Est-il possible de s'affranchir de ces problèmes, malgré sa forte impédance? Une possibilité serait de mesurer une quantité qui soit déjà une moyenne dans le temps de l'information qui nous intéresse, *ie.* le temps d'occupation des différents niveaux d'énergie du SCPT.

Analogue d'une mesure de réflectométrie 'on-chip'

Les expériences à base d'électronique haute-fréquence rencontrent des problèmes similaires avec le SCPT: sa forte impédance impose des restrictions sur la vitesse de mesure. Une alternative bien connue est d'insérer le transistor dans un circuit résonant [35][36]: à l'équilibre, le SCPT s'apparente à une inductance (effet Josephson DC), qui est reliée à son

couplage Josephson effectif. Il est possible de remonter à cette inductance en mesurant la fréquence de résonance de ce circuit (expérience de réflectométrie): chaque niveau d'énergie ayant son couplage Josephson effectif propre, en mesurant cette résonance, on doit pouvoir remonter à l'information qui nous intéresse, *ie*. l'occupation des niveaux d'énergie du SCPT en fonction de la fréquence d'irradiation. Néanmoins, dans notre cas nous ne disposons pas de circuit résonant, et il nous a fallu trouver une autre quantité à regarder. Il se trouve qu'à cause de son environnement, la branche du supercourant de notre SCPT présentait une pente finie, qui se trouve être reliée à l'inductance du transistor: nous avons donc mesuré cette pente, en fonction de l'irradiation haute-fréquence, et avons ainsi pu remonter à des informations sur la spectroscopie de ce système (cf. figure 1.19).
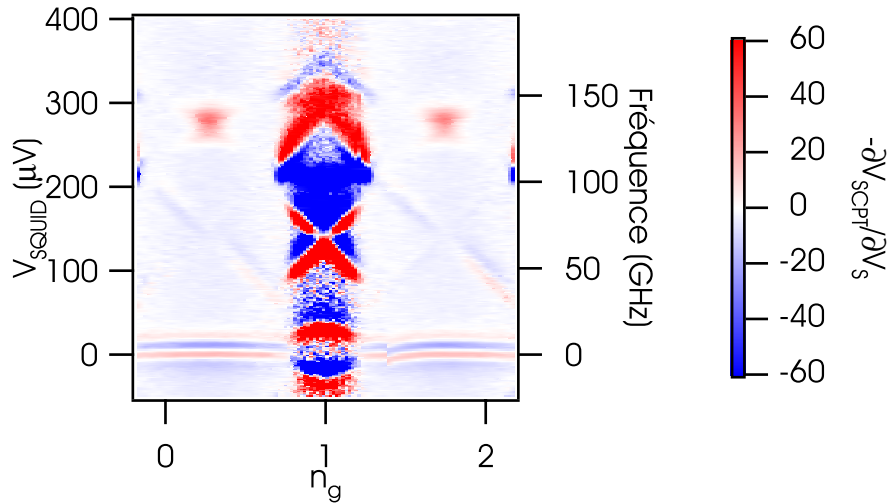
Figure 1.19: Pente de la branche Josephson du transistor en fonction de la fréquence d'irradiation, pour différentes valeurs de la tension de grille (T = 90 mK).

On distingue plusieurs jeux de transitions

- $|n = 0\rangle \rightarrow |n = 2\rangle$: C'est la transition étudiée habituellement dans les expériences de spectrosopie sur des boîtes à paires de Cooper: cette transition nous permet de vérifier que notre dispositif fonctionne correctement.

- $|n = 0\rangle \rightarrow |n = 1\rangle$: Cette transition fait partie de ce qui était recherché pour répondre aux questions qui se posent autour des processus "d'empoisonnement": on peut induire le passage de quasiparticules sur l'îlot supraconducteur, ce qui explique par exemple pourquoi on était en mesure de réduire fortement l'amplitude du super-courant autour de $n_{\mathrm{g}} = 1$ dans l'expérience précédente, pour des fréquences de l'ordre de 100 GHz $\approx 2\Delta/h$. Mais si il est possible de diminuer le supercourant, peut-on aussi facilement l'augmenter? On va voir que deux possibilités s'offrent à nous.

- $|n = 1\rangle \rightarrow |n = 3\rangle$: Si le transistor est dans un état à une quasiparticule (*ie*. qu'il est "empoisonné"), on peut induire le passage d'une paire de Cooper sur l'îlot. On passe alors dans l'état $|n = 3\rangle$, qui relaxe spontanément vers l'état $|n = 2\rangle$ en évacuant une quasiparticule vers un des réservoirs: ce processus est permis tant que $(\mathrm{E}_{|3\rangle} - \mathrm{E}_{|1\rangle}) > \Delta$. On revient alors vers un niveau pair, donc avec un plus fort supercourant autour de $n_{\mathrm{g}} = 0$.

- $|n = 1\rangle \rightarrow |n = 0\rangle$**:** Autre cas de figure possible pour accroître le supercourant si le SCPT est dans un état à une quasiparticule: apporter au système suffisamment d'énergie (soit $\Delta - (E_{|1\rangle} - E_{|0\rangle})$) pour extraire la quasiparticule.

Cette étude de spectrocopie, dans une gamme de fréquence difficile à explorer sur ce type de système, a permis d'identifier différents types de processus de transport mettant en jeu des états à une quasiparticule: il révèle qu'il est possible d'induire, comme d'extraire des quasiparticules dans un dispositif SCPT/CPB par une irradiation haute-fréquence appropriée. Il reste à savoir si ces effets peuvent avoir un intérêt dans le domaine des qubits: en effet, chasser ces quasiparticules est une chose, encore faut-il les chasser plus vite qu'elles n'entrent dans le système si l'on veut améliorer les propriétés de cohérence d'un qubit. On peut aussi entrevoir des applications potentielles dans le domaine des bolomètres, étant donnée la grande sensibilité du supercourant à de faibles puissances d'irradiation.

Part II

Detection of non-symmetrized noise correlator in mesoscopic devices

Chapter 2

Current fluctuations: classical and quantum regimes

I Classical limit

1 Noise time correlator and spectral density

Let us consider a conductor: the current flowing through it is measured by an ideal ammeter (see figure 2.1-a). Whether it is voltage biased or not, the measured current $I(t)$ presents some fluctuations $\delta I(t)$ around its average value $\langle I(t) \rangle$ (see figure 2.1-b). These fluctuations can be characterized by a time current-current correlator

$$C(\tau) = \langle \delta I(t + \tau) \delta I(t) \rangle$$
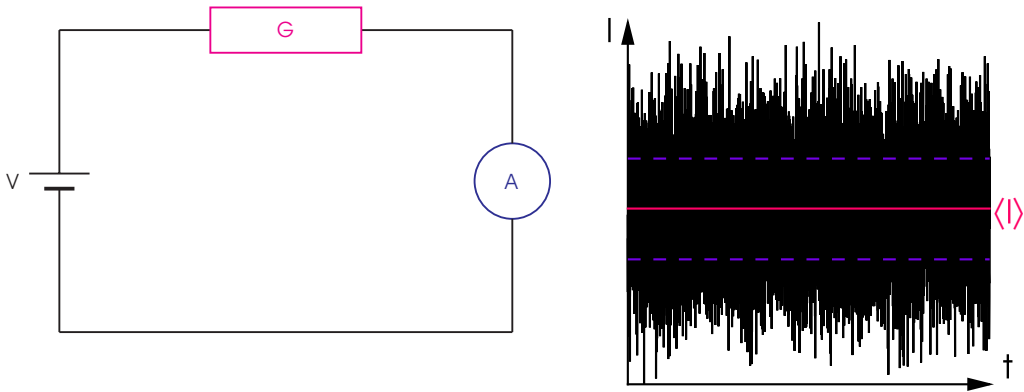
Figure 2.1: (a) - The device under test is voltage biased by an ideal voltage source: the current $I(t)$ is measured by an ideal ammeter. (b) - Example of the recorded signal $I(t)$.

When characterizing fluctuation phenomena, one prefers to work on another quantity, the spectral density $S_I(\omega)$, which is simply the Fourier transform of the current-current correlator $C(\tau)$

$$S_I(\omega) = \frac{1}{2\pi} \int_{-\infty}^{+\infty} d\tau e^{i\omega\tau} \langle \delta I(t + \tau) \delta I(t) \rangle$$

Wiener-Khintchine theorem

Let us consider a WSS[1] stochastic process $\mathrm{I}(n)$. Its spectral density $\mathrm{S}(\omega)$ is defined as its squared fourier transform

$$\mathrm{S}(\omega) = \lim_{\mathrm{N}\to\infty} \frac{1}{2\mathrm{N}+1} \left\langle \left(\sum_{m=-\mathrm{N}}^{\mathrm{N}} \mathrm{I}(m)\, e^{-i\,\omega m} \right) \left(\sum_{n=-\mathrm{N}}^{\mathrm{N}} \mathrm{I}(n)\, e^{-i\,\omega n} \right)^{\star} \right\rangle$$

This expression can be developped

$$\mathrm{S}(\omega) = \lim_{\mathrm{N}\to\infty} \frac{1}{2\mathrm{N}+1} \left\langle \sum_{m=-\mathrm{N}}^{\mathrm{N}} \sum_{n=-\mathrm{N}}^{\mathrm{N}} \mathrm{I}(m)\,\mathrm{I}(n)\, e^{-i\,(m-n)} \right\rangle$$

$$= \lim_{\mathrm{N}\to\infty} \frac{1}{2\mathrm{N}+1} \sum_{m=-\mathrm{N}}^{\mathrm{N}} \sum_{n=-\mathrm{N}}^{\mathrm{N}} \langle \mathrm{I}(m)\,\mathrm{I}(n) \rangle\, e^{-i\,(m-n)}$$

$$= \lim_{\mathrm{N}\to\infty} \frac{1}{2\mathrm{N}+1} \sum_{m=-\mathrm{N}}^{\mathrm{N}} \sum_{n=-\mathrm{N}}^{\mathrm{N}} \mathrm{C_I}(m-n)\, e^{-i\,(m-n)}$$

$$\mathrm{S}(\omega) = \lim_{\mathrm{M}\to\infty} \lim_{\mathrm{N}\to\infty} \frac{1}{2\mathrm{M}+1} \sum_{m=-\mathrm{M}}^{\mathrm{M}} \sum_{n=-\mathrm{N}}^{\mathrm{N}} \mathrm{C_I}(m-n)\, e^{-i\,(m-n)}$$

At this stage, the demonstration becomes more tricky because one requires to check some convergence requirements on the sums involved. We will simplify the procedure in order to give an insight of the origin of the Wiener-Khintchine theorem:

$$\mathrm{S}(\omega) = \lim_{\mathrm{M}\to\infty} \frac{1}{2\mathrm{M}+1} \sum_{m=-\mathrm{M}}^{\mathrm{M}} \lim_{\mathrm{N}\to\infty} \sum_{n=-\mathrm{N}}^{\mathrm{N}} \mathrm{C_I}(m-n)\, e^{-i\,(m-n)}$$

$$= \left(\lim_{\mathrm{M}\to\infty} \frac{1}{2\mathrm{M}+1} \sum_{m=-\mathrm{M}}^{\mathrm{M}} \right) \lim_{\mathrm{N}\to\infty} \sum_{n=-\mathrm{N}}^{\mathrm{N}} \mathrm{C_I}(n)\, e^{-i\,n}$$

$$\mathrm{S}(\omega) = \sum_{n=-\infty}^{+\infty} \mathrm{C_I}(n)\, e^{-i\,n}$$

It finally appears that the spectral density $\mathrm{S}(\omega)$ of a WSS stochastic process I is the Fourier transform of its correlation function $\mathrm{R_I}$: this result is referred as the Wiener-Khintchne theorem in the literature.

Ergodicity

In the following, it will be assumed that the random process I considered is ergodic: it means that the ensemble averages $\langle\rangle$ previously defined can be identified with time averages of the realizations $\mathrm{I}(t)$. It thus comes

$$\begin{cases} \langle \mathrm{I} \rangle = \displaystyle\int_{t=-\infty}^{+\infty} \mathrm{I}(t)\, dt \\ \mathrm{C_I}(\tau) = \displaystyle\int_{t=-\infty}^{+\infty} \mathrm{I}(t+\tau)\,\mathrm{I}(t)\, dt \end{cases}$$

---

[1]WSS is the acronym for "Wide-Sense Stationnary": it refers to a random process whose first and second moments do not vary over differents realizations: $\forall \mathrm{N} \in \mathbb{Z}$
$$\begin{cases} \mathrm{E[I]} = \langle \mathrm{I}(m) \rangle = \langle \mathrm{I}(m+\mathrm{N}) \rangle \\ \mathrm{R[I]} = \langle \mathrm{I}(m)\,\mathrm{I}(n) \rangle = \langle \mathrm{I}(m+\mathrm{N})\,\mathrm{I}(n+\mathrm{N}) \rangle = \langle \mathrm{I}(m-n)\,\mathrm{I}(0) \rangle \end{cases}$$

2   Equilibrium noise (Johnson-Nyquist)

The Johnson-Nyquist states that

$$S_I(f = 0) = 4k\mathrm{T}\,\mathrm{G}$$

It appears that measuring thermal noise does not bring much more information than a conductance measurement: however, it will be shown that the frequency dependence of the equilibrium noise brings much more physics, and help to understand the distinction between emission and absorption. However, most detectors are not sensitive to equilibrium noise: an experimental test of symmetrization thus requires a device with an asymmetric excess noise.

3   Shot noise

The Fano factor is defined as

$$\mathcal{F} = \frac{S_I(f = 0)}{2\,q\,\mathrm{I}}$$

Such measurement can bring interesting informations about the electronic correlations, or signatures of the charge carriers (fractional charges [6][7][37]) as mentionned in the introduction: in the following, we will also focus on the frequency dependence of shot noise, thus trying to understand the meaning of symmetrization.

II   Quantum limit

1   Quantum description of electronical circuits

In this section, the notations usually employed to describe electrical circuits in the quantum regime will be introduced [38]: the goal is to build the tools required to describe the noise properties of mesoscopic devices. We will apply them to modelize

- the high-frequency (HF) emission/absorption properties of an unspecified impedance $Z(\omega)$ (quantum fluctuation-dissipation theorem)

- the interaction of the device under test and our detector, from the quantum mechanical point of view (dynamical Coulomb blockade)

Hamiltonian description of electrical circuits
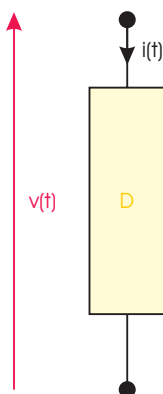
Classically, any electrical dipole can be described by two quantities: voltage $v(t)$ and current $i(t)$. A quantum description of electrical circuits requires to introduce two more quantities, the flux $\phi(t)$ and the charge $q(t)$, defined as

$$\begin{cases} \phi(t) = \displaystyle\int_{-\infty}^{t} v(t')\,\mathrm{d}t' \\[2mm] q(t) = \displaystyle\int_{-\infty}^{t} i(t')\,\mathrm{d}t' \end{cases}$$

Another important quantity is the phase $\varphi = \phi/\phi_0$ where ϕ_0 stands for the flux quantum ($\phi_0 = \hbar/e$).

2   Phase-phase correlation function in the quantum limit

The quantum harmonic oscillator

Let us consider a quantum LC circuit (see figure 2.2-a): this model circuit behaves as a quantum oscillator.
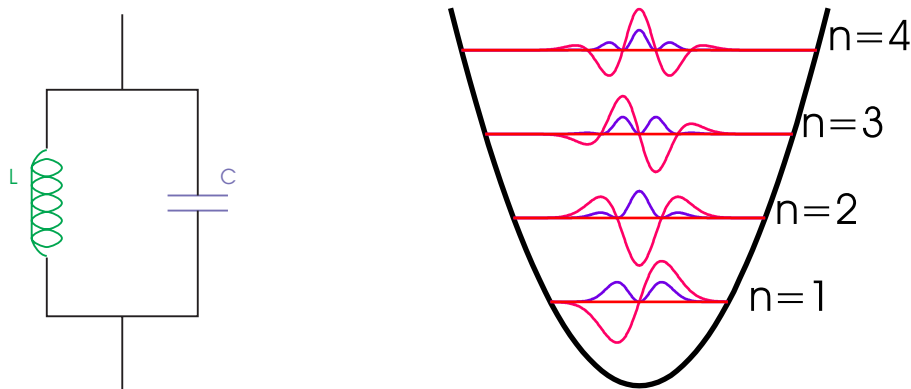
Figure 2.2: (a) - Schematic representation of a quantum harmonic oscillator. (b) - Energy levels of the quantum harmonic oscillator: the wavefunctions $\psi(\varphi)$ and the probability density $|\psi(\varphi)|^2$ of the first four eigenstates are represented.

Its hamiltonian is the sum of potential energy (electric term) and kinetic energy (magnetic term):

$$\mathcal{H}_{\mathrm{LC}} = \frac{(q^{\mathrm{C}})^2}{2\,\mathrm{C}} + \frac{(\phi^{\mathrm{L}})^2}{2\,\mathrm{L}}$$

where q^{C} and ϕ^{L} stand for the charge on the capacitor C, and the flux through the inductance L respectively. These operators obey the following rules, inheritated from their classical counterparts

$$\begin{cases} q_{\mathrm{T}} = q^{\mathrm{C}} + q^{\mathrm{L}} \\ \phi_{\mathrm{T}} = \phi^{\mathrm{C}} = \phi^{\mathrm{L}} \end{cases}$$

From now, we will use the phase φ instead of the flux $\phi = \phi_0 \times \varphi$: this choice is motivated by the fact that our detector is sensitive to phase fluctuations, and it is this quantity which will be relevant later for the modelization of our detection scheme. The hamiltonian can be recast as a combination of creation and anihilation operators (ladder operators a^+ and a)[2]

$$\mathcal{H}_{\mathrm{LC}} = \hbar\omega_0 \left(a^+ a + \frac{1}{2}\right) \qquad \text{with} \qquad \begin{cases} a = \dfrac{\phi_0}{\sqrt{2\,\hbar\,\mathrm{Z}_0}} \left(\varphi^{\mathrm{L}} + \mathrm{i}\,\dfrac{\mathrm{Z}_0}{\phi_0{}^2}\,q^{\mathrm{C}}\right) \\ a^+ = \dfrac{\phi_0}{\sqrt{2\,\hbar\,\mathrm{Z}_0}} \left(\varphi^{\mathrm{L}} - \mathrm{i}\,\dfrac{\mathrm{Z}_0}{\phi_0{}^2}\,q^{\mathrm{C}}\right) \end{cases}$$

where $\omega_0 = 1/\sqrt{\mathrm{LC}}$ and $\mathrm{Z}_0 = \sqrt{\mathrm{L/C}}$. Conversely, the charge and phase operators can be written as a function of these creation/anihilation operators

---

[2]The eigenfunctions in phase representation read

$$\psi_n(\varphi) = \sqrt{\frac{1}{2^n\,n!}} \left(\frac{\phi_0{}^2}{\pi\,\hbar\,\mathrm{Z}_0}\right)^{1/4} \exp\left(-\frac{\phi_0{}^2}{2\,\hbar\,\mathrm{Z}_0}\,\varphi^2\right) \mathrm{H}_n\left(\sqrt{\frac{\phi_0}{\sqrt{\hbar\,\mathrm{Z}_0}}}\,\varphi\right)$$

where H_n stands for the Hermite polynomials.

$$\begin{cases} \varphi^{\mathrm{L}} = \dfrac{1}{\phi_0} \sqrt{\dfrac{\hbar\, Z_0}{2}} \; (a + a^+) \\[4mm] q^{\mathrm{C}} = \dfrac{1}{\mathrm{i}} \sqrt{\dfrac{\hbar}{2\, Z_0}} \; (a - a^+) \end{cases}$$

The phase-phase time correlator thus reads

$$\langle \varphi(t)\, \varphi(t') \rangle = \frac{\hbar\, Z_0}{2\, \phi_0^{\,2}} \left\{ \langle a^+ a \rangle \; \mathrm{e}^{\,\mathrm{i}\,\omega_0(t-t')} + \langle a a^+ \rangle \; \mathrm{e}^{-\mathrm{i}\,\omega_0(t-t')} \right\}$$

Performing a thermal average over all the possible bound eigenstates $|n\rangle$, it comes

$$\langle a^+ a \rangle = \frac{1}{Z_\beta} \sum_n \langle n|\, a^+ a\, \mathrm{e}^{-\beta \mathcal{H}_{\mathrm{LC}}} \,|n\rangle \quad \text{where} \quad Z_\beta = \mathrm{Tr}\left\{ \mathrm{e}^{-\beta \mathcal{H}_{\mathrm{LC}}} \right\} = \sum_n \langle n|\, \mathrm{e}^{-\beta\, \hbar \omega_0 \left(n+\frac{1}{2}\right)} \,|n\rangle$$

The thermal average $\langle a^+ a \rangle$ can be expressed in terms of the thermal factor ${\color{red}\langle n \rangle}$:

$$\langle a^+ a \rangle = \frac{\displaystyle\sum_n n\, \mathrm{e}^{-\beta\, \hbar \omega_0 \left(n+\frac{1}{2}\right)}}{\displaystyle\sum_n \mathrm{e}^{-\beta\, \hbar \omega_0 \left(n+\frac{1}{2}\right)}} = \frac{1}{\mathrm{e}^{\,\beta\, \hbar \omega_0} - 1} = {\color{red}\langle n \rangle}$$

It can be shown that the creation/anihilation operators obey the commutation relation $[a, a^+] = 1$. Consequently, the other thermal average $\langle a a^+ \rangle$ reads

$$\langle a a^+ \rangle = 1 + \langle a^+ a \rangle = 1 + {\color{red}\langle n \rangle}$$

One finally finds out for the emission/absorption spectrum of a quantum harmonic oscillator

$$S_\varphi(\omega) = \int_{-\infty}^{+\infty} \langle \varphi(t)\, \varphi(t') \rangle \, \mathrm{e}^{\,\mathrm{i}\,\omega(t-t')} \, \mathrm{d}t = \frac{\hbar\, Z_0}{2\, \phi_0^{\,2}} \left\{ \underbrace{\delta(\omega + \omega_0)\, {\color{red}\langle n \rangle}}_{\color{blue}\text{Emission}} + \underbrace{\delta(\omega - \omega_0)\, (1 + {\color{red}\langle n \rangle})}_{\color{red}\text{Absorption}} \right\}$$

The first term stands for the emission of the resonator, whereas the second term stands for the absorption. At $T = 0$, the circuit lies in its fundamental state, so $\langle n \rangle = 0$. First of all, we see that even at zero temperature, the oscillator exhibits fluctuations: this is a consequence of Heisenberg uncertainty principle. Moreover, one can see that the spectrum of this device is not symmetric: in its fundamental state, this device can absorb energy from its environment, but it can not emit any photon. This simple example demonstrates why it is necessary to discriminate negative/positive frequencies, *ie.* emission from absorption. At finite temperature ($T \neq 0$), higher energy states are accessible because of thermal activated processes: in this case, the resonator can emit photons and relax to lower energy states: this explains why the emission spectrum is non-zero (indeed, at ($T \neq 0$), $\langle n \rangle \neq 0$), but the spectrum remains non-symmetric. When one reaches the classical limit ($k_{\mathrm{B}} T \geqslant \hbar \omega_0$), $\langle n \rangle \approx \langle n \rangle + 1 \approx k_{\mathrm{B}} T / \hbar \omega_0$: the circuit now absorbs as much as it emits, the zero-point fluctuations being dominated by the thermal fluctuations.

Quantum fluctuation-dissipation theorem. Given the expression of the impedance of an LC oscillator

$$Z_{\mathrm{LC}}(\omega) = \frac{1}{C} \frac{\mathrm{i}\,\omega}{\omega_0^{\,2} - (\omega - \mathrm{i}\varepsilon)^2} \qquad \text{so} \qquad \begin{aligned} \mathrm{Re}\, Z_{\mathrm{LC}}(\omega) &= \frac{\pi}{2\, C} \left[\delta(\omega - \omega_0) + \delta(\omega + \omega_0) \right] \\[2mm] &= \frac{\pi}{2} \left(Z_0\, \omega_0 \right) \left[\delta(\omega - \omega_0) + \delta(\omega + \omega_0) \right] \end{aligned}$$

We thus recover the quantum fluctuation-dissipation theorem for a quantum harmonic oscillator

$$S_\varphi(\omega) = \frac{\mathrm{Re}\ Z_{\mathrm{LC}}(\omega)}{\pi\,R_q}\,\frac{1}{\omega\left[1 - e^{-\beta\,\hbar\omega}\right]}$$

Quantum noise of a resistor

A phenomenological approach   Let us consider now a resistor, of resistance R: it can be modelized by an infinite assembly of LC oscillators (see figure 2.3). Actually, it can be demonstrated that any environment (characterized by its impedance $Z(\omega)$) can be modelized in such a way. At first sight, it seems rather astonishing to model a dissipative circuit element by a set of non-dissipative elements: this paradox is raised when one considers the thermodynamic limit $N \to \infty$. Indeed, in an infinite LC transmission line, the energy is carried by progressive plane waves counterpropagating forward and backward: in the limit $N \to \infty$, a part of this energy propagates towards infinity and appears to be 'lost', which models the dissipation. This approach is often referred as the Caldeira-Leggett model [39].
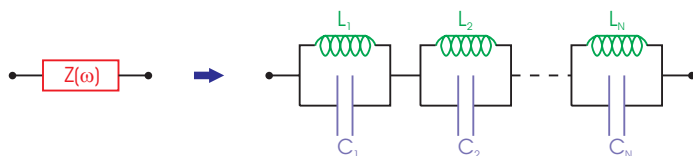
Figure 2.3: Schematic representation of the Caldeira-Leggett model: a linear dissipative element $Z(\omega)$ can be modelized by a set of quantum harmonic oscillators $\{L_k, C_k\}_{k=[1:N]}$, at the thermodynamic limit ($N \to \infty$).

The quantum state of the environment can be described as the tensorial product of the bound eigenstates $|n_k\rangle$ of the oscillators

$$|\mathcal{E}\rangle = \bigotimes_{k=[1:N]} |n_k\rangle$$

The hamiltonian of the environment thus reads

$$\mathcal{H}_{Z(\omega)} = \sum_{k=1}^{N}\left\{\frac{(q^{C_k})^2}{2\,C_k} + \frac{(\varphi^{L_k})^2}{2\,L_k}\right\} = \sum_{k=1}^{N}\hbar\omega_k\left(a_k{}^+a_k + \frac{1}{2}\right)$$

The phase-phase correlation functions $S_{\varphi,\mathrm{LC}}(\omega)$ for each oscillator being linear functions of the real part of the impedances Z_k, their contributions to the phase-phase correlation function of the whole circuit element $Z(\omega)$ add

$$\begin{aligned} S_\varphi(\omega) &= \sum_{k=1}^{N}\left\{\frac{\mathrm{Re}\ Z_k(\omega)}{\pi\,R_q}\,\frac{1}{\omega\left[1 - e^{-\beta\,\hbar\omega}\right]}\right\} \\ &= \frac{\mathrm{Re}\ Z(\omega)}{\pi\,R_q}\,\frac{1}{\omega\left[1 - e^{-\beta\,\hbar\omega}\right]} \end{aligned}$$

Finally, one finds for the current noise spectrum of a linear dissipative element at equilibrium

$$S_{\mathrm{I}}(\omega) = \frac{\mathrm{Re}\ Z^{-1}(\omega)}{\pi}\,\frac{\hbar\omega}{1 - e^{-\beta\,\hbar\omega}}$$

This result is an illustration of the quantum fluctuation-dissipation theorem [11], applied to the case of a linear dissipative electrical circuit. At zero temperature, the noise spectrum reads

$$S_I(\omega) = \frac{\text{Re } Z^{-1}(\omega)}{\pi} \, \hbar\omega \, \Theta(\omega)$$

This result is a manifestation of the zero-point fluctuations (ZPF): as seen for the quantum harmonic oscillator, at zero temperature, there is no emission from the resistor. However, for positive frequencies, one recovers that $S_I(\omega) \propto \omega$. This is the manifestation that a system in its ground state can absorb photons from its environment: the example of the resistor is a generalization of the quantum oscillator, for a system with many modes. At finite temperature, the noise spectrum is rounded by thermal effects, as for the case of the quantum LC circuit.

Quantum and thermal noise. The previous expression of the equilibrium noise can be rewritten in the following way

$$S_I(\omega) = \frac{\text{Re } Z^{-1}(\omega)}{\pi} \left\{ \underbrace{\hbar\omega \, \Theta(\omega)}_{\text{Quantum noise}} + \underbrace{\frac{\hbar \, |\omega|}{e^{\beta \, \hbar|\omega|} - 1}}_{\text{Thermal noise}} \right\}$$

The equilibrium noise is thus composed of two contributions: the so-called quantum noise[3] which originates from vacuum fluctuations (asymmetric component), and thermal noise which is related with thermal fluctuations (symmetric component).

Quantum noise of a resistor. (see figure 2.4)
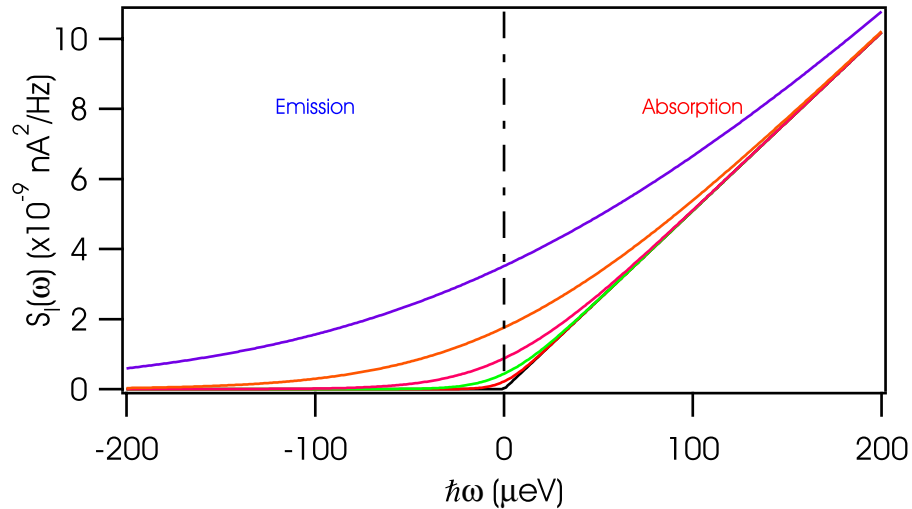

Figure 2.4: Quantum noise of a resistor (R = 1 kΩ) *vs.* ω for different temperatures (T = 0 mK, 50 mK, 100 mK, 200 mK, 400 mK and 800 mK).

---

[3]By extension, in the literature "quantum noise" often refers to the spectral density of noise such as $\hbar\omega > k\text{T}$, and by so does not only refer to zero-point fluctuations.
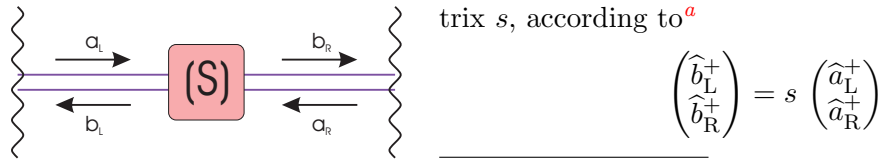
3   Shot noise in the quantum limit

Quantum transport and scattering theory

The scattering theory of shot noise for mesoscopic conductors (without interactions) will be briefly reviewed in this section [40].

2 contacts, 1 channel   Any mesoscopic conductor (by mesoscopic, it is meant fully phase coherent), connected to two leads (let us say L and R), can be described as a set of N channels of transparency $(\mathrm{T}_k)_{k \in [1:\mathrm{N}]}$. Electronic states can be described by fermionic creation/anihilation operators $\widehat{a}_{k,\alpha}, \widehat{a}_{k,\alpha}^+$ and $\widehat{b}_{k,\alpha}, \widehat{b}_{k,\alpha}^+$ ($k \in [1:\mathrm{N}], \alpha = \mathrm{L}, \mathrm{R}$), corresponding respectively to the forward and backward propagation.

These operators are related *via* the scattering matrix s, according to[a]

$$\begin{pmatrix} \widehat{b}_{\mathrm{L}}^+ \\ \widehat{b}_{\mathrm{R}}^+ \end{pmatrix} = s \begin{pmatrix} \widehat{a}_{\mathrm{L}}^+ \\ \widehat{a}_{\mathrm{R}}^+ \end{pmatrix}$$

---

[a]Current conservation imposes the unitarity of this matrix.

Let us consider the current correlation in the left lead for example, of a single channel conductor. The scattering states $\widehat{\psi}_{\mathrm{L}}$ and $\widehat{\psi}_{\mathrm{L}}^+$ can be expressed as

$$\begin{cases} \widehat{\psi}_{\mathrm{L}}(r,t) = \displaystyle\int \frac{\chi_{\mathrm{L}}}{\sqrt{h\,v_{\mathrm{L}}(\mathrm{E})}} \left[\widehat{a}_{\mathrm{L}}(k_x)\mathrm{e}^{-\mathrm{i}\,k_x x} + \widehat{b}_{\mathrm{L}}(k_x)\mathrm{e}^{\mathrm{i}\,k_x x} \right]\,\mathrm{dE} \\ \widehat{\psi}_{\mathrm{L}}^+(r,t) = \displaystyle\int \frac{\chi_{\mathrm{L}}}{\sqrt{h\,v_{\mathrm{L}}(\mathrm{E})}} \left[\widehat{a}_{\mathrm{L}}(k_x)\mathrm{e}^{-\mathrm{i}\,k_x x} + \widehat{b}_{\mathrm{L}}(k_x)\mathrm{e}^{\mathrm{i}\,k_x x} \right]\,\mathrm{dE} \end{cases}$$

The current operator $\widehat{\mathrm{I}}$ in the left lead thus reads

$$\widehat{\mathrm{I}}(x,t) = \frac{e\,\hbar}{2\mathrm{i}\,m} \int_{\mathcal{S}} \left[\frac{\partial \widehat{\psi}_{\mathrm{L}}}{\partial x}(r,t)\widehat{\psi}_{\mathrm{L}}^+(r,t) - \widehat{\psi}_{\mathrm{L}}(r,t)\frac{\partial \widehat{\psi}_{\mathrm{L}}^+}{\partial x}(r,t) \right]\,\mathrm{d}\mathcal{S}$$

With the expression of the scattering states $\widehat{\psi}$ and $\widehat{\psi}^+$ previously written, it comes

$$\widehat{\mathrm{I}}(t) = \frac{2e}{h} \int \left[\widehat{a}_{\mathrm{L}}^+(\mathrm{E})\widehat{a}_{\mathrm{L}}(\mathrm{E}') - \widehat{b}_{\mathrm{L}}^+(\mathrm{E})\widehat{b}_{\mathrm{L}}(\mathrm{E}') \right]\,\mathrm{e}^{\mathrm{i}\,(\mathrm{E}-\mathrm{E}')/\hbar}\,\mathrm{dE}\,\mathrm{dE}'$$

where $\widehat{a}_{\mathrm{L}}(\mathrm{E}) = \dfrac{\widehat{a}(k_x)}{\sqrt{h\,v_{\mathrm{L}}(\mathrm{E})}}$.

It can be noticed that the last expression does not depend on the position x anymore. Introducing the relation between operators $\widehat{a}$ and $\widehat{b}$ by means of the scattering matrix s, it is found that

$$\widehat{\mathrm{I}}(t) = \frac{2e}{h} \int \left\{ \sum_{\alpha,\beta} \widehat{a}_{\alpha}^+(\mathrm{E})\,\mathrm{A}_{\alpha,\beta}(\mathrm{E},\mathrm{E}')\,\widehat{a}_{\beta}(\mathrm{E}') \right\}\,\mathrm{e}^{\mathrm{i}\,(\mathrm{E}-\mathrm{E}')t/\hbar}\,\mathrm{dE}\,\mathrm{dE}'$$

where matrix elements $\mathrm{A}_{\alpha,\beta}$ are related with scattering matrix s through

$$\mathrm{A}_{\alpha,\beta}(\mathrm{L}; \mathrm{E}, \mathrm{E}') = \delta_{\alpha,\mathrm{L}}\delta_{\beta,\mathrm{L}}\,\mathbb{I} - s_{\mathrm{L},\alpha}^{\star}(\mathrm{E})s_{\mathrm{L},\beta}(\mathrm{E}')$$

The Fourier transformed current operator $\widehat{\mathrm{I}}(\omega)$ is straigthforwardly expressed as

$$\widehat{\mathrm{I}}(\omega) = 2e \int \sum_{\alpha,\beta} \widehat{a}_{\alpha}^+(\mathrm{E})\,\mathrm{A}_{\alpha,\beta}(\mathrm{E}, \mathrm{E}+\hbar\omega)\,\widehat{a}_{\beta}(\mathrm{E}+\hbar\omega)$$

The ensemble average of the product of current operators thus reads

$$\left\langle \widehat{I}(\omega)\widehat{I}(\omega') \right\rangle = 2e^2 \int \sum_{\alpha,\beta,\gamma,\delta} A_{\alpha,\beta}(L; E, E + \hbar\omega) A_{\gamma,\delta}(L; E', E' + \hbar\omega')$$

$$\times \left\langle \widehat{a}_\alpha^+(E)\, \widehat{a}_\beta(E + \hbar\omega)\, \widehat{a}_\gamma^+(E')\, \widehat{a}_\delta(E' + \hbar\omega') \right\rangle$$

Finally, the current noise spectral density $S_{LL}(\omega)$ can be expressed as

$$S_{LL}(\omega) = \left\langle \widehat{I}(\omega)\widehat{I}(\omega') \right\rangle \delta(\omega + \omega')$$

$$= \frac{2e^2}{h} \int \sum_{\alpha,\beta} A_{\alpha,\beta}(L; E, E + \hbar\omega) A_{\beta,\alpha}(L; E + \hbar\omega, E)$$

$$\times [f_\alpha(E)(1 - f_\beta(E + \hbar\omega)) + (1 - f_\alpha(E))f_\beta(E + \hbar\omega)]$$

Let us assume the scattering matrix $A(L; E, E')$ is independent of energy (*ie.* $|E - E'| < \hbar\omega_c$). Finally, the current noise spectrum for a quantum conductor with one channel (of transmission T), between two contacts, reads

$$S_{LL}(\omega) = \frac{2e^2}{h} T^2 \frac{2\,\hbar\omega}{1 - e^{-\beta\,\hbar\omega}} + T(1 - T) \left\{ \frac{\hbar\omega + eV}{1 - e^{-\beta(\hbar\omega + eV)}} + \frac{\hbar\omega - eV}{1 - e^{-\beta(\hbar\omega - eV)}} \right\}$$

2 contacts, N channels   The generalization to a conductor with N channels is straightforward

$$S_{LL}(\omega) = \frac{2e^2}{h} \Bigg\{ \sum_n T_n^2 \frac{2\,\hbar\omega}{1 - e^{-\beta\,\hbar\omega}}$$

$$+ \sum_n T_n(1 - T_n) \frac{\hbar\omega + eV}{1 - e^{-\beta(\hbar\omega + eV)}}$$

$$+ \sum_n T_n(1 - T_n) \frac{\hbar\omega - eV}{1 - e^{-\beta(\hbar\omega - eV)}} \Bigg\}$$

At equilibrium ($V = 0$), the quantum fluctuation-dissipation is recovered

$$S_{LL}(\omega) = \frac{2e^2}{h} \left(\sum_n T_n \right) \frac{\hbar\omega}{1 - e^{-\beta\,\hbar\omega}}$$

$$= \frac{G}{\pi} \frac{\hbar\omega}{1 - e^{-\beta\,\hbar\omega}}$$

The Fano factor is defined as

$$\mathcal{F} = \frac{\displaystyle\sum_n T_n(1 - T_n)}{\displaystyle\sum_n T_n}$$

Shot noise: a probe of the inelastic processes

The aim of this section is to show that an intuitive comprehension of the frequency dependence of the noise spectral density $S(\omega)$ can be found: a simple system (a tunnel junction with normal metal electrodes) will be considered, and current correlations will be related to inelastic processes. Again, only the regime without interactions is investigated.

Equilibrium. Let us first consider the equilibrium situation ($V = 0$): following Gavish *et al.* [41][12], the time current-current correlator can be expressed as

$$C(\tau) = \sum_i P_i \langle i | \hat{\jmath}(t + \tau) \hat{\jmath}(t) | i \rangle$$

Introducing another set of eigenstates, by means of the closure relation $\sum_f |f\rangle \langle f|$ and performing a time integration [42], it reads

$$S_I(\omega) = \hbar \sum_{i,f} P_i |\langle f | \hat{\jmath} | i \rangle|^2 \delta(E_i - E_f - \hbar\omega)$$

This relation shows that at equilibrium, the current noise spectral density can be interpretated in terms of inelastic processes: to illustrate this result, let us consider the case of a tunnel junction at equilibrium (see figure 2.5). At zero temperature, there is emission processes, confirming that a system in its ground state cannot emit photons. However, at a given frequency $\hbar\omega$, two sets of absorption processes can be detected. The higher the frequency $\hbar\omega$, the higher the number of available electronic states which contribute to the spectral density, justifying that $S(\omega > 0) \propto \hbar\omega$.
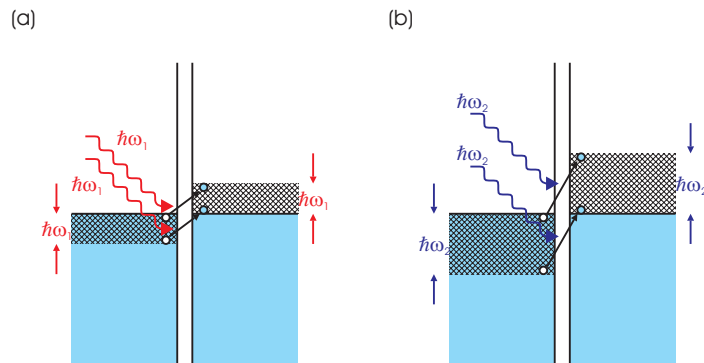
Figure 2.5: **Equilibrium** $V = 0$, $T = 0$. Emission: There is no possible emission processes. Absorption: (a) - $\hbar\omega_1 > 0$. (b) - $\hbar\omega_2 > \hbar\omega_1 > 0$.

Out of equilibrium. This approach can be generalized to the out of equilibrium case: let us consider again a tunnel junction at zero temperature (see figure 2.6). When it is voltage biased, two kinds of inelastic processes add to the equilibrium processes: emission and absorption in a frequency range $0 - eV/h$. The cutoff at eV/h predicted by the scattering theory can be thus understood qualitatively: the junction cannot emit photons of energy higher than provided by the voltage source.
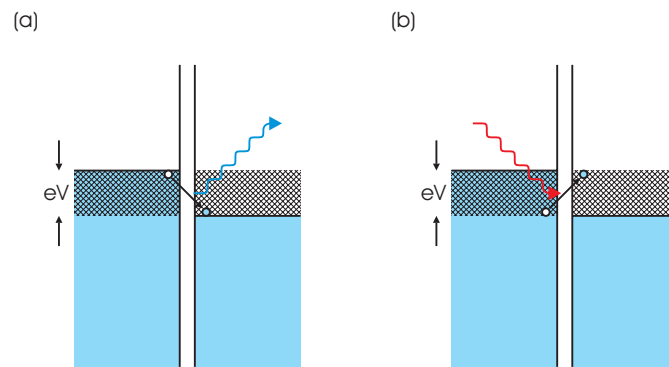
Figure 2.6: **Out of equilibrium,** T = 0. (a) - Emission: . (b) - Absorption: .

Chapter 3

Detection of non-symmetrized noise correlator

I Retrospective on the detection of noise with "classical amplifiers"

There exists a large variety of methods to detect current noise, given the impedance of the device and the range of frequency which has to be probed. The most commonly used will be presented in the following section, in order to motivate the choice for our detection scheme.

1 Low-frequency noise measurements

The most commonly used method to detect current fluctuations at low-frequency relies on cross-correlation technique: the voltage fluctuations across the device under test are amplified by two suposedly independent amplifiers (*ie.* their own noise are supposed to be uncorrelated). By computing the correlation product of their output signal, one can get rid of the contribution of the amplifiers.

Figure 3.1: Detection scheme relying on a cross-correlation technique

2 Finite frequency measurements

The tank-circuit setup

The principle of this detection scheme is to realize a resonant circuit, which selects a range of frequency at the input of the amplifiers (see figure 3.2): the resistance belongs to

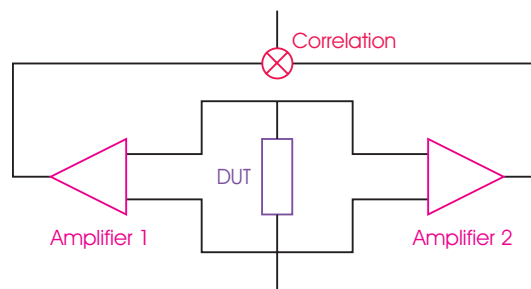the device under study, and the capacitance is provided by the coaxial cables. This kind of setup was used to detect the shot noise associated with fractional charge of Laughlin quasiparticles in the fractional quantum Hall effect [6][37].
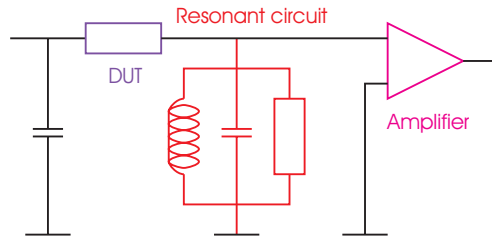

Figure 3.2: Detection scheme relying on a dissipative resonant circuit

Quantum noise measurements

A few examples of such experiments have been reviewed in the introduction.

II   Detection of quantum noise with a quantum detector: "on-chip" coupling

Different detection schemes based on quantum devices will be reviewed in this section: we will see why this class of detectors appear promising to solve the issue of time symmetrization of the noise correlators. Most of these proposals were motivated by the issue of the detection of the zero-point fluctuations (quantum noise): in a first time we will focus on this approach, and then we will consider the possibility to detect excess noise (which corresponds to the added noise induced by applying an external force to the system under study, typically a voltage or current bias in the present case).

The detection of zero-point fluctuations (ZPF) is a difficult task: most of the time, ZPF manifest themselves in an undirect way. Let us cite a few examples:

- **Casimir effect:** In 1948, Casimir predicted that two parallel conducting plates (electrically neutral) experienced an attractive force between them [43]: this attraction is related to the zero-point fluctutations of the electromangetic field between the plates. This prediction has been tested experimentally with a high accuracy [44][45].

- **Lamb shift:** [46] [47]

- Liquid state of helium in the very low temperature limit (T → 0 K).

- **Dynamical Coulomb blockade:** (this point will be extensively developped in the following)

It appears easier to observe manifestations of the ZPF, rather than detecting them directly. Do systems like quantum electrical circuits provide a possibility to detect these fluctuations? The other issue is related to the time symmetrization: as mentionned above, ZPF present a strong asymmetry between negative/positive frequencies, which could allow to answer if symmetrization is relevant. Let us review now different approaches to couple a given conductor to a "quantum" detector.

1   Detection of finite frequency current fluctuations with a quantum resonant circuit

Reference [48] has considered the possibility of detecting finite-frequency current fluctuations in the quantum regime by means of a quantum resonant circuit, inductively coupled to the device under test (DUT). We will try to give a qualitative understanding of this detection scheme.
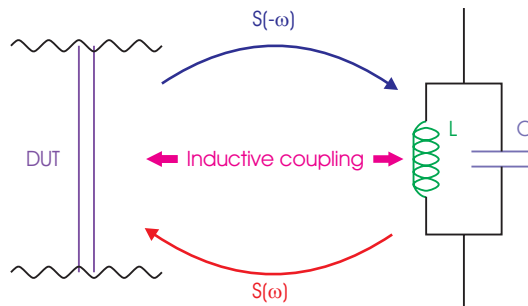

Figure 3.3: Detection scheme proposed by Lesovik *et al.* [48]: it relies on an inductive coupling between the device under test and a quantum harmonic oscillator.

In interaction representation, at first order in perturbation theory

$$\left\langle \varphi^2(0) \right\rangle = (\mathrm{i}\,\alpha)^2 \int_{-\infty}^{0} \mathrm{d}t_1 \int_{-\infty}^{t_1} \mathrm{d}t_2 \mathrm{e}^{\,\eta(t_1+t_2)} \left\langle \left[\left[\varphi^2(0), \varphi(t_1)\dot{\mathrm{I}}(t_1) \right], \varphi(t_2)\dot{\mathrm{I}}(t_2) \right] \right\rangle \Big|_{\eta \to 0}$$

where α stands for the mutual inductance between the conductor and the quantum harmonic oscillator. It was shown in [48], that the measurable signal reads[1]

$$\left\langle \varphi^2(0) \right\rangle = \mathrm{K} \left\{ \mathrm{S}(-\omega_0) + \langle n \rangle \left[\mathrm{S}(-\omega_0) - \mathrm{S}(\omega_0) \right] \right\}$$

Presented this way, this result shows that it is impossible to detect zero-point fluctuations at zero temperature: indeed, as the LC oscillator lies in its fundamental state, it can only be excited by the photons emitted by the quantum conductor under test, but there is no way to detect absorbed photons. However, from the point of detection theory, it is interesting to recast this expression in the following form

$$\left\langle \varphi^2(0) \right\rangle \propto \int_{-\infty}^{+\infty} \mathrm{S}(\omega)\mathrm{S}_{\mathrm{LC}}(-\omega)\mathrm{d}\omega$$

It appears that in the perturbative limit (weak coupling regime), the detected signal results from a rectification effect of the emission/absorption of the device under test: the "negative" frequencies (emission) of the DUT are rectified by the "positive" frequencies of the detector (absorption), and conversely the "positive" frequencies (absorption) of the DUT are rectified by the "negative" frequencies of the detector (emission). This rectification effect can be formulated in such a simple way until one restricts oneself to weak coupling: for stronger coupling, many photon processes will intervene, and the contribution of the HF emission/absorption properties of the DUT to the static phase fluctuations across the detector will be more intricate. This detection scheme can be extended to the detection of finite-frequency current cross-correlations [49][50].

---

[1]This 2nd order contribution adds to the 0th order term of the static phase fluctuations

$$\left\langle \varphi^2(0) \right\rangle = \frac{\mathrm{Z}_0}{\mathrm{R}_q} \left(\langle n \rangle + \frac{1}{2} \right) \quad \text{where } \mathrm{Z}_0 = \sqrt{\frac{\mathrm{L}}{\mathrm{C}}}$$

2   Detection of finite-frequency current fluctuations with a two-level system (TLS)

Another approach to detect current fluctuations is to couple the device under test to a coherent two-level system, described by the Pauli matrices $\{\sigma_x, \sigma_y, \sigma_z\}$[2] [51] (see figure 3.4).
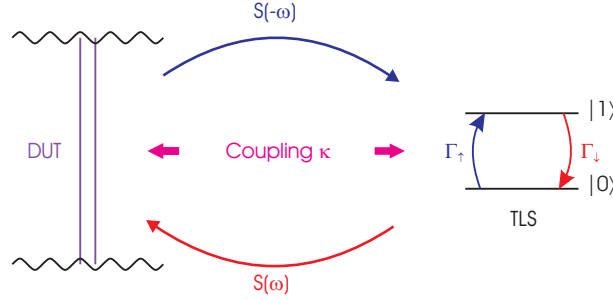

Figure 3.4: Schematic representation of the coupling between a quantum conductor (noise source), and a TLS (detector): parameter κ characterizes the strength of the coupling between them.

The hamiltonian of the whole system thus reads

$$\mathcal{H} = \underbrace{-\frac{\hbar\omega_{01}}{2}\,\sigma_{\mathrm{z}}}_{\text{TLS}} + \underbrace{\sum_{k=1}^{\mathrm{N}}\left\{\frac{(q^{\mathrm{C}_k})^2}{2\,\mathrm{C}_k} + \frac{(\varphi^{\mathrm{L}_k})^2}{2\,\mathrm{L}_k}\right\}}_{\text{Environment }\mathrm{Z}(\omega)} + \underbrace{\kappa\,\mathrm{I}(t)\,\sigma_{\mathrm{x}}}_{\text{Coupling}}$$

It can be shown that the excitation/relaxation rates are related to the noise properties of the environment [51], according to

$$\begin{cases}\Gamma_{\uparrow} = \dfrac{\kappa^2}{\hbar^2}\,\mathrm{S_I}(-\omega_{01}) \\[2mm] \Gamma_{\downarrow} = \dfrac{\kappa^2}{\hbar^2}\,\mathrm{S_I}(+\omega_{01})\end{cases}$$

This detection scheme was implemented by Astafiev *et al.*, using a Cooper pair box (CPB) as a coherent two-level system [19]: however, it seems that the sensitivity of qubits as spectrometers is limited by the coupling with TLS. According to whether the qubits is coupled longitudinally or transversally with an assembly of TLS, it exhibits dephasing ($1/f$ noise) or relaxation/excitation.

III   Detection and theory of environment

1   Dynamical Coulomb blockade and $\mathrm{P}(\varepsilon)$ theory

The aim of this section is to briefly review the dynamical Coulomb blockade theory [52]: a review can be found in [53]. This quantum mechanical description of the interaction of a given mesoscopic device and its environment, will be useful to quantitatively understand our experimental results. The importance of working with non-symmetrized correlators

---

[2]The Pauli matrices read
$$\sigma_x = \begin{pmatrix} 0 & 1 \\ 1 & 0 \end{pmatrix} \quad \sigma_y = \begin{pmatrix} 0 & -\mathrm{i} \\ \mathrm{i} & 0 \end{pmatrix} \quad \sigma_z = \begin{pmatrix} 1 & 0 \\ 0 & -1 \end{pmatrix}$$

will be emphasized: it will be shown that, in the limit of moderately resistive environments, dynamical Coulomb blockade acts as a rectification effect of the emission/absorption properties of mesoscopic systems by their environment, justifying the need to work with non-symmetrized quantities.
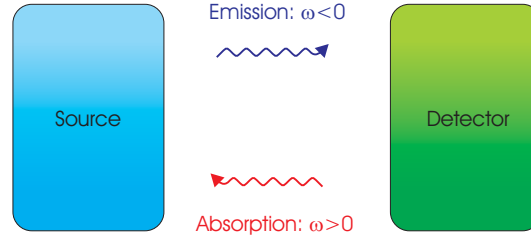
Figure 3.5: Energy exchange between the source and the detector.
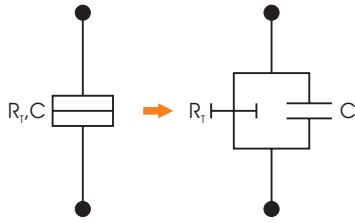
Let us consider a tunnel junction with normal metal electrodes: the progress in nanofabrication allows to realize junctions of submicronic dimensions. The geometric capacitance of such junctions appear to be not negligible, which imply strong charging effects (often referred as Coulomb blockade). In this limit, the junction can be represented as a tunnel element R_T, in parallel with a capacitance C (see opposite figure).

2   Tunneling hamiltonian and effect of the environment

For the sake of simplicity, we will first consider a tunnel junction with normal electrodes (NIN junction), embedded in an electromagnetic environment $Z_{env}(\omega)$ (see figure 3.6).
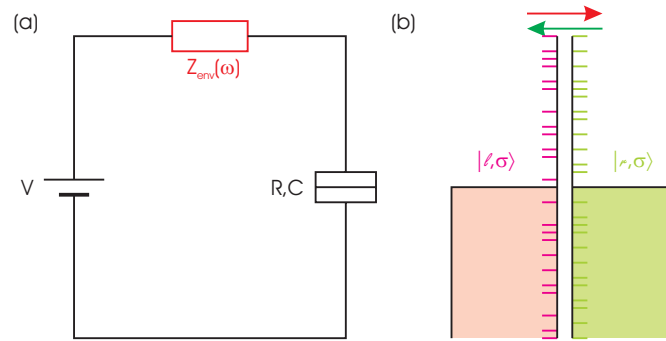
Figure 3.6: (a) - Schematic representation of the normal tunnel junction (NIN) coupled to its environment $Z_{env}(\omega)$. (b) - Representation of the electronic states of the junction.

Let us first consider two limits

- $|\mathbf{Z}(\omega)| \to \mathbf{0}$ This limit corresponds to an ideal voltage bias of the junction: the evolution of the phase φ is imposed by the voltage source. Consequently, there is no phase fluctuation across the junction, *ie.* no inelastic tunneling of quasiparticles.

- $|\mathbf{Z}(\omega)| \rightarrow \infty$ Conversely, in this regime the junction is ideally current biased: the current source imposes the evolution of the quasicharge q.

To explore the intermediate regimes (unspecified $Z(\omega)$), we need to describe the interaction between the electronic modes of the junction and the electromagnetic modes of its surrounding environment. The hamiltonian of the electrical circuit described above is the sum of three terms:

- the first one describes the quasiparticles in the left and right electrodes respectively

$$\mathcal{H}_{\mathrm{qp}} = \mathcal{H}_{\mathrm{L}} + \mathcal{H}_{\mathrm{R}} = \sum_{\ell,\sigma} \varepsilon_\ell c^+_{\ell,\sigma} c_{\ell,\sigma} + \sum_{r,\sigma} \varepsilon_r c^+_{r,\sigma} c_{r,\sigma}$$

- the second one corresponds to the tunneling hamiltonian

$$\mathcal{H}_{\mathrm{T}} = \mathcal{H}^+_{\mathrm{T}} + \mathcal{H}^-_{\mathrm{T}} = \sum_{\ell,r,\sigma} \left\{ \mathrm{T}_{\ell r} c^+_{\ell,\sigma} c_{r,\sigma}\, \mathrm{e}^{-\mathrm{i}\varphi} + \mathrm{T}^\star_{\ell r} c^+_{r,\sigma} c_{\ell,\sigma}\, \mathrm{e}^{\mathrm{i}\varphi} \right\}$$

- the third one accounts for the environment $Z(\omega)$ (in the frame of the Caldeira-Leggett approach)

$$\mathcal{H}_{\mathrm{env}} = \sum_{k=1}^{\mathrm{N}} \left\{ \frac{(q^{\mathrm{C}_k})^2}{2\,\mathrm{C}_k} + \frac{(\varphi^{\mathrm{L}_k})^2}{2\,\mathrm{L}_k} \right\}$$

The coupling of the electromagnetic modes of the environment to the electronic modes of the junction is described by means of the phase term $\mathrm{e}^{-\mathrm{i}\varphi}$ in the tunneling hamiltonian: this term can be understood qualitatively as a translation operator in the quasicharge space

$$\mathrm{e}^{\mathrm{i}\varphi}\, q\, \mathrm{e}^{-\mathrm{i}\varphi} = q - e$$

The main steps of the demonstration will be briefly reviewed (see appendix for details): the coupling to the environment will be taken into account *via* the time correlator of the phase fluctuations across the junction (induced by the external circuit). Later, we will see that similarly to what was found for the quantum harmonic oscillator or the TLS, in the perturbative regime (limit of weak coupling), the effect of the phase noise of the device under test (here $Z(\omega)$) on the detector (here the NIN junction) can be understood as a rectification effect of the emission/absorption properties of the DUT by the emission/absorption properties of the detector. This way, it will appear very intuitively that the relevant quantities are the nonsymmetrized time correlators.

It can be shown that the forward tunneling rate can be expressed as[3]

$$\overrightarrow{\Gamma}(\mathrm{V}) = \frac{1}{e^2\,\mathrm{R}_{\mathrm{T}}} \int_{-\infty}^{+\infty} f(\mathrm{E}) \left[1 - f(\mathrm{E}') \right]$$
$$\times \left\{ \int_{-\infty}^{+\infty} \frac{1}{2\pi\,\hbar}\, \mathrm{e}^{\mathrm{i}\,(\mathrm{E}-\mathrm{E}'+e\mathrm{V})t/\hbar} \left\langle \mathrm{e}^{\mathrm{i}\,\delta\varphi(t)} \mathrm{e}^{-\mathrm{i}\,\delta\varphi(0)} \right\rangle \mathrm{d}t \right\} \mathrm{d}\mathrm{E}\,\mathrm{d}\mathrm{E}'$$

Assuming Gaussian fluctuations, the phase-phase correlation function can be simplified according to Wick theorem so as to one finds

---

[3] $f(\mathrm{E})$ stands for the Fermi-Dirac distribution

$$f(\mathrm{E}) = \frac{1}{1 + \mathrm{e}^{\beta\mathrm{E}}} \quad \text{where} \quad \beta = (k\mathrm{T})^{-1}$$

$$\left\langle e^{i\,\delta\varphi(t)} e^{-i\,\delta\varphi(0)} \right\rangle = e^{\langle [\delta\varphi(t) - \delta\varphi(0)] \delta\varphi(0) \rangle} = e^{J(t)} \quad \text{where} \quad J(t) = \langle [\delta\varphi(t) - \delta\varphi(0)]\, \delta\varphi(0) \rangle$$

Given that $\delta\varphi \propto \int \delta V_D$, it reads

$$\langle \delta\varphi(t)\delta\varphi(0) \rangle = \frac{e^2}{\hbar^2} \int^t dt' \int^0 dt'' \, \langle \delta V_D(t') \delta V_D(t'') \rangle$$

The probability to exchange an amount of energy ε with the environment is related to the phase-phase correlator through

$$P(\varepsilon) = \frac{1}{2\pi\,\hbar} \int_{-\infty}^{+\infty} \exp\left\{ J(t) + i\frac{\varepsilon\,t}{\hbar} \right\} \, dt$$

The forward tunneling rate thus reads

$$\overrightarrow{\Gamma}(V) = \frac{1}{e^2\, R_T} \int_{-\infty}^{+\infty} \frac{E}{1 - e^{-\beta E}} \, P(eV - E) \, dE$$

Finally, the $I(V)$ characteristic of a normal tunnel junction (NIN) coupled to an unspecified electromagnetic environment $Z(\omega)$ can be expressed as a function of the energy exchange probability law $P(E)$

$$I(V) = \frac{1}{e\, R_T} \int_{-\infty}^{+\infty} E \, \frac{1 - e^{-\beta eV}}{1 - e^{-\beta E}} \, P(eV - E) \, dE$$

3 Two simple examples of electromagnetic environments: the quantum harmonic oscillator and an unspecified impedance $Z_{env}(\omega)$

Tunnel junction coupled to a single mode

The aim of this section is to show that a weak coupling is required to distinguish emission/absorption processes: let us consider a single mode circuit element (a quantum harmonic oscillator) coupled to the tunnel junction. In the following, we will recover the expression for the $P(\varepsilon)$ law established in [53]: nevertheless, the following calculation is performed keeping the distinction between emission/absorption terms explicit, thus skipping a tricky Jacobi-Anger expansion. The phase-phase correlation function for a quantum LC circuit has already been calculated earlier in this manuscript. Finally, $J(t)$ reads

$$\begin{aligned}
J(t) &= \int_{-\infty}^{+\infty} \frac{d\omega}{\omega} \frac{\text{Re } Z_{LC}(\omega)}{R_q} \frac{e^{-i\omega t} - 1}{1 - e^{-\beta\,\hbar\omega}} \\
&= \underbrace{\rho_e \left(e^{i\omega_0 t} - 1 \right)}_{\rho_e = \rho\,\langle n \rangle} + \underbrace{\rho_a \left(e^{-i\omega_0 t} - 1 \right)}_{\rho_a = \rho\,(1 + \langle n \rangle)}
\end{aligned}$$

where $\rho = E_c / \hbar\omega$ is the ratio between the charging energy $E_c = e^2/2C$, and the eigenstates excitation energy $\hbar\omega_0$. Let us now calculate the $P(\varepsilon)$ probability law

$$\begin{aligned}
P(\varepsilon) &= \frac{1}{2\pi\,\hbar} \int_{-\infty}^{+\infty} \exp\left\{ J(t) + i\frac{\varepsilon\,t}{\hbar} \right\} \, dt \\
&= \frac{1}{2\pi\,\hbar} \int_{-\infty}^{+\infty} \exp\left\{ \rho_e \left(e^{i\omega_0 t} - 1 \right) + \rho_a \left(e^{-i\omega_0 t} - 1 \right) + i\frac{\varepsilon\,t}{\hbar} \right\} \, dt \\
P(\varepsilon) &= \frac{e^{-(\rho_e + \rho_a)}}{2\pi\,\hbar} \int_{-\infty}^{+\infty} \exp\left\{ \rho_e\, e^{i\omega_0 t} + \rho_a\, e^{-i\omega_0 t} + i\frac{\varepsilon\,t}{\hbar} \right\} \, dt
\end{aligned}$$

Introducing the expression of $x \mapsto e^x$ as an infinite power series, one finds

$$\mathrm{P}(\varepsilon) = \frac{\mathrm{e}^{-(\rho_\mathrm{e}+\rho_\mathrm{a})}}{2\pi\,\hbar} \int_{-\infty}^{+\infty} \exp\left(\rho_\mathrm{e}\,\mathrm{e}^{\mathrm{i}\,\omega_0 t}\right) \times \exp\left(\rho_\mathrm{a}\,\mathrm{e}^{-\mathrm{i}\,\omega_0 t}\right)\,\mathrm{e}^{\mathrm{i}\,\varepsilon\,t/\hbar}\,\mathrm{d}t$$

$$= \frac{\mathrm{e}^{-(\rho_\mathrm{e}+\rho_\mathrm{a})}}{2\pi\,\hbar} \int_{-\infty}^{+\infty} \left(\sum_m \frac{{\rho_\mathrm{e}}^m}{m!}\mathrm{e}^{\mathrm{i}\,m\omega_0 t}\right) \left(\sum_n \frac{{\rho_\mathrm{a}}^n}{n!}\mathrm{e}^{-\mathrm{i}\,n\omega_0 t}\right)\,\mathrm{e}^{\mathrm{i}\,\varepsilon\,t/\hbar}\,\mathrm{d}t$$

$$\mathrm{P}(\varepsilon) = \frac{\mathrm{e}^{-(\rho_\mathrm{e}+\rho_\mathrm{a})}}{2\pi\,\hbar} \sum_{m,n} \frac{{\rho_\mathrm{e}}^m {\rho_\mathrm{a}}^n}{m!n!} \int_{-\infty}^{+\infty} \mathrm{e}^{\mathrm{i}\,[\varepsilon-(n-m)\hbar\omega_0]t/\hbar}\,\mathrm{d}t$$

After performing the Fourier transform, it finally comes

$$\mathrm{P}(\varepsilon) = \mathrm{e}^{-(\rho_\mathrm{e}+\rho_\mathrm{a})} \sum_{m,n} \frac{{\rho_\mathrm{e}}^m {\rho_\mathrm{a}}^n}{m!n!}\,\delta(\varepsilon-(n-m)\,\hbar\omega_0) \quad \text{where} \quad \begin{cases} \rho_\mathrm{e} = \rho\,\langle n\rangle \\ \rho_\mathrm{a} = \rho\,(1+\langle n\rangle) \end{cases}$$

This result can be understood intuitively: if the emission/absorption processes are in-dependant, one expects $\mathrm{P}(\varepsilon)$ to obey a Poissonian distribution. The probability for the junction to simultaneously absorb m quanta emitted/emit n quanta absorbed by the har-monic oscillator thus reads

$$p(n,m) = \frac{\mathrm{e}^{-(\rho_\mathrm{e}+\rho_\mathrm{a})}\,{\rho_\mathrm{e}}^m {\rho_\mathrm{a}}^n}{m!n!}$$

From the point of view of the detection, it is interesting to see that these multiphoton processes complicate the interpretation of the dynamical Coulomb blockade because they mix both emission and absorption. In the following, we will see that in order to distinguish negative/positive frequencies, weak coupling between source and detector is required: the choice of the coupling will be a compromise between the sensitivity of the detection scheme and the requirement to avoid multiphoton processes.

Tunnel junction coupled to an unspecified electromagnetic environment $\mathrm{Z_{env}}(\omega)$

Since the quantum fluctuation-dissipation theorem has been established earlier in this manuscript, at equilibrium $\mathrm{J}(t)$ straightforwardly reads[4]

$$\mathrm{J}(t) = \int_{-\infty}^{+\infty} \frac{\mathrm{d}\omega}{\omega} \frac{\mathrm{Re}\,\mathrm{Z_e}(\omega)}{\mathrm{R}_q} \frac{\mathrm{e}^{-\mathrm{i}\,\omega t}-1}{1-\mathrm{e}^{-\beta\,\hbar\omega}} \quad \text{where} \quad \mathrm{Z_e}(\omega) = \frac{1}{\mathrm{i}\mathrm{C}\omega + \mathrm{Z_{env}^{-1}}(\omega)}$$

This expression can be generalized to the non-equilibrium case, by introducing the voltage noise spectral density $\mathrm{S_{V,env}}(\omega)$ of the environment

$$\mathrm{J}(t) = \frac{2\pi}{\hbar\,\mathrm{R}_q} \int_{-\infty}^{+\infty} \frac{\mathrm{S_{V,env}}(\omega)}{\omega^2} \left(\mathrm{e}^{-\mathrm{i}\,\omega t}-1\right)\,\mathrm{d}\omega$$

4   Intuitive approach of the dynamical Coulomb blockade: a rectification effect of the emission/absorption properties of mesoscopic systems by their environment

The aim of this section is to demonstrate that in order to realize a frequency resolved detection, a weak coupling between the source and the detector is required.

---

[4]Beware that the following expression

$$\mathrm{J}(t) = \int_{0}^{+\infty} \frac{\mathrm{d}\omega}{\omega} \frac{\mathrm{Re}\,\mathrm{Z}(\omega)}{\mathrm{R}_q} \frac{\mathrm{e}^{-\mathrm{i}\,\omega t}-1}{1-\mathrm{e}^{-\beta\,\hbar\omega}}$$

found in some references, only accounts for the absorption processes and is thus valid only at $\mathrm{T}=0$ K.

Low impedance environment $(\mathrm{J(t)} \ll 1)$

Let us consider now a low impedance environment, which means that the condition Re $\mathrm{Z}(\omega) <$ R_q must be fulfilled: one can assume that $\mathrm{J}(t) \ll 1$, and consequently

$$\exp[\mathrm{J}(t)] \approx 1 + \mathrm{J}(t)$$

Under such condition, the probability $\mathrm{P}(\varepsilon)$ to exchange energy with the environment reads (see appendix for details)

$$
\begin{aligned}
\mathrm{P}(\varepsilon) &= \frac{1}{2\pi\,\hbar} \int_{-\infty}^{+\infty} (1 + \mathrm{J}(t))\,\exp\left(\mathrm{i}\frac{\varepsilon t}{\hbar}\right)\,\mathrm{d}t \\
&= \underbrace{\left[1 - \frac{2\pi}{\hbar\,\mathrm{R}_q}\int_{-\infty}^{+\infty}\frac{\mathrm{S_{V,env}}(\omega)}{\omega^2}\,\mathrm{d}\omega\right]\delta(\varepsilon)}_{\text{Renormalized elastic processes}} + \underbrace{\frac{2\pi}{\mathrm{R}_q}\frac{\mathrm{S_{V,env}}(-\varepsilon/\hbar)}{\varepsilon^2}}_{\text{Inelastic processes}}
\end{aligned}
$$

The first term accounts for the renormalization of the elastic tunneling processes by the coupling to the environment, whereas the second term models the inelastic processes. Writing $\mathrm{P}(\varepsilon)$ this way helps to understand qualitatively the underlying physical phenomena involved in dynamical Coulomb blockade: a low impedance environment corresponds to a situation close to an ideally voltage biased junction, which means that phase fluctuations across the tunnel junction are quite small. This justifies the assumption $\exp[\mathrm{J}(t)] \approx 1+\mathrm{J}(t)$, which is equivalent to neglect multiphotons processes. In this regime, dynamical Coulomb blockade can be understood as a simple rectification effect by the environment of the photons emitted/absorbed by the device under test (here a tunnel junction).

Unspecified $\mathbf{J(t)}$

In the more general case of an unspecified environment $\mathrm{Z}(\omega)$, one has to deal with the expansion

$$\exp \mathrm{J}(t) = 1 + \sum_{n>0}\frac{[\mathrm{J}(t)]^n}{n!}$$

Without going further into details, one can qualitatively understand the meaning of this expansion as multiphoton processes: the case of the LC oscillator was interesting, because as there was only one mode, $\mathrm{P}(\varepsilon)$ could be written straightforwardly. For an unspecified environment, given that we deal with an infinite set of modes, $\mathrm{P}(\varepsilon)$ theory becomes more complex.

Similar theory in mesoscopic physics

The dephasing rate for a particle coupled to an environment reads

$$\frac{1}{\tau_\varphi} = \frac{1}{\hbar^2\,(2\pi)^3\,\mathrm{V}}\int \mathrm{d}\overrightarrow{q}\int_{-\infty}^{+\infty}\mathrm{d}\omega\,\left|\mathrm{V}_{\overrightarrow{q}}\right|^2\,\mathrm{S_{part}}(-\overrightarrow{q},\omega)\,\mathrm{S_{env}}(\overrightarrow{q},\omega)$$

Similarly to the DCB theory, this approach of the coupling of a quasiparticle to an electromagnetic environment allows to interpretate dephasing as a rectification effect.

5 Experimental setup: capacitive coupling

The detection scheme relies on a capacitive coupling between the device under test (the source), and the detector circuit: this circuit has been suggested by Aguado and Kouwenhoven [22], in order to probe the non-symmetrized noise correlator of a given mesoscopic

device. In order to avoid that the high-frequency signal 'escapes' in the leads, one requires additionnal on-chip resistances: it will be shown later that these resistances determine the amplitude of the coupling between the source and the detector.
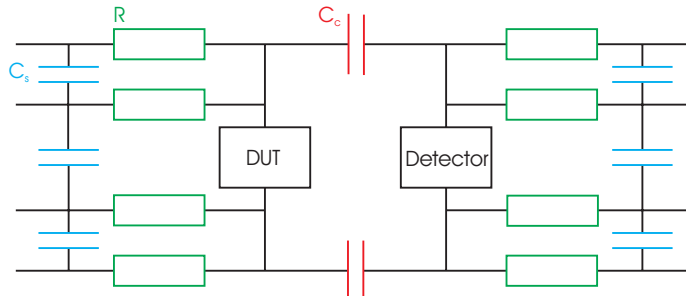

Figure 3.7: Principle of the detection: capacitive coupling between the device under test and the detector.

IV   Detection and photo-assisted tunneling in a SIS junction

1   Choice for the detector: the SIS junction

It remains to choose the appropriate device to play the role of the detector: one can ask which fundamental property should have a 'good' detector? Until now, it is hard to give a criterion to define how acurate is this choice, however one can argue it should be non linear: indeed, since detection relies on a rectifying effect of the emission/absorption properties of the detector, a quantum detector can distinguish emission/absorption if it can be biased in such a way that it only absorbs/emits in the frequency range of interest. It is clear that a gap, and thus non-linearity is required for a good quantum detector[5]. Aguado and Kouwenhoven proposed to use a double dot, an experiment recently implemented by Gustavsson *et al.* [23]. In this case, the non-linearity is given by the Coulomb blockade. Another highly non-linear device, frequently used in mesoscopic physics is the SIS junction: in order to precise the vocabulary used in this thesis, a SIS junction is a Josephson junction which Josephson coupling has been cancelled. SIS junctions have been widely used in the field of radioastronomy, as mixers. In our case, the non-linearity is used in a slightly different way: actually, we use the gap of the superconductor to detect the high frequency photons emitted by the source.

2   SIS junctions and photo-assisted tunneling

Description

A SIS junction is a Josephson junction which supercurrent has been cancelled. In practice, a SQUID geometry can be used in order to tune the effective Josephson coupling of the whole system to zero, by means of a magnetic field: that is the reason why the two capacitively coupled junctions of our device are designed in this SQUID geometry (with

---

[5]In the frame of DCB theory, NIN junction seemed to be sensitive to emission/absorption: but as its excess noise spectrum is symmetric, there is no way to distinguish emission/absorption.

incommensurate areas). One can thus turn one of the two junctions into a SIS junction, independently from the other: this will allow to use one of them as a detector (SIS junction), and the other as a source (Josephson junction).

General transport properties

Without irradiation, the $I(V)$ characteristic of a SIS junction is determined by the BCS density of states $\mathcal{N}_{\mathrm{S}}(\mathrm{E})$[6]

$$\mathrm{I}_{\mathrm{qp},0}(\mathrm{V}) = \frac{1}{e\,\mathrm{R}_{\mathrm{T}}} \int_{-\infty}^{+\infty} \frac{\mathcal{N}_{\mathrm{S}}(\mathrm{E})\,\mathcal{N}_{\mathrm{S}}(\mathrm{E}+e\mathrm{V})}{\mathcal{N}(0)^2} \left[f(\mathrm{E}) - f(\mathrm{E}+e\mathrm{V})\right]\,\mathrm{dE}$$

It can be shown, after integration, that it reads

$$\mathrm{I}_{\mathrm{qp},0}(\mathrm{V}) = \begin{cases} \dfrac{\mathrm{V}}{\mathrm{R}_{\mathrm{T}}} \left\{ \mathrm{E}\left(\sqrt{1 - \left|\dfrac{2\Delta}{e\mathrm{V}}\right|^2}\right) - 2\left|\dfrac{\Delta}{e\mathrm{V}}\right|^2 \mathrm{K}\left(\sqrt{1 - \left|\dfrac{2\Delta}{e\mathrm{V}}\right|^2}\right) \right\} & \text{if } |e\mathrm{V}| > 2\Delta \\[4mm] 0 & \text{if } |e\mathrm{V}| < 2\Delta \end{cases}$$

where Δ stand for the superconducting gap, and R the normal state resistance of the junction. Functions K and E are complete elliptic integrals of the first and second kind respectively[7].

Photo-assisted tunneling

Under irradiation, whether the SIS junction is voltage biased below or above the gap, two different scenarios are possible

- $e\mathrm{V}_{\mathrm{D}} < 2\Delta$**:** this situation corresponds to the subgap regime (infinite DC resistance in theory). In the so-called 'semiconductor representation', one can clearly see that no quasiparticles can tunnel from one electrode to the other (see figure 3.8-a): however, under HF irradiation, quasiparticles can absorb photons of energy $\hbar\omega = (2\Delta - e\mathrm{V}_{\mathrm{D}})$, which gives them enough energy to tunnel through the tunnel barrier (see mechanism on figure 3.8-a). This leads to the appearance of a small step of photo-assisted tunneling (PAT) current, which corresponds to photons emitted by the device under test (absorbed by the junction).

- $e\mathrm{V}_{\mathrm{D}} > 2\Delta$**:** in this case, there is a quasiparticle current (quasiparticle branch). Conversely, quasiparticles can relax and emit photons of energy $\hbar\omega = (e\mathrm{V}_{\mathrm{D}} - 2\Delta)$, while tunneling (these photons being absorbed by the device coupled to the SIS junction: see mechanism on figure 3.8-b). Consequently, the quasiparticle current is decreased, leading to a 'negative' step corresponding to the absorption of the device under test.

---

[6] $\dfrac{\mathcal{N}_{\mathrm{S}}(\mathrm{E})}{\mathcal{N}(0)} = \begin{cases} \dfrac{|\mathrm{E}|}{\sqrt{\mathrm{E}^2 - \Delta^2}} & \text{if } |\mathrm{E}| > \Delta \\[2mm] 0 & \text{if } |\mathrm{E}| < \Delta \end{cases}$

[7] $\begin{cases} \mathrm{K}(x) = \displaystyle\int_{\theta=0}^{\pi/2} \sqrt{1 - x^2\,\sin^2\theta}\,\mathrm{d}\theta \\[4mm] \mathrm{E}(x) = \displaystyle\int_{\theta=0}^{\pi/2} \dfrac{1}{\sqrt{1 - x^2\,\sin^2\theta}}\,\mathrm{d}\theta \end{cases}$

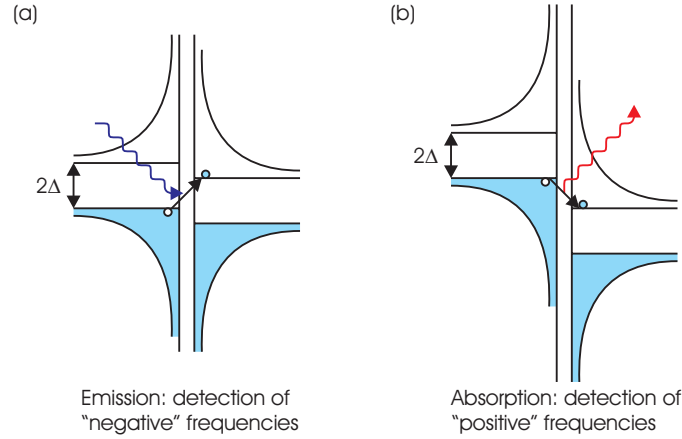Figure 3.8: (a) - Emission: a photon emitted by the source is absorbed by the detector. (b) - Absorption: the source absorbs a photon emitted by the detector.

This effect has been first observed by Dayem and Martin [54], and subsequently explained by Tien and Gordon [55]. Let us briefly consider the effect of a microwave field on quasi-particle states

$$\psi(\overrightarrow{r}, t) = f(\overrightarrow{r}) \, \mathrm{e}^{-\mathrm{i}\,[\mathrm{E}t + \int_0^t e\mathrm{V}_{\mathrm{ac}} \cos(\omega t') \mathrm{d}t']/\hbar}$$

Performing a Jacobi-Anger expansion, it comes[8]

$$\psi(\overrightarrow{r}, t) = f(\overrightarrow{r}) \, \mathrm{e}^{-\mathrm{i}\,\mathrm{E}t/\hbar} \sum_{n=-\infty}^{+\infty} \mathrm{J}_n(e\mathrm{V}_{\mathrm{ac}}/\hbar\omega) \, \mathrm{e}^{-\mathrm{i}\,n\,\omega t}$$

where J_n stands for the Bessel functions of the first kind. It is deduced that under HF irradiation, the density of states reads

$$\mathcal{N}_{\mathrm{S}}'(\mathrm{E}) = \sum_{n=-\infty}^{+\infty} \mathrm{J}_n{}^2(e\mathrm{V}_{\mathrm{ac}}/\hbar\omega)\,\mathcal{N}_{\mathrm{S}}(\mathrm{E} + n\hbar\omega)$$

Reinjecting this in the expression of the tunneling current of a SIS junction, it is found after integration that under periodic drive, the $I(V)$ characteristic of the junction is modified according to

$$\mathrm{I}_{\mathrm{qp}}(\mathrm{V}_{\mathrm{DC}}) = \sum_{n=-\infty}^{+\infty} \mathrm{J}_n{}^2(e\mathrm{V}_{\mathrm{ac}}/\hbar\omega)\mathrm{I}_{\mathrm{qp},0}(\mathrm{V}_{\mathrm{DC}} + n\hbar\omega/e)$$

The power of the HF excitation intervenes through factor $\mathrm{J}_n{}^2(e\mathrm{V}_{\mathrm{ac}}/\hbar\omega)$: the higher the ratio $e\mathrm{V}_{\mathrm{ac}}/\hbar\omega$, the higher the number of photo-assisted steps in the characteristic. These multiple replicas are a manifestation of multiphoton processes. In the following, we will restrict ourselves to sufficiently low emitted/absorbed power in order to neglect multi-photon process: this assumption reads $\mathrm{J}(t) \ll 1$ (moderate coupling *ie.* lowly resistive environment $\mathrm{Z}(\omega) \ll \mathrm{R}_q$). An example of the effect of HF irradiation on the transport properties of a SIS junction is represented on figure 3.9.

---

[8]Normalization of the wave function $\psi(\overrightarrow{r}, t)$ is ensured given that

$$\forall x \in \mathbb{R} \quad \left(\sum_{n \in \mathbb{N}} \mathrm{J}_n(x)\right)^2 = 1$$
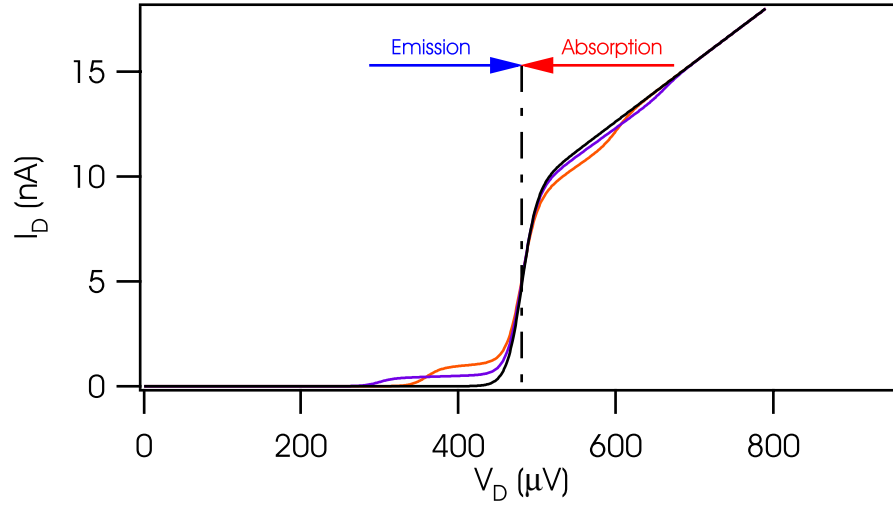
Figure 3.9: Numeric calculation of the $I(V)$ characteristic of the junction which will be used as a detector in the following for two different frequencies (29 GHz and 44 GHz) and the same irradiation power (which is voluntarily exagerated in this simulation, in order to make the PAT current steps clearly visible: at such power, one should observe multiphoton processes).

3   Dynamical properties of a SIS junction

Dynamical conductance

The real part of the dynamical conductance of a SIS junction reads [56][57]

$$G_Q(\omega, V) = \frac{e}{2\,\hbar\,\omega} \left[I_{qp}(V + \hbar\omega/e) - I_{qp}(V - \hbar\omega/e) \right]$$

In the frame of linear response theory, causality imposes that the imaginary part is related to the real part through a Kramers-Kronig transform

$$B_Q(\omega, V) = P \int_{-\infty}^{+\infty} \frac{d\omega'}{\pi} \frac{G_Q(\omega')}{\omega' - \omega}$$

It can be shown that

$$B_Q(\omega, V) = \frac{e}{2\,\hbar\,\omega} \left[I_{KK}(V + \hbar\omega/e) + I_{KK}(V - \hbar\omega/e) - 2\,I_{KK}(V) \right]$$

where $I_{KK}(V)$ stands for the Hilbert transform of $I_{qp}(V)$ (see figure 3.10)

$$I_{KK}(V) = P \int_{-\infty}^{+\infty} \frac{dV'}{\pi} \frac{I_{qp}(V') - V'/R_T}{V' - V}$$

This has already been checked experimentally[9] [59][58].

---

[9]We acknowledge D.E. Prober for pointing out the importance of this imaginary part in the quantitative interpretation of some of our data, and for bringing to our attention reference [58].
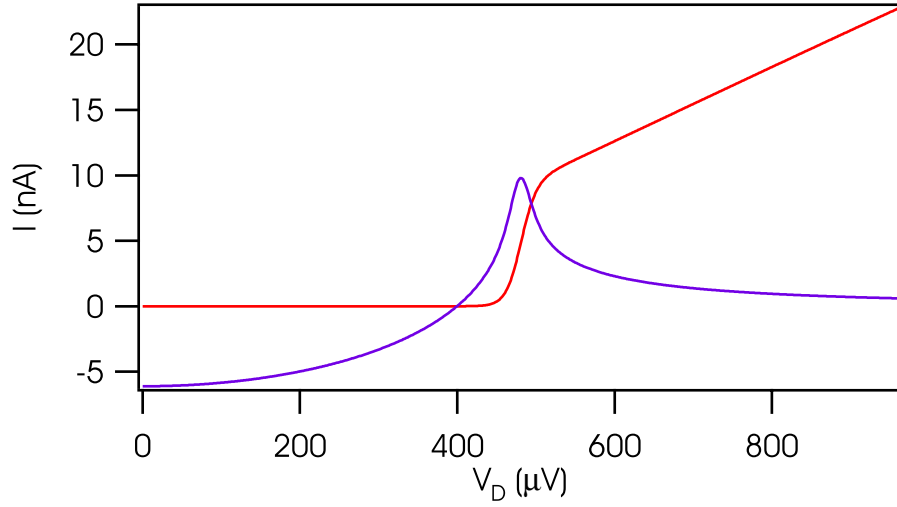
Figure 3.10: DC $I(V)$ characteristic $\mathbf{I_{qp}}$ of the junction which will be used as a detector in this experiment (experimental data), and its Kramers-Kronig transform $\mathbf{I_{KK}}$ (numerical calculation).

Quasiparticles current fluctuations of a SIS junction

Nonsymmetrized noise correlator.   It can be shown (see appendix) that the current noise spectrum of a SIS junction (or alternately the quasiparticle current noise spectrum of a Josephson junction) reads

$$S_I(\omega, V) = \frac{e}{2\pi} \left[\frac{I_{qp}(\hbar\omega/e + V)}{1 - e^{-\beta(\hbar\omega + eV)}} + \frac{I_{qp}(\hbar\omega/e - V)}{1 - e^{-\beta(\hbar\omega - eV)}} \right]$$
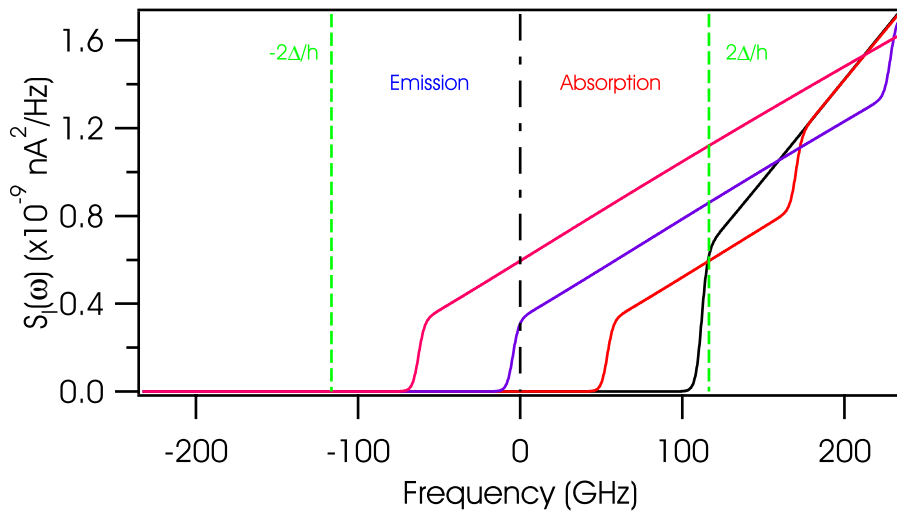
Figure 3.11: Nonsymmetrized current noise spectrum $S_I(\omega)$ of a SIS junction *vs.* frequency, at equilibrium and for different voltage biases (V = 0, Δ/e, $2\Delta/e$ and $3\Delta/e$).

Interpretation: inelastic processes. The nonsymmetrized spectral density can be understood in terms of inelastic processes (see appandix & figure 3.12).
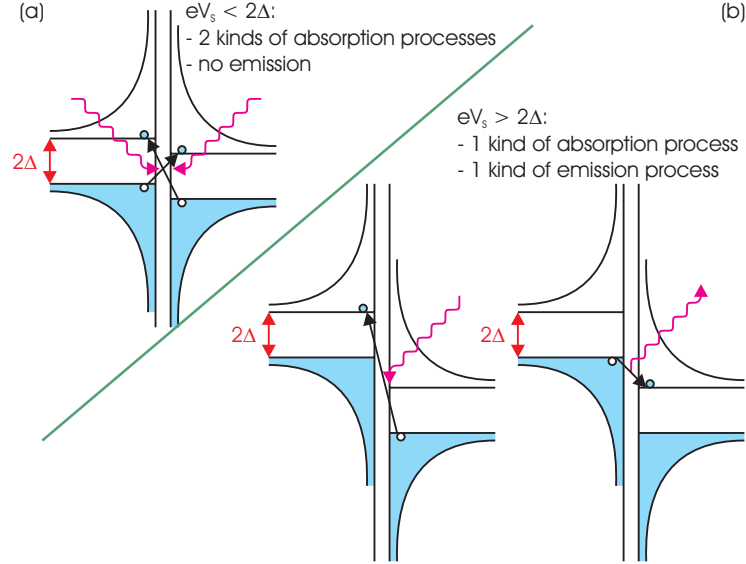

Figure 3.12: Inelastic processes.

We thus recover that the quasiparticle current noise spectrum of a Josephson junction presents a singularity in absorption at $\hbar\omega = (2\Delta + eV_S)$, whatever the bias regime, and a singularity in absorption at $\hbar\omega = (2\Delta - eV_S)$ if $eV_S < 2\Delta$, and in emission at $\hbar\omega = (eV_S - 2\Delta)$ if $eV_S > 2\Delta$.

Non symmetrization vs symmetrization. Starting from this expression of the non-symmetrized noise spectral density, one can rebuild the symmetrized one

$$S_I(\omega, V) = \frac{e}{4\pi} \left[\; I_{qp}(\hbar\omega/e + V) \coth\left(-\frac{\beta}{2}(\hbar\omega + eV)\right) \right.$$
$$\left. + \; I_{qp}(\hbar\omega/e - V) \coth\left(-\frac{\beta}{2}(\hbar\omega - eV)\right) \right]$$

The expression established in [60] is recovered: it is plotted on figure 3.13. One can first notice that contrarily to most mesoscopic devices (NIN tunnel junctions, diffusive wires), the nonsymmetrized/symmetrized noise spectral density $S_I(\omega)$ of a SIS junction are clearly distinguishable

- **Nonsymmetrized case:** If $eV_S < 2\Delta$, two singularities occur in absorption ($\omega > 0$) at $\hbar\omega = (2\Delta \pm eV_S)$, whereas if $eV_S > 2\Delta$, one can notice one singularity in absorption ($\omega > 0$) at $\hbar\omega = (2\Delta + eV_S)$ and another one in emission ($\omega < 0$) at $\hbar\omega = (eV_S - 2\Delta)$.

- **Symmetrized case:** Whatever the voltage bias V_S, two singularities both in emission and absorption at $|2\Delta \pm eV_S|$ can be distinguished.
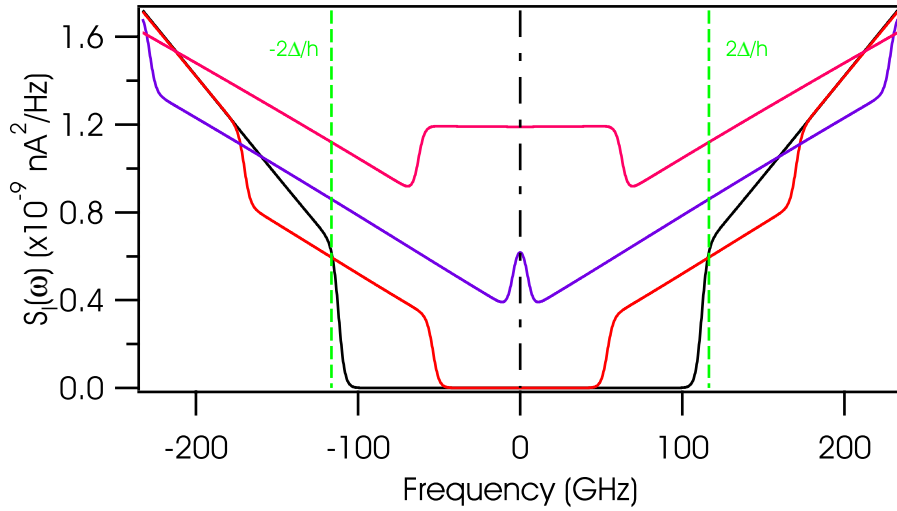
Figure 3.13: Symmetrized current noise spectrum $S_I(\omega)$ of a SIS junction *vs.* frequency, at equilibrium and for different voltage biases (V $= 0, \Delta/e, 2\Delta/e$ and $3\Delta/e$).

A SIS junction is thus an ideal candidate to test the ability of a noise detector to distinguish nonsymmetrized/symmetrized noise correlators: it is worth to notice that this asymmetry in the excess noise of a SIS junction is strongly related with the strong nonlinearity of its $I(V)$ characteristic. This nonlinearity is also the reason why SIS junction stands as an ideal candidate for quantum noise detection: this reciprocity between the properties of the noise source and the detector can be misleading in the interpretation of the experiment, however it is not fortuitous. It can be thus pointed out that the PAT mechanisms the detection rely on, are the same inelastic processes hidden behind the quantum noise spectral density.

Detection of excess noise   As explained previously, our detector is sensitive to excess noise (the equilibrium noise of the source being already included in the equilibrium $I(V)$ characteristic of the detector, through dynamical Coulomb blockade). The excess noise of a SIS junction is plotted on figure 3.14. The fact that the excess noise spectral density is negative in a limited range of the absorption side is another interesting feature of the SIS junction: however it will not be possible to detect it in our experiment, this singularity occuring at frequencies $\hbar\omega > 2\Delta$.
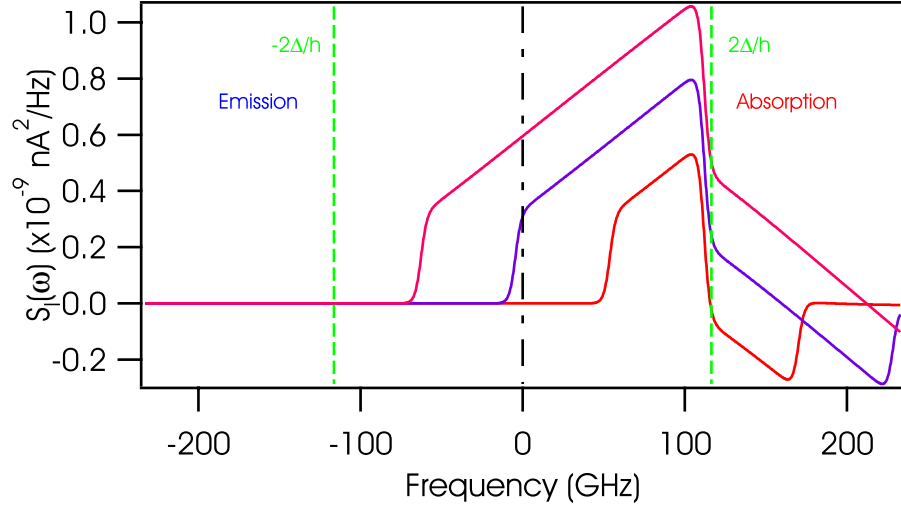
Figure 3.14: Nonsymmetrized excess current noise spectrum $S_I(\omega)$ of a SIS junction *vs.* frequency, for different voltage biases (V $= \Delta/e, 2\Delta/e$ and $3\Delta/e$).

4   Derivation of the PAT current for a SIS junction in the frame of the P(ε) theory

Replacing the equilibrium current noise spectral density of the environment by the current noise spectral density of the biased device under test, it comes

$$J(t) = \frac{2\pi}{\hbar R_q} \int_{-\infty}^{+\infty} d\omega \frac{|Z(\omega)|^2}{\omega^2} S_I(\omega) \left[\exp(-i\omega t) - 1\right]$$

Aguado *et al.* have shown that in the limit of low-impedance environment, the expression of the energy exchange probability P(ε) can be simplified according to [22] (see appendix B for details)

$$P(\varepsilon) = \left[1 - \frac{2\pi}{\hbar R_q} \int_{-\infty}^{+\infty} d\omega \frac{|Z(\omega)|^2}{\omega^2} S_I(\omega)\right] \delta(\varepsilon) + \frac{2\pi}{R_q} \frac{|Z(\varepsilon/\hbar)|^2}{\varepsilon^2} S_I(\varepsilon/\hbar)$$

The $I(V)$ characteristic I_{qp} of the SIS junction in presence of an environment (non-ideal voltage bias) is related with the $I(V)$ characteristic $I_{qp,0}$ of the junction without environment, *via* a convolution with the energy exchange probability P(ε)

$$I_{qp}(V_D) = P \otimes I_{qp}\left[eV_D\right] = \int_0^{+\infty} d\varepsilon' P(eV_D - \varepsilon') I_{qp}\left(\frac{\varepsilon'}{e}\right)$$

Deblock *et al.* have shown that the PAT current can be decomposed into three terms [21] (see appendix C for details):

$$
\begin{aligned}
I_{PAT}(V_D) &= I_{qp}(V_D) - I_{qp,0}(V_D) \\
&= \underbrace{\int_0^{+\infty} d\omega \left(\frac{e}{\hbar\omega}\right)^2 S_V(-\omega)\, I_{qp,0}\left(V_D + \frac{\hbar\omega}{e}\right)}_{\text{Emission contribution to the PAT current}} \\
&\quad + \underbrace{\int_0^{eV_D} d\omega \left(\frac{e}{\hbar\omega}\right)^2 S_V(\omega)\, I_{qp,0}\left(V_D - \frac{\hbar\omega}{e}\right)}_{\text{Absorption contribution to the PAT current}} \\
&\quad - \underbrace{\int_{-\infty}^{-\infty} d\omega \left(\frac{e}{\hbar\omega}\right)^2 S_V(\omega)\, I_{qp,0}(V_D)}_{\text{Renormalization of the elastic current}}
\end{aligned}
$$

This expression shows the different contributions of the emission/absorption HF signals to the PAT current: the last term takes into account the fact that elastic processes must be renormalized by the sum of all inelastic processes. It can be seen that when the junction is biased below the gap, it is only sensitive to emission, a feature that can be intuitively understood with the schematic representation of the detection processes in the semiconductor representation (see figure 3.12).

Chapter 4

Detection of non-symmetrized noise correlator

I Detection scheme

1 General principle

Our detection scheme relies on a capacitive coupling between the device under test, and our detector (following the proposal by Aguado *et al.* [22]: see figure 4.1): this way, the source and the detector can be DC biased independently, while ensuring a good coupling at high-frequency. In the Delft experiment [21], the environment was shunted at HF by stray capacitances between the leads. In order to get a better control on our environment, "on-chip" capacitances C_s have been added (see figure 4.1 & 4.2): at HF, these capacitances act as short circuits which completely isolate our device from the external apparatus, thus ensuring a good shielding from the external sources of noise.
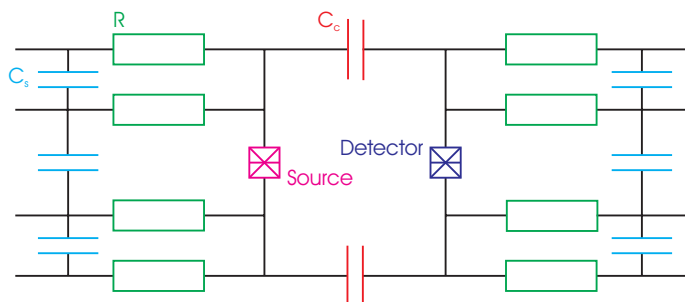

Figure 4.1: Principle of the detection: capacitive coupling between a Josephson junction (the source) and a SIS junction (the detector)

Another important requirement to fulfill if one wants to neglect retardation effects, is to ensure that the typical size of the circuit is lower than the wavelength λ associated with the HF signals under study: at 10 GHz, $\lambda \approx 3$ mm. Our HF environment is delimited by the shunt capacitances, and thus extends over approximately 200 μm $< \lambda$. Retardation effects can be neglect, and by so the P(ε) theory is valid.

2   Description of the sample

This sample has been realized in collaboration with F. Pierre (LPN-Marcoussis). The optical picture presented on figure 4.2-a allows to distinguish the different elements constituting the circuit:

- **The coupling capacitances C_c:** two metallic plates (size $23 \times 25 \ \mu m^2$), with a dielectric layer (65 nm of alumina) between them. Estimated value: $C_c \approx 750$ fF.

- **The polarization resistances:** 8 platinum wires length= 40 μm, width= 750 nm, thickness= 15 nm. Measured value: R = 750 Ω.

- **The source** and **the detector:** both are constituted of two Josephson junctions, embedded in a SQUID geometry, thus allowing to tune the Josephson coupling with a magnetic field.
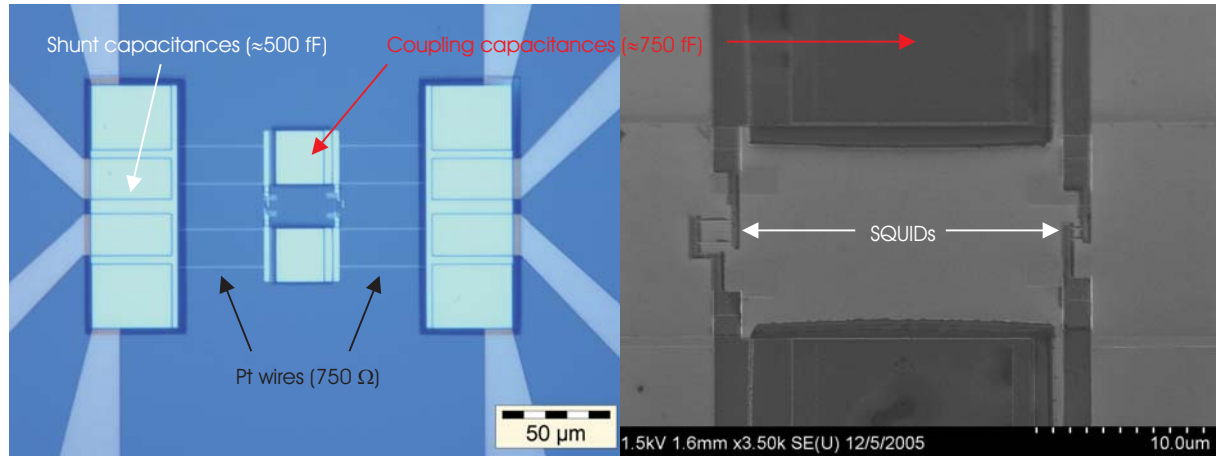

Figure 4.2: (a) - Optical microscopy picture of the sample. The different elements of the "on-chip" environment can be seen: notice that its size is lower than the typical wavelength of the HF signals detected ($\lambda \approx 3$ mm at 100 GHz), thus allowing to neglect retardation effects. (b) - Electronic microscopy picture of the sample: the areas of the loop of the two SQUIDs are different.

Let us motivate the choice of the different elements of the detection scheme. Firstly, as we wish to work in the limit of weak coupling, the polarization resistances must fulfill R $\ll$ R$_q$: consequently, 750 Ω seems a good compromise (a too low impedance would decrease the coupling). Since the coupling and shunt capacitances must act as short circuits in the frequency range of interest (*ie.* between 10 and 100 GHz), their impedance in this range is required to be lower than the impedance of the polarization resistances: a capacitance of 500 fF at 10 GHz has an impedance of 30 Ω. Finally, both Josephson junctions are required to be resistive in order to limit their influence on the frequency dependence of the transimpedance Z(ω): moreover, the P(ε) theory is valid in the weak tunneling limit (R$_T \ll$ R$_q$). We finally chose R$_T \approx 25$ kΩ. The geometric capacitance C of the junction must fulfill R$_T$C$\omega \approx 1$: with the usual oxidation conditions, it leads approximately to a 100×100 nm^2 junction.
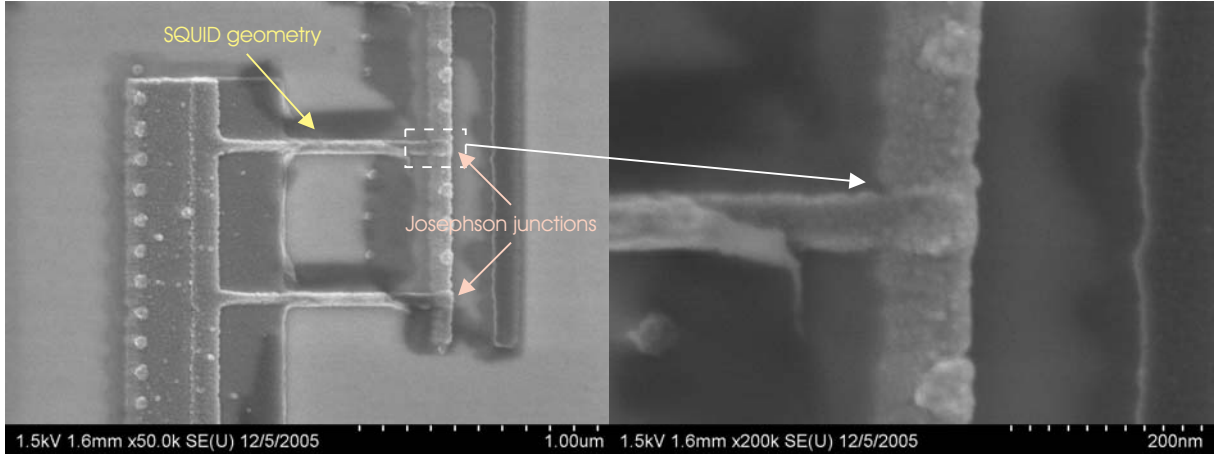
Figure 4.3: (a) Electronic microscopy picture of a SQUID: features due to the two-angle evaporation technique can be seen. (b) Electronic microscopy picture of one of the two junctions embedded in the SQUID: area of the junctions can be estimated around 200 nm× 200 nm.

3   Transimpedance $Z(\omega)$

The current fluctuations through the source are related to the voltage fluctuations across the detector *via* the transimpedance $Z(\omega)$, defined such as

$$S_{V_D}(\omega) = |Z(\omega)|^2\, S_{I_S}(\omega)$$

This quantity characterizes the electromagnetic environment of the detector, similarly to what is done in the theory of dynamical Coulomb blockade. In the frequency range we are interested in, between 10 GHz and 100 GHz, the transimpedance is more or less defined by the value of the on-chip resistances. In order to check this, one can draw the high-frequency equivalent circuit (see figure 4.4).
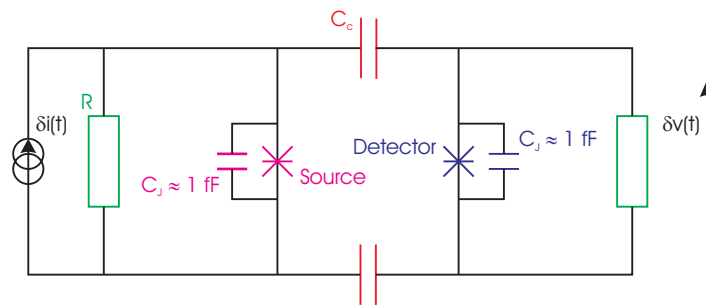

Figure 4.4: HF equivalent circuit of our detection scheme.

It is assumed that the shunt capacitances C_s act as short circuits in the frequency range of interest. The transimpedance $Z(\omega)$ can thus be expressed as a function of the impedances of the other circuit elements

$$Z(\omega) = \frac{\delta v(\omega)}{\delta i(\omega)} = \frac{i\omega R C_c}{2 + i\omega R (2C + C_c)} \left\{ R^{-1} + Y_S(\omega, V_S) + \left[\frac{2}{iC_c\omega} + \frac{R}{1 + i\omega RC} \right]^{-1} \right\}$$

where $Y_S(\omega, V_S)$ stands for the admittance of the source.

$$Y_S(\omega, V_S) = \underbrace{(G_Q(\omega, V_S) + iB_Q(\omega, V_S))}_{\text{Tunneling term}} + \underbrace{iC\omega}_{\substack{\text{Geometric} \\ \text{capacitance}}}$$
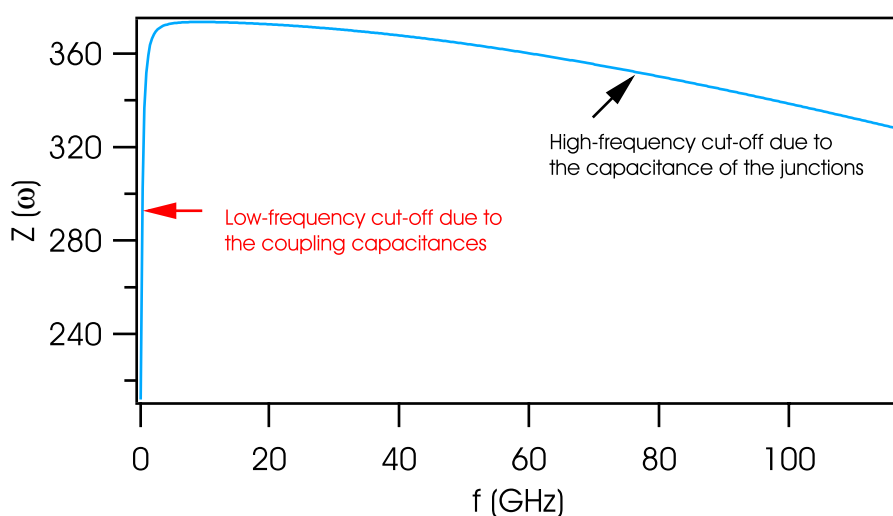

Figure 4.5: Transimpedance *vs.* frequency.

We will see later that we will need to calibrate our detection circuit: there is some kind of disagreement between the predicted value of the transimpedance and the measured one.

It can be noticed that contrarily to the case of a low-impedance ohmic environment, $P(\varepsilon)$ does not diverge at low energy (see figure 4.6): this is due to the capacitive coupling. Indeed, in the low-frequency limit, the source and the detector are decoupled $(Z(\omega) \underset{\omega \to 0}{\sim} iC_c\omega\, R^2)$. The $1/\varepsilon^2$ divergence of the energy exchange law $P(\varepsilon)$ (due to the phase sensitivity of the detector) is thus cured by the capacitive coupling. It is also worth to point out that $P(\varepsilon)$ is very sensitive to temperature: given our moderately resistive environment $(|Z(\omega)| < R_q)$, the dynamical Coulomb blockade acts mainly at low energy (quasi-elastic regime). This regime is required for the detection, because it ensures the measurement is frequency resolved. In such conditions, it is not surprising that $P(\varepsilon)$ is sensitive to a temperature of a few tens of mK. Actually, the coupling is not well controlled at low frequency given that the shunt capacitances C_s do not act as good short circuits in the limit $\varepsilon \to 0$: the environment being not well defined in this frequency range, $P(\varepsilon)$ is not well known. However, it does not constitute an issue given that we aim at exploring higher frequencies $(\hbar\omega \gg k\mathrm{T})$.
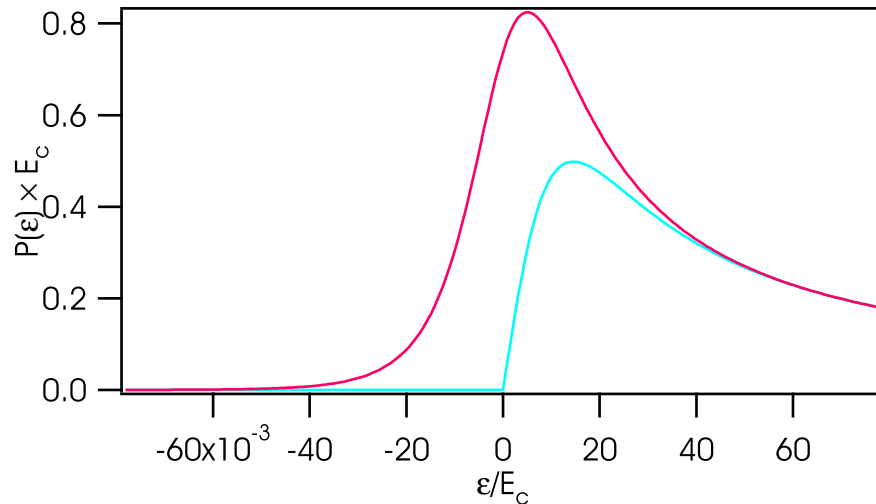
Figure 4.6: Inelastic contribution to the energy exchange law P(ε) *vs.* reduced energy ε/E_c for the environment designed in our experiment (T = 0 K, T = 10 mK).

II Emission

1 Measurement

In this section, the HF emission properties of a Josephson junction is investigated: as explained earlier in this manuscript, the emitted photons (negative frequencies) are detected by the SIS junction in the subgap regime ($eV_D < 2\Delta$). In this bias regime, the detector has an infinite impedance (almost infinite actually, because in a real experiment the subgap conductance of a SIS junction presents some resonances): it seems more suitable in this case to voltage bias the detector. The source must be voltage biased in the subgap regime in order to observe AC Josephson effect, whereas for $eV_S > 2\Delta$, it can be voltage or current biased. For the sake of simplicity, we choose to voltage bias the source in both regimes, thus allowing to record the emission in the AC Josephson effect and shot noise regimes in similar conditions. To improve the accuracy of the measurement, we modulate the amplitude of the voltage bias on the source V_S, and record the associated variations of the photo-assisted tunneling current I_{PAT} induced through the detector. The source being a Josephson junction, its DC dynamical impedance presents some variations whether the bias regime (Josephson branch, subgap regime or quasiparticle branch): consequently we also record the effective voltage modulation on the source. We can then rebuild the following quantity $\partial I_{PAT}/\partial V_S$, which can be numerically calculated using the P(ε) theory precedently exposed. We have checked that the cross-talked signal on the detector by the modulation on the source was negligible: the signal measured on the detector is thus entirely due to the HF photons emitted by the source. An example of the measured signal is represented on figure 4.7.
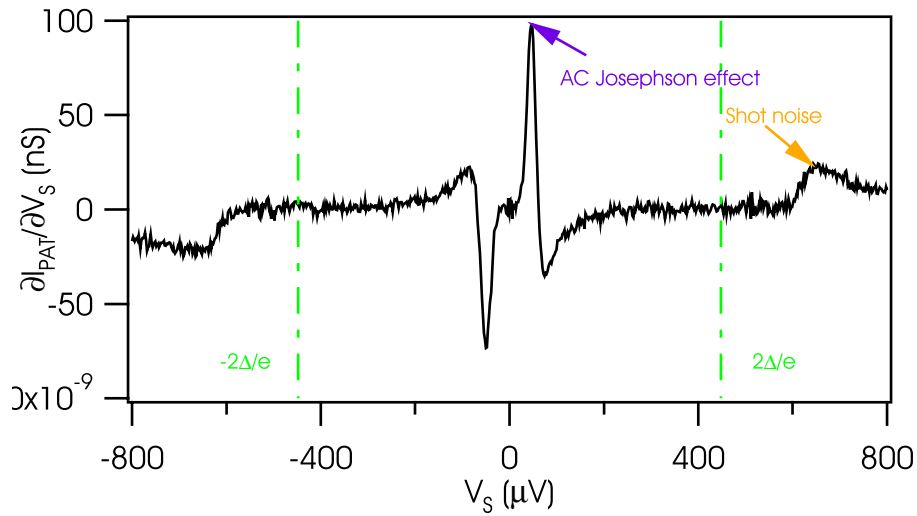
Figure 4.7: Example of the measured signal in the emission regime: $V_D = 398$ μV, *ie.* $f = 20$ GHz: two singularities can be distinguished, one being related to the AC Josephson effect (low bias), and the other to the shot noise regime (quasiparticle branch)

One can clearly see two different peaks, depending on whether the source junction is biased below or above the gap $2\Delta/e$:

- **At low bias** ($V_S < 2\Delta/e$)**:** this peak is followed by a dip when the voltage bias on the source V_S is increased, and then the PAT current is constant again: this lets us think that this emission process acts in a limited bandwidth. This would be consistent with the AC Josephson effect regime (expected in the subgap regime), which is supposed to be almost monochromatic (a certain bandwidth is expected due to thermal and environmental effects).

- **At higher bias** ($V_S > 2\Delta/e$)**:** this peak looks much broader, and the PAT current keeps increasing when the voltage bias is increased. Conversely, this is the signature of an emission process with a large bandwidth: it can be associated with shot noise (expected for $eV_S > 2\Delta$ as observed).

One can notice that the amplitude of the low-bias peak is clearly non-symmetric when compared at positive and negative voltage bias V_S: we have no clear understanding of this, but it seems that this asymmetry is reversed when the magnetic field is reversed. In the following, the fits to the experimental data will be performed on the larger of the two peaks. To confirm our intuitions, we have recorded the PAT current for different voltage bias on the detector V_D, in order to discriminate both emission processes from their frequency dependence: the data are represented on figure 4.8.
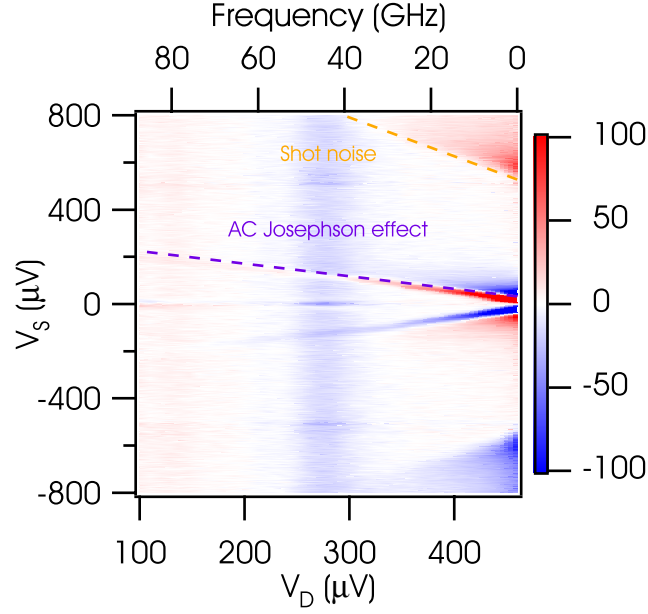
Figure 4.8: Derivative of the PAT current with respect to the voltage bias on the source $\partial I_{PAT}/\partial V_S$ for different DC voltage bias on the source: one can notice that the peaks discussed above have different frequency dependence.

The singularities previously described have different frequency dependence *vs.* the DC voltage bias on the source V_S. The position of the maximum of the low bias peak unambiguously obeys the Josephson relation $\omega_J = 2eV_S/\hbar$, whereas the higher bias peak position follows a $(eV_S - 2\Delta)$ law when $eV_S > 2\Delta$. This last feature is one of the key result of this experiment, and will be discussed in details later.

2 AC Josephson effect

As previously mentionned, we need to calibrate the high-frequency coupling between the source and the detector: fortunately, by tuning the Josephson coupling to its maximum value, using the SQUID geometry, one can use the AC Josephson effect to turn the Josephson junction into a high-frequency generator. We will assume that the high-frequency emission spectrum is almost monochromatic, though our environment is quite resistive. When it is voltage biased, the high-frequency current emitted by the junction is given by

$$I_J(t) = I_C \sin\left(\frac{2eV_S}{\hbar}t\right) \quad \text{where} \quad I_C = \frac{\pi\,\Delta}{2e\,R}$$

The amplitude I_C is related to the transparency of the junction, by the so-called Ambegaokar-Baratoff formula [61]: it is the result of a treatment to the second order of the tunneling Hamiltonian of a Josephson junction, neglecting the environmental degrees of freedom and thermal broadening.

Fit of the data

For a monochromatic irradiation $(S_I(\omega) = I_C{}^2\,\delta[\omega \pm 2eV_S/\hbar])$, the expression of the PAT current reads

$$I_{PAT}(V_D) = \frac{1}{4}\left(\frac{|Z(\omega)|\,I_C}{2\,V_S}\right)^2 [I_{qp,0}(V_D + 2eV_S) + I_{qp,0}(V_D - 2eV_S) - 2\,I_{qp,0}(V_D)]$$

One recovers the result by Tien *et al.* [55], in the limit of small irradiation power ($\alpha = eV_{ac}/\hbar\omega \ll 1$), by expanding the Bessel function ($J_{\pm 1}(x \ll 1) \approx \pm x/2$)[1].
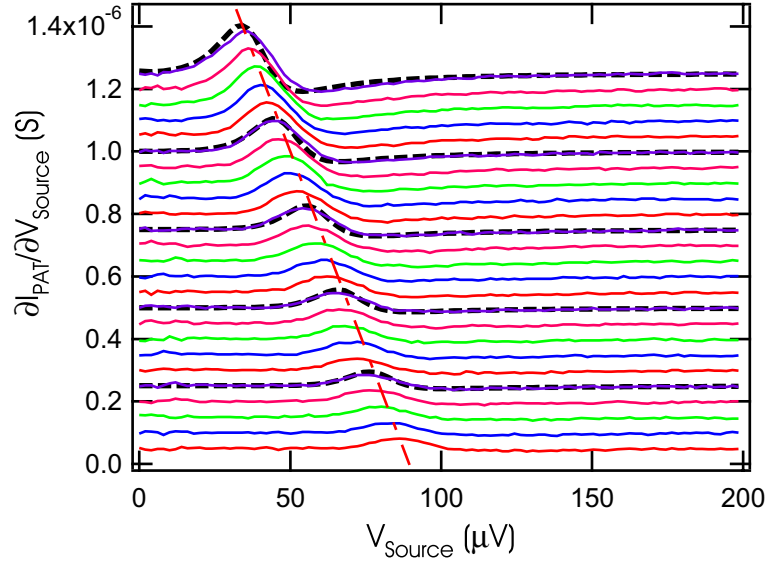

Figure 4.9: AC Josephson effect: derivative of the PAT current with respect to the voltage bias on the source $\partial I_{PAT}/\partial V_S$ *vs.* DC voltage bias on the source, for different DC voltage bias on the detector. Dashed lines are numeric simulations of the expected PAT current in the frame of DCB theory, calculated with transimpedance $Z(\omega)$ as adjustable parameter.

Extraction of the transimpedance

We can extract the value of the transimpedance $Z(\omega)$ from the numeric simulations performed to fit the AC Josephson effect data in emission (see figure 4.10).

---

[1]Among other formulas concerning Bessel functions of the first kind, one can show that

$$J_n(x) = \sum_{\ell=0}^{+\infty} \frac{(-1)^\ell}{2^{2\ell+n}\ell!(\ell+n)!} x^{2\ell+n}, \ J_{-n}(x) = (-1)^n J_n(x) \quad (n \in \mathbb{N})$$
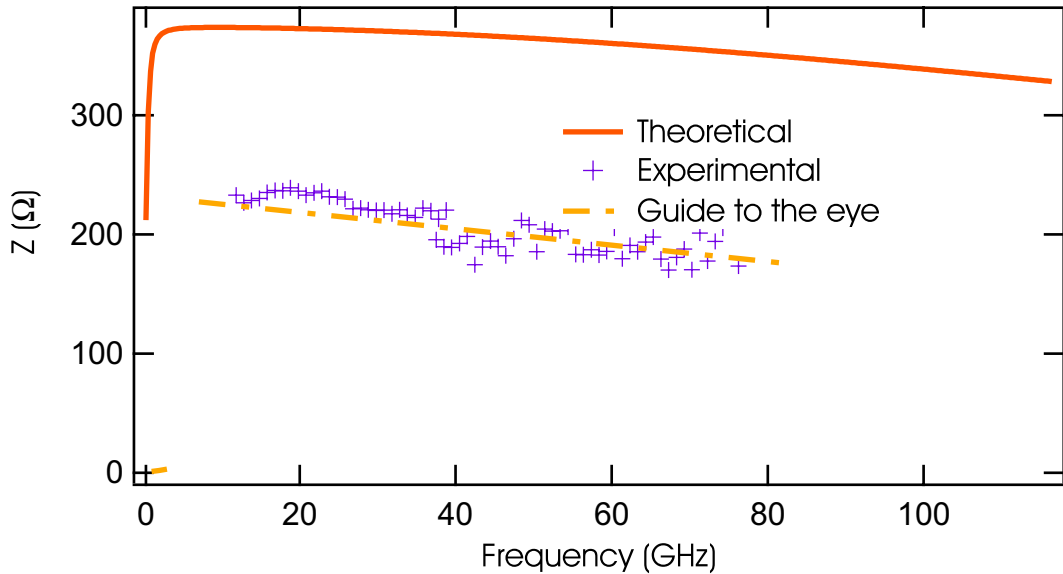
Figure 4.10: Transimpedance *vs.* frequency: both theoretical prediction and experimental data extracted from the emission of the AC Josephson effect are represented.

It is seen that there is a disagreement between the predicted and measured values of the transimpedance: the frequency dependence appears to be similar, however the average of the measured value is found to be lower than predicted.

3 Shot noise

Symmetrized *vs.* nonsymmetrized noise correlator

Let us turn to the key discussion concerning this experiment: the issue of nonsymmetrizing *vs.* symmetrizing the time correlator has been discussed previously in the introduction of this part of the manuscript. It is considered that the answer to this question depends on the detection scheme. Here, we use a quantum detector, *ie.* we guess that the SIS junction is able to distinguish the flow of energy coming from the device under test, and the flow of energy coming to the detector: in this case, we expect that our detection scheme separates emitted and absorbed photons. In practice, one cannot claim that it does so because most mesoscopic devices have a symmetric excess noise: however, SIS junction has a nonsymmetric excess noise spectrum due to the peaked density of states of the superconductor constituting the electrodes. Both situations have been investigated previously:

- **Nonsymmetrized correlator:** this case corresponds to the spectrum plotted on figure 3.13. We expect to detect a singularity at $\hbar\omega = (eV_S - 2\Delta)$ when the junction is biased on the quasiparticle branch ($eV_S > 2\Delta$): as mentionned earlier, this peak has a clear interpretation in terms of inelastic processes (it corresponds to the relaxation of a quasiparticle).

- **Symmetrized correlator:** this case corresponds to the spectrum plotted on figure 3.11. Under this assumption, two singularities are expected: one at $\hbar\omega = (2\Delta - eV_S)$ if $eV_S < 2\Delta$, and one at $\hbar\omega = (eV_S - 2\Delta)$ if $eV_S > 2\Delta$. This is just a consequence of

the symmetrization, and has no physical interpretation in terms of energy exchange between the source and the detector.

From our data, it is clear that our detection scheme is unambiguously sensitive to the nonsymmetrized noise correlator because we only detect a singularity at $\hbar\omega = (eV_S - 2\Delta)$ when $eV_S > 2\Delta$. We want to stress out that these two singularities have a similar spectral density, so if we detect this singularity at $(eV_S - 2\Delta)$, we have enough sensitivity to detect the other possible singularity: the fact that we do not detect it is not an issue of sensitivity. Consequently, from the emission data, we can conclude that this detection scheme can clearly distinguish emitted/absorbed photons: the relevant quantity when a quantum detector is used to detect quantum noise is the nonsymmetrized correlator. This result is consistent with the physical intuition, based on a qualitative interpretation of quantum noise in terms of inelastic processes (starting from the Fermi golden rule): symmetrization aims to turn the noise correlator into a hermitian quantity, which is not necessary. This mathematical procedure has luckily no consequences in most practical cases because detection schemes relying on HF electronics seem to be sensitive to symmetrized correlators, and also because most devices have a symmetric excess noise. In order to confirm this interpretation, let us turn to the absorption: an intuitive vision of the detection has been given on figure 3.8, which let us think that one could detect photons absorbed by the device under test when the detector is biased on the quasiparticle branch. Let us see if this simple approach is correct.

Fit of the data

We have also performed a numeric calculation of the expected PAT current, with the expression of the non-symmetrized current noise spectral density (see figure 4.11).
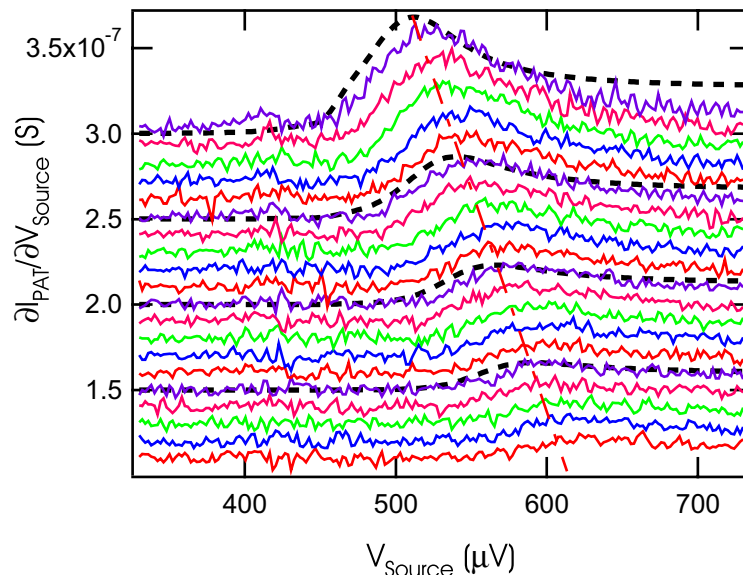

Figure 4.11: Shot noise: derivative of the PAT current with respect to the voltage bias on the source $\partial I_{PAT}/\partial V_S$ *vs.* DC voltage bias on the source, for different DC voltage bias on the detector. Dashed lines are numeric simulations of the expected PAT current, calculated with the value of the transimpedance $Z(\omega)$ previously measured.

These calculations are in good quantitative agreement with the experimental data, and confirm that our detector is sensitive to the non-symmetrized noise correlator.

III Absorption

1 Measurement

The data concerning absorption are taken in a slightly different way: indeed, one now has to bias the detector on the quasiparticle branch. In this case, the detector has a finite impedance (contrarily to the subgap regime explored in the emission regime): consequently, we chose to current bias the detector. This method has a clear advantage in terms of sensitivity: due to the shape of the PAT current, a small variation of the current through the detector implies a large variation of the voltage across it. The source is again voltage biased: we also modulated the voltage across the source, and used a lock-in technique to detect the voltage variations at the same frequency across the detector. By means of accurate transformations, we will present the same quantity as the one presented for the emission regime, *ie.* $\partial I_{PAT}/\partial V_S$.
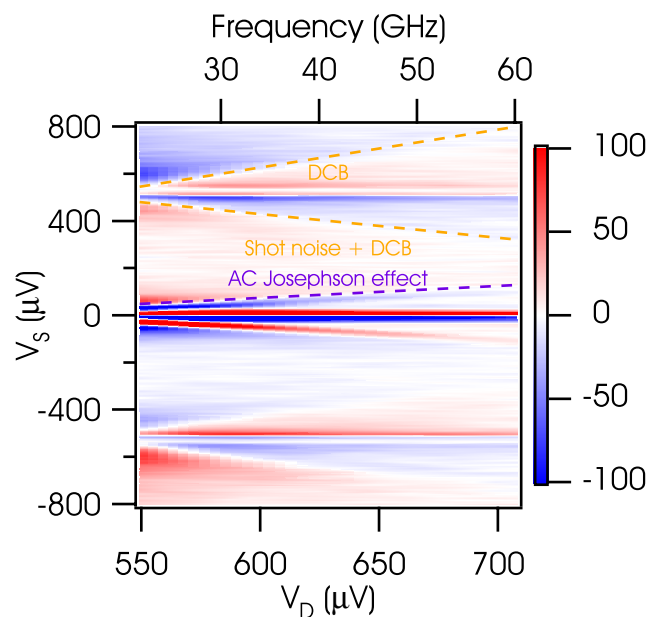

Figure 4.12: Derivative of the PAT current with respect to the voltage bias on the source $\partial I_{PAT}/\partial V_S$ for different DC voltage bias on the source: we detect again a peak due to the AC Josephson effect, and a set of two other peaks varying as $(2\Delta - eV_S)$ when $eV_S < 2\Delta$, and $(eV_S - 2\Delta)$ when $eV_S > 2\Delta$.

2 AC Josephson effect

It is interesting to check the sensitivity of our detection scheme to absorption in a well known regime, before exploring the quantum noise of the SIS junction which is a bit more controversial. The AC Josephson effect is a good candidate to do so, and it is clearly detected (see figure 4.12) in the low-bias regime. Following the position of the maximum of the PAT current edge, we recover the expected Josephson relation $\omega_J = 2eV_S/\hbar$. Using

the transimpedance extracted from the emission data, we have performed a numerical calculation of $\partial I_{PAT}/\partial V_S$, and compared it with the experimental data (see figure 4.13).
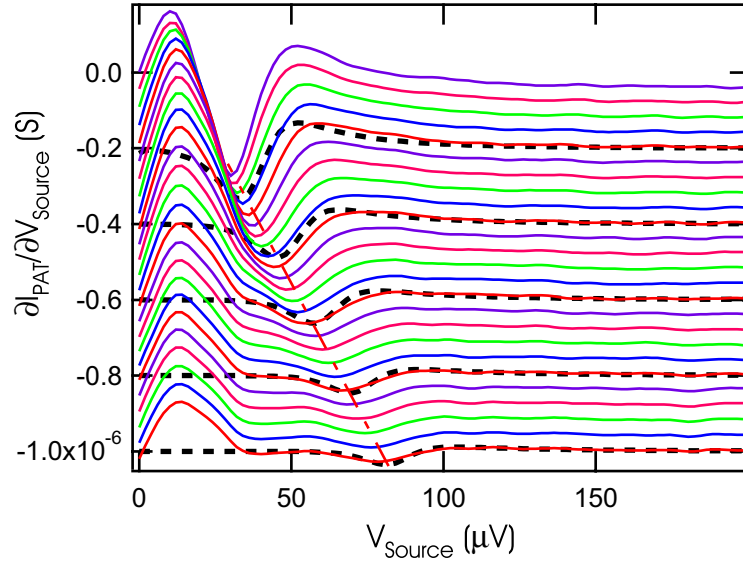

Figure 4.13: AC Josephson effect: derivative of the PAT current with respect to the voltage bias on the source $\partial I_{PAT}/\partial V_S$ *vs.* DC voltage bias on the source, for different DC voltage bias on the detector.

Again, the predictions based on dynamical Coulomb blockade are in good agreement with the experiments: this is an interesting point, because it shows that the SIS junction biased above the gap is sensitive to HF irradiation, but more importantly it confirms the validity of the DCB theory in this regime (not tested in previous experiments).

3   Shot noise and environmental effects

The situation is more intricate concerning shot noise: indeed we observe two singularities, one at $\hbar\omega = (2\Delta - eV_S)$ when $eV_S < 2\Delta$, and the other at $\hbar\omega = (eV_S - 2\Delta)$ when $eV_S > 2\Delta$ (see figure 4.12). At first sight, this result seems to be in stark contradiction with the conclusion of the emission measurements because this set of two singularities is consistent with the symmetrized current noise correlator. Actually, the situation is a bit more subtle in absorption: indeed, this side of the $I(V)$ characteristic of the detector is sensitive to the absorption noise of all the resistive elements of the circuit, *ie.* the source and the polarisation resistances. Until now, we assumed that the current noise of the on-chip resistances was equilibrium noise, and was thus already included into the $I(V)$ characteristic of the detector. However, the voltage fluctuations induced across the detector by these current fluctuations through the resistances strongly depend on the voltage bias on the source, due to the dynamic conductance of the source (SIS junction). The voltage fluctuations across the detector is thus the sum of two contributions:

$$S_V(\omega, V_S) = \underbrace{|Z(\omega, V_S)|^2\, S_{I,SIS}(\omega, V_S)}_{\text{Josephson junction qp noise}} + \underbrace{|Z'(\omega, V_S)|^2\, S_{I,R}(\omega)}_{\text{On-chip resistances}}$$

On the absorption side $(eV_D > 2\Delta)$, our detector is sensitive to environment effects (DCB) associated with the modification of the impedance of the environment: given that

the equilibrium noise of the resistances varies as $G\hbar\omega$, this contribution is presumably not negligible. We were not sensitive to these effects on the emission side, the thermal noise of the resistances being not significant at our working temperature (20 mK). To check the validity of this explanation, we have performed a numeric calculation of the expected PAT current, including these two contributions (shot noise of the source junction and dynamical Coulomb blockade effects): it appears that this scenario is in good agreement with the experimental data (see figure 4.14).
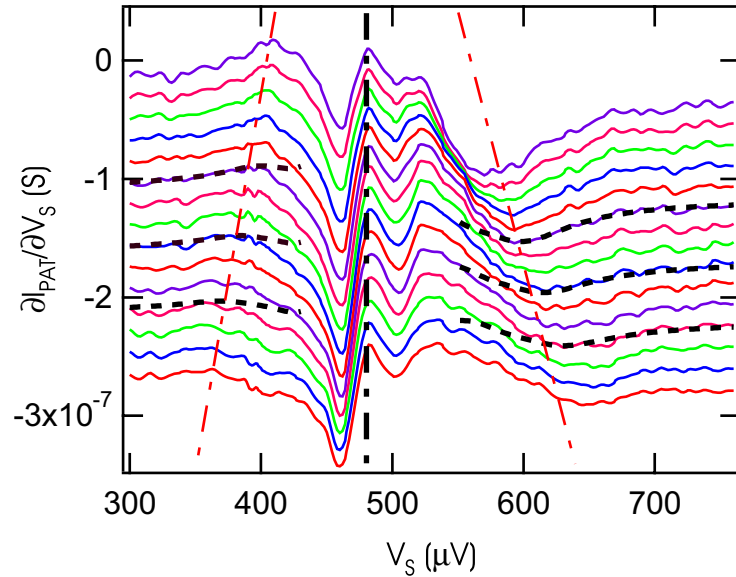

Figure 4.14: Shot noise and environment effects (DCB): derivative of the PAT current with respect to the voltage bias on the source $\partial I_{PAT}/\partial V_S$ *vs.* DC voltage bias on the source, for different DC voltage bias on the detector.

We have thus confirmed that our detector is sensitive to the non-symetrized noise correlator, and it can measure both emission and absorption. These environmental effects are interesting in a sense, because they reveal the presence of vacuum fluctuations (equilibrium noise of the polarization resistances), even though we observe them in an undirect way. The fact that we are not sensitive to these effects of environment on the emission regime ($eV_D < 2\Delta$) is another proof of the ability of our detector to distinguish emission from absorption.

Chapter 5

Conclusions and perspectives

In this experiment, we have shown that the distinction between negative/positive frequencies is relevant: in the quantum limit ($\hbar\omega \gg k\mathrm{T}$), time ordering of current operators must be considered. We checked that some detectors (said "quantum detectors") can distinguish the flow of energy coming from the device uner study (absorption), from the one flowing to it (emission). We also determine a criterion to predict what kind of detector is a good quantum detector: indeed, the theory of DCB shows that in a sense a NIN junction distinguishes emission/absorption processes, but there is no way for the experimentalist to separate the two contributions, since they all contribute at any bias. Let us now consider the DCB as a rectification process of the emission/absorption properties of the detector by its environment (actually the source and polarization resistances in our experiment): this is true in the limit of weak coupling ($\mathrm{R} < \mathrm{R}_q$). Thus, as mentionned earlier, the mechanisms of noise and detection are strongly related: the SIS junction is able to detect only emission processes when biased below the gap because its emission spectrum is zero in this range, and by so it cannot detect absorption processes. On the other hand, when it is biased above the gap, it is sensitive to both emission and absorption processes. However, as the absorption spectrum is almost flat, and the emission spectrum presents a singularity, it is more sensitive to absorption. To conclude, the reason why the SIS junction is a good quantum detector also explains the asymmetry of its noise spectrum.

It remains other issues to solve in the future:

- It would be interesting to detect the singularity at $(2\Delta + e\mathrm{V_S})/h$ in absorption: our detection scheme was sensitive to the frequency range $0 - 2\Delta/h$. Two approaches can used to detect this other type of emission processes: using a superconductor with a higher superconducting gap (niobium for example) in order to increase the range of sensitivity of the detection, or looking at the noise of a NIS junction. Indeed, a calculation in the frame of linear response theory (similarly to what is done to determine the emission/absorption properties of a SIS junction) predicts two singularities, as for the case of the SIS junction: one is the analog of the $(2\Delta + e\mathrm{V_S})/h$ absorption singularity, but is found at $(\Delta + e\mathrm{V_S})/h$. It would also be interesting reverse the roles played by the Josephson/NIS junctions, and see if a NIS junction could be a good noise detector (though its range of sensitivity is restricted to $0 - \Delta/h$).

- Another interesting approach would be to see if polarization resistances can be replaced by "on-chip" inductances. Indeed, as noticed in the experiment, our sensitivity decreases at high frequency due to the phase-sensitivity of our detector ($1/\omega^2$ dependence of the integrand in the expression of the PAT current). Replacing the polarization resistances by inductances would compensate this $1/\omega^2$ dependence, since

the transimpedance would then follow a ω dependence. Moreover, as these elements are non-dissipative, the measurement in absorption would be greatly simplified because they would emit no noise. There is just to ensure that the association of these inductances with the capacitances of the circuit create no parasitic resonances in the environment.

There are also many other ways to explore with "quantum detectors", among which the detection of cross-correlations [49][50], and third order cumulants [62][63]. However, methods involving qubits could reveal to be more tricky to realize than it appears at first sight: indeed, as the experiments of Astafiev *et al.* [19] revealed it, the coupling of qubits to two-level systems does not induce only dephasing. There might be also some coupling between the qubit and TLS at high frequency (inducing relaxation/excitation according to whether one considers absorption/emission), reducing the sensitivity of the qubit as a spectrometer: this issue might also be relevant for the detection of higher order cumulants.

Appendix A

I   Tunnel junction

A tunnel junction is characterized by low transmittency channels ($\forall\, n\mathrm{T}_n \ll 1$). Consequently, the Fano factor reads $\mathcal{F} = 1$. Let us now turn to devices with open channels, which leads to subpoissonian noise. Few conducting channels [64]

II   Chaotic cavity

In the frame of scattering theory, it can be shown that the transport properties of a chaotic cavity (without interactions) are fully characterized by the following transmittency probability law (see figure 5.1)

$$\mathrm{P(T)} = \frac{1}{\pi}\, \frac{1}{\sqrt{\mathrm{T}\,(1-\mathrm{T})}}$$
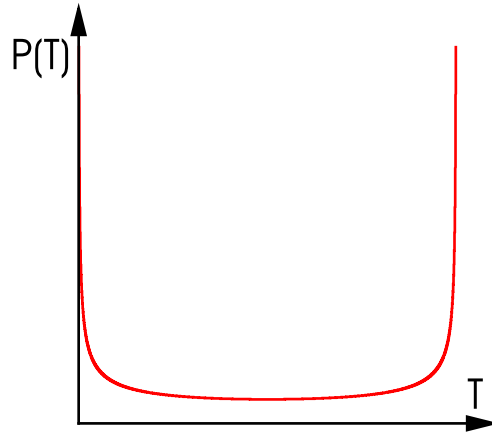

Figure 5.1: Distribution function of transmission coefficients T in a chaotic cavity.

The factor $1/\pi$ is a normalization factor which ensures that $\sum \mathrm{P(T)} = 1$. Indeed

$$\int_{\varepsilon}^{1-\varepsilon} \mathrm{P(T)} = \frac{1}{\pi}\int_{\varepsilon}^{1-\varepsilon} \frac{1}{\sqrt{\mathrm{T}\,(1-\mathrm{T})}} = \frac{1}{\pi}\left[2\,\mathrm{Arcsin}\,\sqrt{\mathrm{T}}\right]_{\varepsilon}^{1-\varepsilon} = 1$$

Consequently, the fano factor $\mathcal{F}$ reads

$$\mathcal{F} = \frac{\int_{\varepsilon}^{1-\varepsilon} T\,(1-T)\,P(T)dT}{\int_{\varepsilon}^{1-\varepsilon} T\,P(T)dT} = \frac{\int_{0}^{1} \sqrt{T\,(1-T)}dT}{\int_{0}^{1-\varepsilon} \sqrt{\frac{T}{(1-T)}}dT} = \frac{\pi/8}{\pi/2} = \frac{1}{4}$$

III   Diffusive wire

For a diffusive wire, the transmittency probability law reads[64][65] (see figure 5.2)

$$P(T) = \begin{cases} \dfrac{\ell_{\mathrm{el}}}{2\,L} \dfrac{1}{T\,\sqrt{1-T}} & \text{if } T_{\min} < T < 1 \; (T_{\min} = 4\,\exp[-2\,L/\ell_{\mathrm{el}}]) \\[2mm] 0 & \text{otherwise} \end{cases}$$
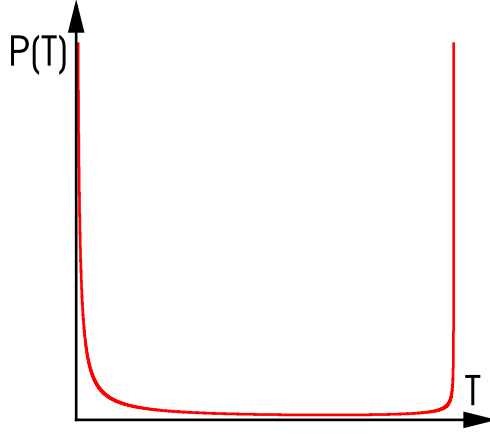

Figure 5.2: Distribution function of transmission coefficients T in a diffusive wire.

Similarly to the case of the chaotic cavity, the factor $\ell_{\mathrm{el}}/2\,L$ ensures the normalization of the probablity law $P(T)$

$$\begin{aligned}
\int_{T_{\min}}^{1-\varepsilon} P(T)dT &= \frac{\ell_{\mathrm{el}}}{2\,L} \int_{T_{\min}}^{1-\varepsilon} \frac{1}{T\,\sqrt{(1-T)}}dT \\
&= \frac{\ell_{\mathrm{el}}}{2\,L} \left[\ln T - 2\,\ln\left(1 + \sqrt{1-T}\right)\right]_{T_{\min}}^{1-\varepsilon} \\
&= \frac{\ell_{\mathrm{el}}}{2\,L}\,\ln\left(\frac{4}{T_{\min}}\right) = 1
\end{aligned}$$

The last approximation relies on the assumption that $T_{\min} \ll 1$: indeed, in a typical diffusive wire, the elastic mean free path ℓ_{el} is much smaller than the length of the wire L, so that $\exp(-L/\ell_{\mathrm{el}}) \gg 1$. The fano factor $\mathcal{F}$ reads

$$\mathcal{F} = \frac{\int_{T_{\min}}^{1-\varepsilon} T\,(1-T)\,P(T)dT}{\int_{T_{\min}}^{1-\varepsilon} T\,P(T)dT} = \frac{\int_{T_{\min}}^{1} \sqrt{1-T}dT}{\int_{T_{\min}}^{1-\varepsilon} \frac{1}{\sqrt{(1-T)}}dT} = \frac{\ell_{\mathrm{el}}/(3\,L)}{\ell_{\mathrm{el}}/L} = \frac{1}{3}$$

Appendix B

IV Derivation of the nonsymmetrized spectral density of the quasiparticle current in a Josephson junction

In this appendix, the expression of the non-symmetrized noise spectrum of a SIS junction is derived in the frame of linear response theory: the procedure used is very similar to the one developped by Rogovin and Scalapino [60] for the symmetrized case.
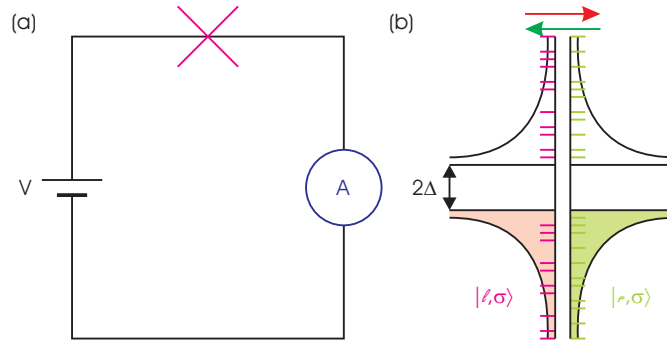

Figure 5.3: (a) - The SIS junction is supposed to be ideally voltage biased $(Z(\omega) = 0)$. (b) - Representation of the SIS junction $(T = 0)$: the eigenstates of the left and right electrodes, $|\ell, \sigma\rangle$ and $|r, \sigma\rangle$ respectively, are represented.

The hamiltonian of the junction, neglecting the environmental degrees of freedom, reads

$$\mathcal{H} = \mathcal{H}_{\mathrm{L}} + \mathcal{H}_{\mathrm{R}} + \mathcal{H}_{\mathrm{T}}$$

where $\mathcal{H}_{\mathrm{L}}$ and $\mathcal{H}_{\mathrm{R}}$ stand for the full many-body hamiltonians of the left and right electrode respectively, and $\mathcal{H}_{\mathrm{T}}$ is the tunneling hamiltonian[1]. It reads

$$\begin{cases} \mathcal{H}_{\mathrm{L}} = \sum\limits_{\ell,\sigma} \varepsilon_{\ell,\sigma} c^+_{\ell,\sigma} c_{\ell,\sigma} \quad \text{and} \quad \mathcal{H}_{\mathrm{R}} = \sum\limits_{r,\sigma} \varepsilon_{r,\sigma} c^+_{r,\sigma} c_{r,\sigma} \\ \mathcal{H}_{\mathrm{T}} = \mathcal{H}^+_{\mathrm{T}} + \mathcal{H}^-_{\mathrm{T}} = \sum\limits_{\ell,r,\sigma} \left\{ \mathrm{T}_{\ell r} c^+_{\ell,\sigma} c_{r,\sigma} + \mathrm{T}^\star_{\ell r} c^+_{r,\sigma} c_{\ell,\sigma} \right\} \end{cases}$$

One defines now two more operators N_{L} and N_{R}, for the number of quasiparticles in the left and right electrodes respectively

$$\begin{cases} N_{\mathrm{L}} = \sum\limits_{\ell,\sigma} c^+_{\ell,\sigma} c_{\ell,\sigma} \\ N_{\mathrm{R}} = \sum\limits_{r,\sigma} c^+_{r,\sigma} c_{r,\sigma} \end{cases}$$

---

[1]It is usually assumed that there is no spin-flip processes during tunneling.

Since N_L commute with the hamiltonian of the electrodes $\mathcal{H}_L$ and $\mathcal{H}_R$, the exact equation of motion for N_L reads

$$\dot{N}_L = \frac{1}{i\hbar}[N_L, \mathcal{H}] = \frac{1}{i\hbar}[N_L, \mathcal{H}_T]$$

Consequently, one finds for the current operator

$$I = \frac{ie}{\hbar}[N_L, \mathcal{H}_T] = \sum_{\ell r \sigma}\left\{ T_{\ell r}\left\langle\left[N_L, c_{\ell,\sigma}^+ c_{r,\sigma}\right]\right\rangle + T_{\ell r}^\star\left\langle\left[N_L, c_{r,\sigma}^+ c_{\ell,\sigma}\right]\right\rangle \right\} = I_+ + I_-$$

where I_+ and I_- stand for the backward and forward currents respectively. In the Schrödinger representation, it comes

$$\begin{cases} I_+(t) = \dfrac{ie}{\hbar}e^{i\frac{(\mathcal{H}_L+\mathcal{H}_R)t}{\hbar}}\, I_+\, e^{-i\frac{(\mathcal{H}_L+\mathcal{H}_R)t}{\hbar}} \\[2mm] I_-(t) = \dfrac{ie}{\hbar}e^{i\frac{(\mathcal{H}_L+\mathcal{H}_R)t}{\hbar}}\, I_-\, e^{-i\frac{(\mathcal{H}_L+\mathcal{H}_R)t}{\hbar}} \end{cases}$$

To first order in tunneling hamiltonian, the out of equilibrium current reads

$$I^1(t) = I^0(t) + \frac{i}{\hbar}\int_0^t\left[\mathcal{H}_T^0(t'), I^0(t)\right]\theta(t-t')\,dt'$$

The response functions read

$$\begin{cases} G_{+-}(t) = -i\left\langle[I_+(t), I_-(t')]\right\rangle\theta(t-t') \\[2mm] G_{-+}(t) = -i\left\langle[I_-(t), I_+(t')]\right\rangle\theta(t-t') \end{cases}$$

The $I(V)$ characteristic of the quasiparticle current through the junction can be related to the current-current response functions *via*

$$I_{qp,0}(V) = -\frac{2}{e}\text{Im}G_{-+}\frac{eV}{\hbar} = -\frac{2}{e}\text{Im}G_{+-}\frac{eV}{\hbar}$$

$$I_{qp,0}(V) = \frac{2\pi}{e}\left(1-e^{-\beta eV}\right)\sum_{\alpha,\beta}\frac{e^{-\beta E_\alpha}}{Z}|\langle\alpha|I_+|\beta\rangle|^2\,\delta\left(\omega_{\alpha\beta}-\frac{eV}{\hbar}\right)$$

Let us turn now to the nonsymmetrized current-current time correlator: the goal is to write this correlator as a spectral decomposition, similarly to what has been done for the quasiparticle current, in order to establish a relation between them. We first decompose the correlator in two parts,

$$C_I(t,t') = C_I^+(t) + C_I^-(t)$$

$$= e^{i\frac{eV(t-t')}{\hbar}}\langle I_+(t)I_-(t')\rangle + e^{-i\frac{eV(t-t')}{\hbar}}\langle I_-(t)I_+(t')\rangle$$

In the frame of linear response theory, the statistical average is performed as a thermal average over a set of eigenstates $|\alpha\rangle$ of the hamiltonian of the junction $(\mathcal{H}_L + \mathcal{H}_R)$ at equilibrium (assuming that the tunneling hamiltonian acts as a perturbation)

$$C_I^+(t,t') = e^{i\frac{eV(t-t')}{\hbar}}\sum_\alpha\frac{e^{-\beta E_\alpha}}{Z}\langle\alpha|e^{i\frac{(\mathcal{H}_L+\mathcal{H}_R)t}{\hbar}}I_+e^{-i\frac{(\mathcal{H}_L+\mathcal{H}_R)t}{\hbar}}e^{i\frac{(\mathcal{H}_L+\mathcal{H}_R)}{\hbar}t'}I_-e^{-i\frac{(\mathcal{H}_L+\mathcal{H}_R)}{\hbar}t'}|\alpha\rangle$$

Using the closure relation $\sum_\beta|\beta\rangle\langle\beta| = \mathbb{I}$, it comes

$$C_I^+(t,t') = e^{i\frac{eV(t-t')}{\hbar}}\sum_\alpha\frac{e^{-\beta E_\alpha}}{Z}\langle\alpha|e^{i\frac{(\mathcal{H}_L+\mathcal{H}_R)t}{\hbar}}I_+e^{-i\frac{(\mathcal{H}_L+\mathcal{H}_R)t}{\hbar}}|\beta\rangle$$

$$\times\langle\beta|e^{i\frac{(\mathcal{H}_L+\mathcal{H}_R)t'}{\hbar}}I_-e^{-i\frac{(\mathcal{H}_L+\mathcal{H}_R)t'}{\hbar}}|\alpha\rangle$$

By definition of the eigenstates $|\alpha\rangle$ and $|\beta\rangle$, one finds

$$C_I^+(t,t') = e^{i\frac{eV(t-t')}{\hbar}} \sum_\alpha \frac{e^{-\beta E_\alpha}}{Z} \langle\alpha| e^{i\frac{E_\alpha t}{\hbar}} I_+ e^{-i\frac{E_\beta t}{\hbar}} |\beta\rangle \langle\beta| e^{i\frac{E_\beta t'}{\hbar}} I_- e^{-i\frac{E_\alpha t'}{\hbar}} |\alpha\rangle$$

$$= C_I^+(t,t') = e^{i\frac{eV(t-t')}{\hbar}} \sum_\alpha \frac{e^{-\beta E_\alpha}}{Z} \langle\alpha| I_+ |\beta\rangle \langle\beta| I_- |\alpha\rangle e^{i(E_\alpha-E_\beta)(t-t')}$$

$$C_I^+(t,t') = \sum_{\alpha,\beta} \frac{e^{-\beta E_\alpha}}{Z} |\langle\alpha| I_+ |\beta\rangle|^2 e^{i\left(\omega_{\alpha\beta}+\frac{eV}{\hbar}\right)(t-t')}$$

The correlator is found to be only dependent of the time difference $(t-t')$, which is a sign of the time invariance. The nonsymmetrized current-current time correlator is thus expressed as a spectral decomposition

$$S_I^+(\omega, V) = \sum_{\alpha,\beta} \frac{e^{-\beta E_\alpha}}{Z} |\langle\alpha| I_+ |\beta\rangle|^2 \delta\left(\omega - \frac{eV}{\hbar}\right)$$

We have expressed both the $I(V)$ characteristic and current spectral density as a spectral decomposition over eigenstates of the hamiltonian of the electrodes. By identification between these two expressions, it comes

$$\begin{cases} I_{qp,0}\left(\hbar\omega/e - V\right) = \dfrac{2\pi}{e} \left(1 - e^{-\beta(\hbar\omega-eV)}\right) S_I^+(\omega, V) \\[2mm] I_{qp,0}\left(\hbar\omega/e + V\right) = \dfrac{2\pi}{e} \left(1 - e^{-\beta(\hbar\omega+eV)}\right) S_I^-(\omega, V) \end{cases}$$

The spectral density associated with the backward and forward currents respectively read

$$\begin{cases} S_I^+(\omega, V) = \dfrac{e}{2\pi} \dfrac{I_{qp,0}\left(\hbar\omega/e - V\right)}{1 - e^{-\beta(\hbar\omega-eV)}} \\[3mm] S_I^-(\omega, V) = \dfrac{e}{2\pi} \dfrac{I_{qp,0}\left(\hbar\omega/e + V\right)}{1 - e^{-\beta(\hbar\omega+eV)}} \end{cases}$$

These two contributions to the quasiparticle current noise spectral density of a Josephson junction can be understood qualitatively in terms of inelastic processes

- $S_I^+(\omega, V)$ corresponds to the backward tunneling current (eV is supposed to be positive): according to whether the junction is biased below or above the gap $2\Delta/e$, its noise spectrum presents a singularity in absorption at $(2\Delta - eV)/h$ or in emission at $(eV - 2\Delta)/h$ respectively (see figure 5.4).

- $S_I^-(\omega, V)$ corresponds to the forward tunneling current: whatever the bias regime on the junction, its noise spectrum presents a singularity in absorption at $(2\Delta + eV)/h$ (see figure 5.4).
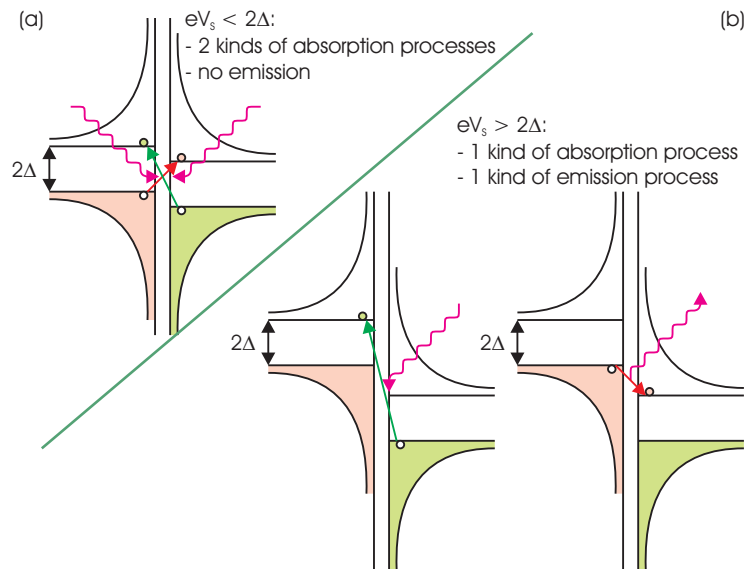
Figure 5.4: Inelastic processes involved in the tunneling of quasiparticles: these emission/absorption processes can be related with the current noise spectral density, and give an intuitive understanding of its asymmetry between negative/positive frequencies.

The noise spectral density of the quasiparticle current in a Josephson junction finally reads

$$
S_{I,0}(\omega, V) = \frac{e}{2\pi} \left[\frac{I_{qp,0}(\hbar\omega/e + V)}{1 - e^{-\beta(\hbar\omega + eV)}} + \frac{I_{qp,0}(\hbar\omega/e - V)}{1 - e^{-\beta(\hbar\omega - eV)}} \right]
$$

It can be checked that the quantum fluctuation-dissipation theorem is recovered [11]

$$
S_{I,0}(\omega, V = 0) = \frac{e}{\pi} \frac{I_{qp,0}(\hbar\omega/e)}{1 - e^{-\beta\,\hbar\omega}} = \frac{G_Q(\omega, V = 0)}{\pi} \frac{\hbar\omega}{1 - e^{-\beta\,\hbar\omega}}
$$

V   Environmental effects

In this section, the retroaction of the environment on the current noise spectrum of a SIS junction will be evaluated: the junction is considereded to be non-ideally voltage biased, which is taken into account by means of a finite impedance $Z(\omega)$ in series with the junction (see figure 5.5).
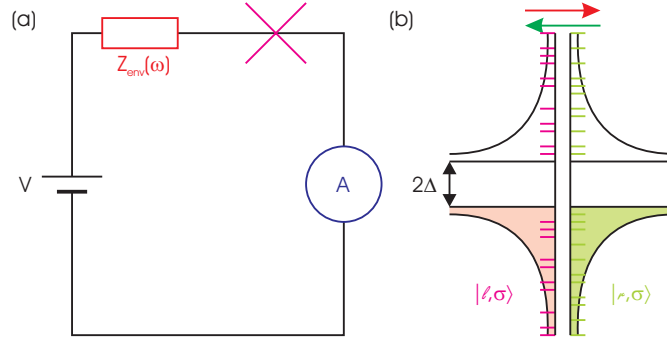
Figure 5.5: (a) - The SIS junction is biased by a non-ideal voltage source ($Z(\omega) \neq 0$). (b) - Representation of the SIS junction ($T = 0$): the eigenstates of the left and right electrodes, $|\ell, \sigma\rangle$ and $|r, \sigma\rangle$ respectively, are represented.

The eigenstates for the quasiparticle states in the left/right electrodes are slightly modified by the environment

$$\begin{cases} |\mathcal{A}\rangle = |\alpha\rangle \otimes |\mathcal{E}\rangle \\ |\mathcal{B}\rangle = |\beta\rangle \otimes |\mathcal{E}'\rangle \end{cases}$$

In presence of an unspecified environment $Z(\omega)$, the tunneling hamiltonian $\mathcal{H}_T$ is modified according to

$$\mathcal{H}_T = \mathcal{H}_T^+ + \mathcal{H}_T^- = \sum_{\ell, r, \sigma} \left\{ T_{\ell r} c_{\ell,\sigma}^+ c_{r,\sigma} \, e^{-i\,\delta\varphi} + T_{\ell r}^\star c_{r,\sigma}^+ c_{\ell,\sigma} \, e^{i\,\delta\varphi} \right\}$$

The spectral decomposition previously established is thus slightly modified by the coupling to the environment

$$I_{qp}(V) = \frac{2\pi}{e} \left(1 - e^{-\beta e V} \right) \sum_{\alpha, \beta, \mathcal{E}, \mathcal{E}'} \frac{e^{-\beta E_\alpha}}{Z} |\langle \alpha | I_+ | \beta \rangle|^2 \, P\left(\omega_{\alpha\beta} - \frac{eV}{\hbar} \right)$$

Similarly, it can be shown that the contributions of the backward and forward tunneling currents to the current noise spectral density read

$$\begin{cases} S_I^+(\omega, V) = \sum_{\alpha, \beta} \frac{e^{-\beta E_\alpha}}{Z} |\langle \alpha | I_+ | \beta \rangle|^2 \, P\left(-\frac{eV}{\hbar} \right) \\ S_I^-(\omega, V) = \sum_{\alpha, \beta} \frac{e^{-\beta E_\alpha}}{Z} |\langle \alpha | I_- | \beta \rangle|^2 \, P\left(\frac{eV}{\hbar} \right) \end{cases}$$

One finally finds out

$$S_I(\omega, V) = \frac{e}{2\pi} \left[\frac{I_{qp}(\hbar\omega/e + V)}{1 - e^{-\beta(\hbar\omega + eV)}} + \frac{I_{qp}(\hbar\omega/e - V)}{1 - e^{-\beta(\hbar\omega - eV)}} \right]$$

where I_{qp} stands for the $I(V)$ characteristic of the SIS junction, in presence of an unspecified environment.

Appendix C

VI Derivation of the expression for the PAT current in a SIS junction

If one assume that $J(t) \ll 1$, the energy exchange probability $P(\varepsilon)$ reads

$$P(\varepsilon) = \frac{1}{2\pi\,\hbar} \int_{-\infty}^{+\infty} \exp[J(t)]\, e^{i\varepsilon t/\hbar}\, dt$$

$$= \frac{1}{2\pi\,\hbar} \int_{-\infty}^{+\infty} [1 + J(t)]\, e^{i\varepsilon t/\hbar}\, dt$$

$$= \frac{1}{2\pi\,\hbar} \int_{-\infty}^{+\infty} e^{i\varepsilon t/\hbar}\, dt + \frac{1}{2\pi\,\hbar} \int_{-\infty}^{+\infty} J(t)\, e^{i\varepsilon t/\hbar}\, dt$$

$$P(\varepsilon) = \frac{1}{2\pi\,\hbar}\, \delta(\varepsilon) + \frac{1}{2\pi\,\hbar} \int_{-\infty}^{+\infty} J(t)\, e^{i\varepsilon t/\hbar}\, dt$$

The phase-phase correlator is related to the current fluctuations through the source *via*

$$J(t) = \frac{2\pi}{\hbar\,R_q} \int_{-\infty}^{+\infty} \frac{|Z(\omega)|^2}{\omega^2} S_I(\omega)\, [\exp(-i\omega t) - 1]\, d\omega$$

It thus comes

$$\frac{1}{2\pi\,\hbar} \int_{-\infty}^{+\infty} J(t)\, e^{i\varepsilon t/\hbar}\, dt \;=\; \frac{1}{2\pi\,\hbar} \int_{-\infty}^{+\infty} \frac{2\pi}{\hbar\,R_q} \int_{-\infty}^{+\infty} \frac{|Z(\omega)|^2}{\omega^2} S_I(\omega)\, [\exp(-i\omega t) - 1]\, d\omega\, e^{i\varepsilon t/\hbar}\, dt$$

$$= \frac{1}{\hbar^2\,R_q} \int_{-\infty}^{+\infty} \frac{|Z(\omega)|^2}{\omega^2} S_I(\omega) \left\{ \int_{-\infty}^{+\infty} [\exp(-i\omega t) - 1]\, e^{i\varepsilon t/\hbar}\, dt \right\} d\omega$$

$$= \frac{1}{\hbar^2\,R_q} \int_{-\infty}^{+\infty} \frac{|Z(\omega)|^2}{\omega^2} S_I(\omega) \left\{ \int_{-\infty}^{+\infty} e^{i\,(\varepsilon/\hbar - \omega)t}\, dt \right\} d\omega$$

$$- \frac{2\pi}{\hbar\,R_q} \int_{-\infty}^{+\infty} d\omega \frac{|Z(\omega)|^2}{\omega^2} S_I(\omega)\delta(\varepsilon)$$

$$= \frac{1}{\hbar^2\,R_q} \int_{-\infty}^{+\infty} \frac{|Z(\omega)|^2}{\omega^2} S_I(\omega)\, [2\pi\,\hbar\,\delta(\varepsilon - \hbar\omega)]\, d\omega$$

$$- \frac{2\pi}{\hbar\,R_q} \int_{-\infty}^{+\infty} d\omega \frac{|Z(\omega)|^2}{\omega^2} S_I(\omega)\delta(\varepsilon)$$

$$\frac{1}{2\pi\,\hbar} \int_{-\infty}^{+\infty} J(t)\, e^{i\varepsilon t/\hbar}\, dt \;=\; \frac{2\pi}{R_q} \frac{|Z(\varepsilon/\hbar)|^2}{\varepsilon^2} S_I(\varepsilon/\hbar) - \frac{2\pi}{\hbar\,R_q} \int_{-\infty}^{+\infty} d\omega \frac{|Z(\omega)|^2}{\omega^2} S_I(\omega)\delta(\varepsilon)$$

The relation between $P(\varepsilon)$ and the noise properties of the environment established by Aguado *et al.* [22] is recovered

$$
\boxed{P(\varepsilon) = \left[1 - \frac{2\pi}{\hbar\,R_q} \int_{-\infty}^{+\infty} d\omega \frac{|Z(\omega)|^2}{\omega^2} S_I(\omega) \right] \delta(\varepsilon) + \frac{2\pi}{R_q} \frac{|Z(\varepsilon/\hbar)|^2}{\varepsilon^2} S_I(\varepsilon/\hbar)}
$$

$$
I_{\mathrm{PAT}}(V) = I_{\mathrm{qp}}(V) - I_{\mathrm{qp},0}(V)
$$

$$
= \int_0^{+\infty} P(eV - \varepsilon)\, I_{\mathrm{qp},0}(\varepsilon/e)\, d\varepsilon - I_{\mathrm{qp},0}(V)
$$

The elastic contributions compensate each other

$$
\begin{aligned}
I_{\mathrm{PAT}}(V) \;=\;& \int_0^{+\infty} \left\{ \left[1 - \frac{2\pi}{\hbar\,R_q} \int_{-\infty}^{+\infty} d\omega \frac{|Z(\omega)|^2}{\omega^2} S_I(\omega) \right] \delta(eV - \varepsilon) \right. \\
& \left. + \frac{2\pi}{R_q} \frac{|Z[(eV - \varepsilon)/\hbar]|^2}{(eV - \varepsilon)^2} S_I[(eV - \varepsilon)/\hbar] \right\} I_{\mathrm{qp},0}(\varepsilon/e)\, d\varepsilon - I_{\mathrm{qp},0}(V) \\
\;=\;& \left[\cancel{1} - \frac{2\pi}{\hbar\,R_q} \int_{-\infty}^{+\infty} d\omega \frac{|Z(\omega)|^2}{\omega^2} S_I(\omega) \right] I_{\mathrm{qp},0}(V) \\
& + \frac{2\pi}{R_q} \int_0^{+\infty} \frac{|Z[(eV - \varepsilon)/\hbar]|^2}{(eV - \varepsilon)^2} S_I[(eV - \varepsilon)/\hbar]\, I_{\mathrm{qp},0}(\varepsilon/e)\, d\varepsilon - \cancel{I_{\mathrm{qp},0}(V)}
\end{aligned}
$$

The first term can be recast in the following way

$$
-\frac{2\pi}{\hbar\,R_q} \int_{-\infty}^{+\infty} d\omega \frac{|Z(\omega)|^2}{\omega^2} S_I(\omega)\, I_{\mathrm{qp},0}(V) = -\int_{-\infty}^{+\infty} \left(\frac{e}{\hbar\omega} \right)^2 S_V(\omega)\, I_{\mathrm{qp},0}(V)\, d\omega
$$

The $1/\omega^2$ dependence of the integrand is related to the fact that our detector is sensitive to phase fluctuations: it fixes a limit to our sensitivity at high frequency. We now perform the change of variable $\omega = (eV - \varepsilon)/\hbar$ for the second term, and it comes

$$
\begin{aligned}
& \frac{2\pi}{R_q} \int_0^{+\infty} \frac{|Z[(eV - \varepsilon)/\hbar]|^2}{(eV - \varepsilon)^2} S_I[(eV - \varepsilon)/\hbar]\, I_{\mathrm{qp},0}(\varepsilon/e)\, d\varepsilon \\
& \hspace{4cm} = \frac{2\pi}{R_q} \int_{eV/\hbar}^{-\infty} \frac{S_V(\omega)}{(\hbar\omega)^2} I_{\mathrm{qp},0}\left(V - \frac{\hbar\omega}{e} \right) (-\hbar\, d\omega)
\end{aligned}
$$

This last integral can be cut in two terms: the first one corresponding to the emission ($\omega < 0$), and the second one to the absorption ($\omega > 0$). It is thus found

$$
\begin{aligned}
& \frac{2\pi\,\hbar}{R_q} \int_{-\infty}^{eV/\hbar} \frac{S_V(\omega)}{(\hbar\omega)^2} I_{\mathrm{qp},0}\left(V - \frac{\hbar\omega}{e} \right) d\omega \\
& = \int_{-\infty}^0 \left(\frac{e}{\hbar\omega} \right)^2 S_V(\omega)\, I_{\mathrm{qp},0}\left(V - \frac{\hbar\omega}{e} \right) d\omega + \int_0^{eV/\hbar} \left(\frac{e}{\hbar\omega} \right)^2 S_V(\omega)\, I_{\mathrm{qp},0}\left(V - \frac{\hbar\omega}{e} \right) d\omega
\end{aligned}
$$

After performing a last change of variable on the first term ($\omega' = -\omega$), the expression of the PAT current finally reads

$$
\begin{aligned}
\mathrm{I}_{\mathrm{PAT}}(\mathrm{V}) \ = \ & \int_0^{+\infty} \mathrm{d}\omega \left(\frac{e}{\hbar\omega}\right)^2 \mathrm{S_V}(-\omega)\,\mathrm{I}_{\mathrm{qp},0}\left(\mathrm{V}+\frac{\hbar\omega}{e}\right) \\
& + \int_0^{e\mathrm{V}} \mathrm{d}\omega \left(\frac{e}{\hbar\omega}\right)^2 \mathrm{S_V}(\omega)\,\mathrm{I}_{\mathrm{qp},0}\left(\mathrm{V}-\frac{\hbar\omega}{e}\right) \\
& - \int_{-\infty}^{-\infty} \mathrm{d}\omega \left(\frac{e}{\hbar\omega}\right)^2 \mathrm{S_V}(\omega)\,\mathrm{I}_{\mathrm{qp},0}(\mathrm{V})
\end{aligned}
$$

PHYSICAL REVIEW LETTERS

Emission and Absorption Asymmetry in the Quantum Noise of a Josephson Junction

P.-M. Billangeon,[1] F. Pierre,[2] H. Bouchiat,[1] and R. Deblock[1]

[1]*Laboratoire de Physique des Solides, associé au CNRS, Bâtiment 510 Université Paris-Sud, 91405 Orsay Cedex, France*
[2]*Laboratoire de Photonique et Nanostructures, associé au CNRS, Route de Nozay, 91460 Marcoussis, France*

We measure current fluctuations of mesoscopic devices in the quantum regime, when the frequency is of the order of or higher than the applied voltage or temperature. Detection is designed to probe separately the absorption and emission contributions of current fluctuations, i.e. the positive and negative frequencies of the Fourier transformed nonsymmetrized noise correlator. It relies on measuring the quasiparticles photon assisted tunneling current across a superconductor-insulator-superconductor junction (the detector junction) caused by the excess current fluctuations generated by quasiparticles tunneling across a Josephson junction (the source junction). We demonstrate unambiguously that the negative and positive frequency parts of the *nonsymmetrized* noise correlator are separately detected and that the excess current fluctuations of a voltage biased Josephson junction present a strong asymmetry between emission and absorption.

Non equilibrium current fluctuations detection is a powerful tool to get information not accessible by transport experiments on mesoscopic systems [1]. Whereas there are now a number of current noise measurements at low frequencies on different systems, there have been only a few measurements in the frequency range 1–100 GHz, which is experimentally more challenging [2–4]. Such frequencies correspond to the typical energy scales and inverse propagation times involved in most mesoscopic phenomena. They also correspond to the transition to quantum noise, when $\hbar\omega \gtrsim eV, k_B T$. Whereas book knowledge is that the measurable physical quantity in such experiments is the *symmetrized* noise correlator, i.e., $C_{\text{sym}}(\tau) = \langle I(t + \tau)I(t) + I(t)I(t + \tau)\rangle$ [or alternatively the symmetrized density spectrum $S_{\text{sym}}(\omega)$ of the noise, i.e., the Fourier transform of $C_{\text{sym}}(\tau)$], several recent theoretical works have pointed out that with an appropriate detection scheme, one could measure the spectral density $S(\omega)$ [5] of the *nonsymmetrized* noise correlator $C(\tau) = \langle I(t)I(t + \tau)\rangle$ [6–8]. Measuring the nonsymmetrized noise means being able to distinguish between emission ($\omega < 0$, energy flows to the detector) and absorption ($\omega > 0$, energy flows from the detector) of the device under test. Experimentally it is difficult to distinguish unambiguously between symmetrized and nonsymmetrized noise, partly because what is often measured is the excess noise, i.e., the difference between current fluctuations at a given bias and zero bias. In most systems studied so far at high frequencies (diffusive wire [2], normal tunnel junction, quantum point contact [8], Josephson junction at high voltage [4]) the spectral density of the nonsymmetrized excess noise $S^{\text{exc}}(\omega)$ is an even function of the frequency [$S^{\text{exc}}(\omega) = S^{\text{exc}}(-\omega)$] when $\hbar\omega \gg k_B T$. Consequently, the excess symmetrized noise $S_{\text{sym}}^{\text{exc}}(\omega) = S^{\text{exc}}(\omega) + S^{\text{exc}}(-\omega)$ differs only by a factor of 2 (measured in Ref. [4]) from the nonsymmetrized excess noise. Thus excess noise experiments in the quantum regime can usually indifferently be explained by using nonsymmetrized or symmetrized noise expression. To know precisely what quantity is measured in such experiments a noise source with an asymmetric excess nonsymmetrized noise is needed together with a good understanding of the detection process. In this Letter we show that the current fluctuations due to quasiparticles tunneling across a Josephson junction have a clear and testable difference between absorption and emission noise. This allows us to prove that, with the detection scheme described hereafter, the emission and absorption part of nonsymmetrized noise are separately measured.

The device probed in this experiment consists of two small Josephson junctions (estimated capacitance 1 fF) coupled capacitively to each other. Both junctions are made of aluminum (superconducting gap $\Delta = 240$ μeV) and embedded in an on-chip environment constituted by resistances (8 Pt wires, $R = 750$ Ω, length $= 40$ μm, width $= 750$ nm, thickness $= 15$ nm) and capacitances (estimated value $C_C \approx 750$ fF, size: 23×25 μm^2, insulator: 65 nm of Al$_2$O$_3$) designed to provide a good high-frequency coupling between the two junctions (Fig. 1). The design of the sample is similar to Ref. [4], with the addition of shunt capacitances (estimated value 500 fF $< C_S <$ 750 fF) after the on-chip resistances. Those capacitances act as short circuits at high frequencies thus isolating the on-chip circuit from the external circuit. Each junction has a SQUID geometry in order to tune the critical current with a magnetic flux. By using different SQUID areas for the two junctions the magnetic flux is adjusted to have a high critical current for one junction and a small one for the other. The junctions will hereafter be called source and detector junction. The sample is measured through filtered lines in a dilution refrigerator of base temperature 20 mK. The detection is performed by studying how the current-voltage characteristics of the detector is modified by the presence of the source and its dc polarization [4]. There have been recently several proposals and/or experiments of similar detection schemes using as detector double dots

[8], quantum bits [9], or the Josephson branch of a superconducting junction [10,11].

In the present work we measure the photon assisted tunneling (PAT) quasiparticle current through the detector due to the high-frequency current fluctuations of the source. This current can be calculated by considering how the detector characteristic is modified by its electromagnetic environment, i.e., the source junction and the on-chip circuit [4,8,12]. Note that such a detection scheme is very general and requires only a detector with a nonlinear $I(V)$ characteristic. For the particular case of a superconductor-insulator-superconductor junction the PAT current $I_{\mathrm{PAT}}(V_D)$ of the detector, in the regime eV_D, $\hbar\omega \gg k_B T$, is:

$$
\begin{aligned}
I_{\mathrm{PAT}}(V_D) &= I_{\mathrm{QP}}(V_D) - I_{\mathrm{QP},0}(V_D) \\
&= \int_0^{+\infty} d\omega \left(\frac{e}{\hbar\omega}\right)^2 S_V(-\omega) I_{\mathrm{QP},0}\left(V_D + \frac{\hbar\omega}{e}\right) \\
&\quad + \int_0^{eV_D} d\omega \left(\frac{e}{\hbar\omega}\right)^2 S_V(\omega) I_{\mathrm{QP},0}\left(V_D - \frac{\hbar\omega}{e}\right) \\
&\quad - \int_{-\infty}^{+\infty} d\omega \left(\frac{e}{\hbar\omega}\right)^2 S_V(\omega) I_{\mathrm{QP},0}(V_D) \qquad (1)
\end{aligned}
$$

with $S_V(\omega)$ the nonsymmetrized spectral density of excess voltage fluctuations at frequency ω across the detector and $I_{\mathrm{QP},0}(V_D)$ the $I(V)$ characteristic of the detector when the source is not polarized. $S_V(\omega)$ is related to the current fluctuations of the source $S_I(\omega, V_S)$ through the transimpedance $Z(\omega)$ determined by the on-chip circuitry $[S_V(\omega) = |Z(\omega)|^2 S_I(\omega, V_S)]$. Note that this experiment is only sensitive to the excess noise of the source, its equilibrium noise being accounted for in $I_{\mathrm{QP},0}(V_D)$. The different terms of Eq. (1) contribute only when the argument of $I_{\mathrm{QP},0}$ is higher than $2\Delta/e$ (i.e., $I_{\mathrm{QP},0} \neq 0$). This defines two regimes of detection. When $|eV_D| < 2\Delta$ only the first term in Eq. (1) contributes: we are then measuring the emission of the source [Fig. 1(a), left]. When $|eV_D| > 2\Delta$, all the terms contribute but with a stronger weight for the absorption by the source [Fig. 1(a), right]. Note that the measurement sensitivity is similar in emission and absorption.

We first present data when $|eV_S| < \Delta$, with V_S the bias of the source. The high-frequency current across the source is then nearly monochromatic and originates from the ac Josephson effect. This current is $I(t) = I_C \sin(2\pi\nu_J t)$ with $\nu_J = 2eV_S/h$ the Josephson frequency and $I_C = \pi\Delta/(2eR_T)$ the critical current determined by the source's normal state resistance R_T [13]. In the frequency domain it leads to a peak in absorption at $+\nu_J$ and one in emission at $-\nu_J$. Consequently, the spectrum of the current fluctuations of the source is symmetric between emission and absorption. The PAT current through the detector is shown on Fig. 2. To maximize sensitivity we modulate the source voltage V_S and use a lock-in detection technique to measure $\partial I_{\mathrm{PAT}}(V_D)/\partial V_S$. Whereas this quantity is not directly the derivative of the noise of the source $\partial S_I(\omega, V_S)/\partial V_S$, both look alike and display the same features, thanks to the
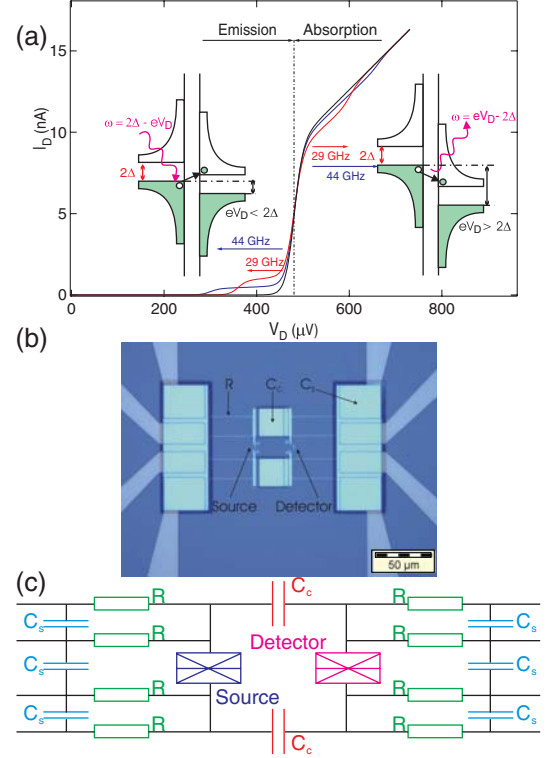

FIG. 1 (color online). (a) Calculated $I(V)$ of the detector under monochromatic irradiation (black curve without irradiation), with frequency indicated on the figure and high enough amplitude to have a visible PAT current, and schematic pictures of the tunneling process involved in the PAT current through the detector. Left: $|V_D| < 2\Delta/e$, only emission by the source can lead to PAT. Right: $|V_D| > 2\Delta/e$ the detector is mainly sensitive to absorption by the source. (b) Optical picture of the sample, showing the two junctions and the on-chip circuitry. (c) Equivalent circuit of the sample, with $R = 750\ \Omega$, $C_C \approx 750$ fF.

sharp BCS density of states near the gap. Figure 2(a) corresponds to the case where the detector is polarized to be sensitive only to the emission of the source ($eV_D < 2\Delta$). For Fig. 2(b), $eV_D > 2\Delta$ so the detector is mainly sensitive to absorption by the source. Both curves display a peak in frequency at $2eV_S/h$, which is expected from the frequency dependence of the ac Josephson effect. This similarity between emission and absorption data reflects the symmetry of current fluctuations. As done in Ref. [4] this signal can be used to extract the value of the transimpedance $Z(\omega)$ of the on-chip circuit versus frequency [Fig. 2(c)]. Despite the careful design of the on-chip circuitry, there is a difference between the measured and predicted transimpedance, which is attributed to not negligible capacitive coupling between electrodes and ground planes, or cross talk between on-chip elements. The frequency independent peak observed in absorption close to $V_S = 0$ is related to the change of the source junction impedance on the Josephson branch. This slightly changes the impedance Z_{env} of the detector electromagnetic environment and thus the current of the detector [12].
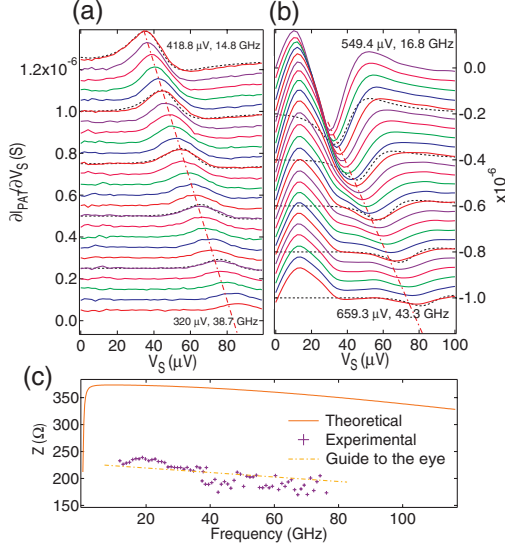
FIG. 2 (color online). (a), (b) PAT current at different detector bias (indicated on the figure) due to the ac Josephson effect ($eV_S < \Delta$). The curves are shifted vertically for clarity. (a) corresponds to the emission part ($V_D < 2\Delta/e$) and (b) to the absorption part ($V_D > 2\Delta/e$). Both exhibit a signature of the ac Josephson effect at the Josephson frequency $2eV_S/h$ (indicated by the dot-dashed lines). The peak near $V_S = 0$ in absorption is due to the variation of the source impedance on the Josephson branch. The dashed lines are calculated curves with the transimpedance as adjustable parameter. (c) Transimpedance extracted from the data.

We now present data taken with the source polarized in the vicinity of the quasiparticle branch ($eV_S \approx 2\Delta$). This regime, dominated by the shot noise of quasiparticles, was considered to be nearly frequency independent in previous studies for bias high compared with $2\Delta/e$ [4]. Our data shows a frequency dependence of this noise, both in emission [Fig. 3(a)], with a singularity at frequency ($eV_S - 2\Delta)/h$ for $eV_S > 2\Delta$, and in absorption [Fig. 3(b)], in particular with a singularity at frequency ($2\Delta - eV_S)/h$ for $eV_S < 2\Delta$. These differences in the data reflect an asymmetry between emission and absorption. The singularities are related, *via* the $I(V)$ characteristic of the source, to the superconducting density of states in the vicinity of the gap according to the calculated following expression for the nonsymmetrized current fluctuations spectrum due to quasiparticle tunneling (the symmetrized spectrum was derived in Ref. [14]):

$$S_I(\omega, V_S) = \frac{e}{2\pi}\left[\frac{I_{\mathrm{QP}}(\hbar\omega/e + V_S)}{1 - \exp(-\frac{\hbar\omega + eV_S}{kT})}\right.$$
$$\left. + \frac{I_{\mathrm{QP}}(\hbar\omega/e - V_S)}{1 - \exp(-\frac{\hbar\omega - eV_S}{kT})}\right] \quad (2)$$

From Eq. (2), in the limit of low temperature, for $0 < eV_S < 2\Delta$ there is only *absorption noise* with steplike singularities (which derivative gives rise to peaks) at $\hbar\omega = 2\Delta \pm eV_S$, whereas for $eV_S > 2\Delta$ there are *both emission*
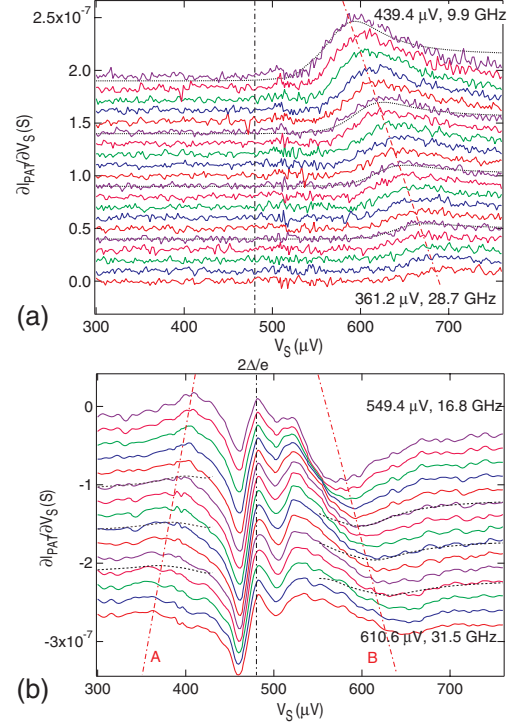

FIG. 3 (color online). PAT current at different bias of the detector (indicated on the figure) when the source is polarized in the vicinity of 2Δ. The curves are shifted vertically for clarity. (a) Emission part ($eV_D < 2\Delta$): there is a singularity at frequency ($eV_S - 2\Delta)/h$ for $eV_S > 2\Delta$ related to the emission of the source (indicated by the dot-dashed line). (b) Absorption part ($eV_D > 2\Delta$): there are two singularities, one at $2\Delta - eV_S$ for $eV_S < 2\Delta$ (line A) and one at $eV_S - 2\Delta$ for $eV_S > 2\Delta$ (line B). They are related to the absorption spectrum of the source and to a change of the environment impedance (see text). The dashed lines are simulations of the expected signal taking into account the measured value of $Z(\omega)$.

and absorption noise, with a singularity in emission at $\hbar\omega = eV_S - 2\Delta$, and a singularity in absorption at $\hbar\omega = 2\Delta + eV_S$ (Fig. 4). This system thus exhibits a very interesting feature in the context of noise detection: the excess current noise has an asymmetry between emission and absorption. Note that at $V_S = 0$ and $T = 0$, up to frequency $2\Delta/h$ there is no absorption noise so that excess noise and noise coincide. At higher frequencies, the excess (absorption) noise can be negative. This feature is beyond our detection range, limited to $|\hbar\omega| < 2\Delta$.

For emission ($eV_D < 2\Delta$), from the transimpedance and the $I(V)$ characteristic of the detector we numerically calculate the expected signal for the PAT current (dashed lines in Fig. 3). Our calculation reproduces accurately the data, and notably the existence of a peak at $eV_S > 2\Delta$ (source emission) and the absence of peak at $eV_S < 2\Delta$ (source absorption). Using Eq. (2) one can calculate the symmetrized noise (inset of Fig. 4). It presents the singularity in the emission noise ($eV_S > 2\Delta$) described before but also another singularity at frequency ($2\Delta - eV_S)/h$, when $eV_S < 2\Delta$, which is related to the absorption side of
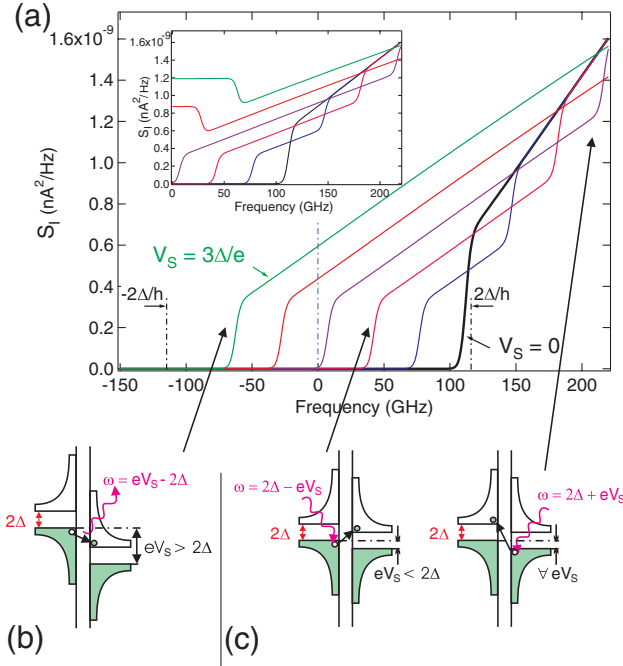
FIG. 4 (color online). (a) Predicted nonsymmetrized current fluctuations of the quasiparticle current of a Josephson junction at low temperature for different bias conditions. The highest frequency the experiment is sensitive to is $2\Delta/h = 115$ GHz. Inset: corresponding symmetrized current fluctuations. (b) Illustration of the tunneling process leading to the singularity in the emission noise ($eV_S > 2\Delta$). (c) Tunneling processes for singularities in absorption noise.

the current fluctuations. This singularity is not present in our data for emission, proving that, when $eV_D < 2\Delta$, only the emission part of the current fluctuations is detected.

The situation is more complicated for the absorption part ($eV_D > 2\Delta$) because there are two contributions to the excess voltage fluctuations across the detector, leading to a modification of its characteristic $I(V_D)$ with V_S: (1) the contribution of the absorption part of the excess current fluctuations spectrum of the source, given by Eq. (2) which leads to a singularity at frequency $(2\Delta - eV_S)/h$ for $eV_S < 2\Delta$; (2) the contribution to the excess voltage fluctuations due to the absorption current noise of the resistive part of the on-chip circuitry ($S_I(\omega) = 2\hbar\omega/(2\pi R)$) for a resistance R at $T = 0$ K). Contribution 2 is not zero due to the change of the impedance $Z_{\text{env}}(\omega)$ of the detector environment with V_S, *via* the source impedance. The source impedance is significantly modified when $eV_S \approx 2\Delta$ [leading to the frequency independent features at $V_S \approx 2\Delta/e$ on Fig. 3(b)] and presents also a high-frequency dependence [15], with a real part given by

$$\sigma(\omega, V_S) = e\frac{I_{\text{QP}}(V_S + \hbar\omega/e) - I_{\text{QP}}(V_S - \hbar\omega/e)}{2\hbar\omega}, \quad (3)$$

leading to a significant change when $\hbar\omega = \pm|2\Delta - eV_S|$.

Whereas the singularity at $V_S > 2\Delta/e$ [line B of Fig. 3(b)] is only related to contribution 2, the feature at $V_S < 2\Delta/e$ (line A) results from contributions 1 and 2, which add with different sign. This is supported by numerical calculation [dashed lines on Fig. 3(b)], which reproduces qualitatively these features. The signature of the singularity in the absorption of the source junction is the reduced peak amplitude at $V_S < 2\Delta/e$ (line A) compared with the dip at $V_S > 2\Delta/e$ (line B).

In conclusion, we have shown in this work that by measuring the PAT current of a superconducting junction we are able to measure separately, and with comparable sensitivities, the contribution of emission and absorption to the *nonsymmetrized* current fluctuations of the source. For this particular detection scheme, the symmetrized current fluctuations are not relevant, because they mix emission and absorption. Whether this is a general property of any current fluctuations detection scheme in the quantum regime is an interesting issue. We also showed that the current fluctuations due to quasiparticle tunneling in a Josephson junction present a strong asymmetry between emission and absorption, with singularities in emission or absorption depending on the bias condition.

[1] Y. M. Blanter and M. Büttiker, Phys. Rep. **336**, 1 (2000).
[2] R. J. Schoelkopf *et al.*, Phys. Rev. Lett. **78**, 3370 (1997).
[3] R. H. Koch, D. J. Van Harlingen, and J. Clarke, Phys. Rev. Lett. **47**, 1216 (1981).
[4] R. Deblock, E. Onac, L. Gurevich, and L. P. Kouwenhoven, Science **301**, 203 (2003).
[5] Note that whereas $C(\tau)$ is not a real quantity, due to the noncommutation of the current operator at different times, $S(\omega)$ is a real quantity.
[6] G. B. Lesovik and R. Loosen, JETP Lett. **65**, 295 (1997).
[7] U. Gavish, Y. Levinson, and Y. Imry, Phys. Rev. B **62**, R10637 (2000).
[8] R. Aguado and L. P. Kouwenhoven, Phys. Rev. Lett. **84**, 1986 (2000).
[9] R. J. Schoelkopf *et al.*, in *Quantum Noise in Mesoscopic Physics*, edited by Y. V. Nazarov, NATO Science Series (Kluwer, Dordrecht, 2003).
[10] T. T. Heikkilä, P. Virtanen, G. Johansson, and F. K. Wilhelm, Phys. Rev. Lett. **93**, 247005 (2004).
[11] R. K. Lindell *et al.*, Phys. Rev. Lett. **93**, 197002 (2004).
[12] G. L. Ingold and Yu. V. Nazarov, in *Single-Charge Tunneling*, edited by H. Grabert and M. H. Devoret (Plenum, New York, 1992).
[13] M. Tinkham, *Introduction to Superconductivity* (McGraw-Hill, Singapore, 1996), 2nd ed.
[14] A. J. Dahm *et al.*, Phys. Rev. Lett. **22**, 1416 (1969).
[15] A. H. Worsham *et al.*, Phys. Rev. Lett. **67**, 3034 (1991).

Part III

High-frequency characterization of a single-Cooper pair transistor

Chapter 6

Single Cooper-pair transistor (SCPT)

I Introduction

The single Cooper-pair transistor (SCPT) consists in a superconducting island connected to two superconducting leads *via* tunnel junctions: moreover, the electrostatic potential of the island can be tuned by means of a nearby gate. It is the analog of the single-electron transistor [26], with an additional competing correlation effect (given by superconductivity). As already mentioned earlier in this manuscript, quantum circuits can be described by two conjugate variables: the quasicharge k, and the phase δ. In an ultrasmall tunnel junction for example, the charging energy tends to localize the charge, which in this case becomes a good quantum number, whereas in a pure Josephson element, the phase is localized by the superconducting order, which is conversely a good quantum number. The properties of ultrasmall Josephson junctions result from the interplay of the charging energy $E_c = e^2/2C_\Sigma$ (where C_Σ stands for the total capacitance of the island), and the Josephson coupling E_J of each junction: however, a device whose ratio between E_c and E_J could be tuned by an external parameter, would be more interesting because it would allow to understand the way these two competing orders modify the evolution of charge and phase. Since its first implementation in an experiment by Fulton and Dolan, this device has been extensively studied in the last 15 years: first studies consisted in transport measurements. These experiments confirmed some predictions concerning the different transport processes involved in the SCPT: for example, they gave some information about the spectroscopy of the device [30]. But the increasing interest for the SCPT is related to its potential applications in the field of quantum information, and charge detection (*ie.* SCPT is a good electrometer). In this chapter, a brief overview of the SCPT will be given: some notations will be introduced, its hamiltonian will be derived. This will allow later to have a better comprehension of the transport processes involved, when the SCPT is biased.

II Charge representation of the SCPT

A simplified representation of the SCPT is given in figure 6.1: k_i ($i = 1, 2$) are the number of Cooper pairs flowing through junction i, whereas δ_i ($i = 1, 2$) stand for their conjugate variables, *ie.* the superconducting phase across junction i. One can then define the excess number of Cooper pairs on the island n as $n = (k_1 - k_2)$, and the superconducting phase δ

across the transistor as $\delta = (\delta_1 + \delta_2)$. It is worth to point out that the conjugate variable of n is not δ, but $\theta = (\delta_1 - \delta_2)/2$: conversely, the conjugate variable of δ is $k = (k_1 + k_2)$. This variable corresponds to the total number of Cooper pairs which have flown across the transistor: this parameter will be useful later to index charge states involved in the so called resonant Cooper pair tunneling process for example.
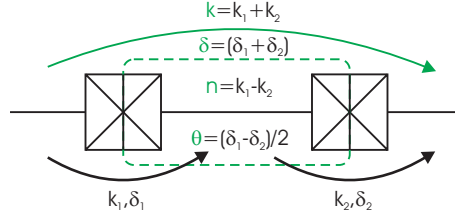

Figure 6.1: Schematic representation of the single-Cooper pair transistor: the different variables describing the evolution of charge and phase are represented. We adopted a convention defining k_1 and k_2, and by so n and k in number of Cooper pairs: following this choice, δ_1 and δ_2, and consequently δ are superconducting phases.

1   Ideal case: symmetric junctions

We will first consider the simplified example of symmetric junctions, which in the case ultrasmall junctions is never achieved: however, it greatly simplifies the derivation of the hamiltonian of the SCPT, and does not change much the underlying physics. Let us first write the electrostatic term of the hamiltonian: as mentionned earlier, this term localizes the charge, thus corresponding to a diagonal term in the charge state basis

$$\mathcal{H}_{el} = E_c \sum_n (n - n_g)^2 \, |n\rangle \langle n| \quad \text{where} \quad n_g = \frac{C_g V_g}{e}$$

The Josephson energy of the transistor is the sum of the Josephson coupling hamiltonians of the two junctions, which couple neighbouring charge states

$$\mathcal{H}_J = \mathcal{H}_{J1} + \mathcal{H}_{J2} \quad \text{where} \quad \begin{cases} \mathcal{H}_{J1} = -E_J \cos(\delta_1) \\ \mathcal{H}_{J2} = -E_J \cos(\delta_2) \end{cases}$$

Since $\delta = \delta_1 + \delta_2$ and $\theta = (\delta_1 - \delta_2)/2$, it reads

$$\mathcal{H}_J = -E_J \left[\cos\left(\frac{\delta}{2} + \theta\right) + \cos\left(\frac{\delta}{2} - \theta\right) \right] = -2 E_J \cos\left(\frac{\delta}{2}\right) \cos(\theta)$$

It finally comes

$$\mathcal{H}_J = -\sum_n E_J \cos\left(\frac{\delta}{2}\right) (|n\rangle \langle n+2| + |n+2\rangle \langle n|)$$

The hamiltonian of the transistor is thus given by

$$\boxed{\mathcal{H}_0 = \sum_n \left\{ E_c (n - n_g)^2 \, |n\rangle \langle n| - E_J \cos\left(\frac{\delta}{2}\right) (|n\rangle \langle n+2| + |n+2\rangle \langle n|) \right\}}$$

The derivation of this hamiltonian allows to realize that at equilibrium, the transistor behaves as a Josephson junction, which Josephson coupling can be adjusted with the gate. As for an ultrasmall Josephson junction, the total Hamiltonian is the sum of two

competing terms: the charging energy (localization of the charge), and the Josephson coupling (delocalization of the charge). Two opposite regimes can be distinguished:

- At $n_g = 0[2]$: the charging effects dominate (of course, we consider a device such as $E_c > E_J$). Two neighbouring charge states are energetically well separated, and thus are weakly coupled by Josephson coupling: the dependence of the energy *vs.* phase δ is negligible. A small supercurrent is expected.

- At $n_g = 1[2]$: considering only electrostatic energy, two neighbouring charge states are degenerate: the effect of the Josephson energy is maximum, by lifting this degeneracy. The amplitude of the supercurrent is expected to be maximum.

One of the most important consequences, is the ability to tune the amplitude of the supercurrent of the transistor with the gate [30] (*ie.* DC Josephson effect is tuned by the gate). At this stage, an intriguing question arises: how is AC Josephson effect affected by the gate? Not only its amplitude, but also in terms of frequency content?
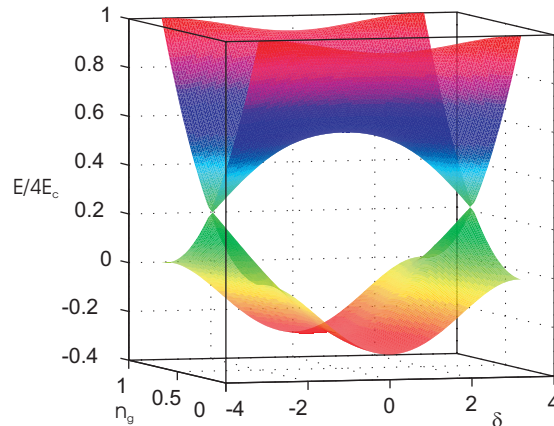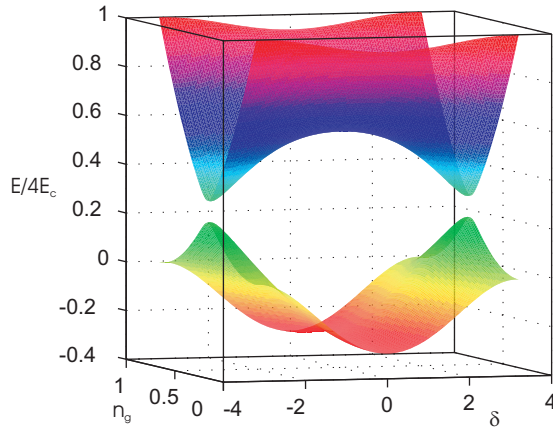

Figure 6.2: Two lowest energy bands E_0 and E_2 *vs.* n_g and δ plotted for the parameters of our sample $E_J = 28~\mu eV$ and $E_c = 65~\mu eV$: notice the degeneracies occuring at ($n_g = 1[2], \delta = \pi[2\pi]$).

2 Non-symmetric junctions

Experimentally, the junctions are not perfectly equivalent: due to some asymmetry of the areas of the junctions, their Josephson coupling is slightly different. This effect is particularly relevant in the case of ultrasmall junctions, which is typically the kind of device we are dealing with in this experiment. In practice, the effect of this asymmetry is to open a small gap at the degeneracy point, located at ($n_g = 1[2], \delta = \pi[2\pi]$). Let us introduce a new parameter d, which allows to quantify this asymmetry

$$\begin{cases} E_{J1} = E_J \left(1 + d\right) \\ E_{J2} = E_J \left(1 - d\right) \end{cases}$$

Following the procedure described in the previous section, the transistor hamiltonian reads

$$
\begin{aligned}
\mathcal{H}_0 \;=\; \sum_n \Bigg\{ & \mathrm{E_c}\,(n - n_\mathrm{g})^2\,|n\rangle\,\langle n| \\
& - \mathrm{E_J}\left[\cos\left(\frac{\delta}{2}\right) - \mathrm{i}\,d\,\sin\left(\frac{\delta}{2}\right)\right]|n\rangle\,\langle n+2| \\
& - \mathrm{E_J}\left[\cos\left(\frac{\delta}{2}\right) + \mathrm{i}\,d\,\sin\left(\frac{\delta}{2}\right)\right]|n+2\rangle\,\langle n| \Bigg\}
\end{aligned}
$$

A numeric diagonalization of this hamiltonian allows to show how the asymmetry of the junctions lifts the degeneracy occuring at $(n_\mathrm{g} = 1[2], \delta = \pi[2\pi])$ (see figure 6.3).

Figure 6.3: Two lowest energy bands $\mathrm{E_0}$ and $\mathrm{E_2}$ *vs.* n_g and δ plotted for the parameters of our sample ($\mathrm{E_J} = 28\ \mu\mathrm{eV}$ and $\mathrm{E_c} = 65\ \mu\mathrm{eV}$): notice the degeneracies occuring at $(n_\mathrm{g} = 1[2], \delta = \pi[2\pi])$ for the symmetric case are lifted by the asymmetry of the junctions.

3   Estimation of the asymmetry of the junctions

In order to estimate the asymmetry of the junctions, we performed a measurement of the switching current of a Squid realized during the same fabrication process: indeed, these junctions are similar in size to the junctions of the transistor, so one can assume that their asymmetry will be about the same.
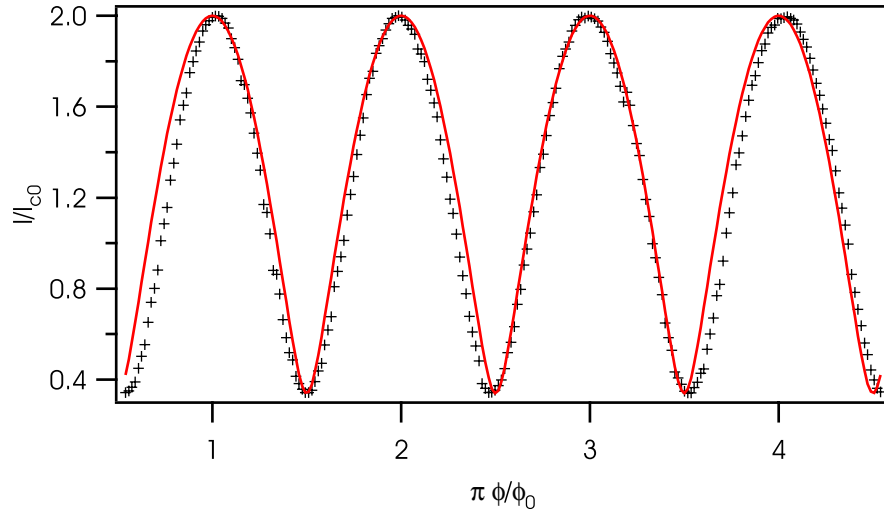
Figure 6.4: Determination of the critical current of the SQUID *vs.* reduced flux ϕ/ϕ_0: experimental points (dots) and best fit (line).

Considering two asymmetric Josephson junctions, embedded in a Squid geometry ($I_{c1} = I_{c0}(1+d), I_{c2} = I_{c0}(1-d)$), one can show that the critical current of the whole system reads

$$I_c(\phi) = 2 \sqrt{d^2 \sin^2\left(\frac{\pi\,\phi}{\phi_0}\right) + \cos^2\left(\frac{\pi\,\phi}{\phi_0}\right)}$$

It is thus deduced that the asymmetry of the junctions is approximately $d = 0.17$.

III   BCS term and odd states

Until now, charge states involving only Cooper pairs have been considered (*ie.* even states): however, one should also include a BCS term accounting for quasiparticle states on the island. It reads [66]

$$\mathcal{H}_{\text{BCS}} = \sum_i \varepsilon_i\, \gamma_i^+\, \gamma_i$$

In the previous expression, the spin indices have been omitted for the sake of clarity: the expression of the hamiltonian of the quasiparticle states in the frame of BCS theory is obviously slightly more complicated. The main consequence of this term is that at equilibrium it costs a free energy $\mathcal{F}_{\text{e/o}}$ to add a quasiparticle on the island [67]

$$\mathcal{F}_{\text{e/o}}(\text{T}) = \Delta - k_{\text{B}}\text{T} \log \text{N}_{\text{eff}}$$

Here, N_{eff} stands for the number of available states on the island: roughly, N_{eff} is equal to the density of states times the volume of the island. This expression can be understood qualitatively: at zero temperature, one recovers that it costs an energy 2Δ to extract a quasiparticle in the leads, before sending it onto the island. At finite temperature, quasiparticles can tunnel onto the island by thermal activation: consequently, the energy cost to send a quasiparticle in the island is renormalized by thermal effects. Obviously, the larger the number of available states on the island and the higher the temperature, the higher the probability for a quasiparticle to stay in the island. More formally, this

expression is obtained by integrating over energy the density of states times the thermal activation factor. This effect has been extensively tested experimentally [67][68]: it is often referred as poisoning effects. However, there has been a renewed interest for this phenomenon more recently: indeed, in the field of quantum information, superconducting circuits similar to the SCPT could provide coherent two-level systems (qubits) which has the advantage to be easily scalable (a goal which appears more difficult to achieve with ion-traps for example [69]). These poisoning effects remain a strong limitation to the coherence of such devices: this partly explains why a better comprehension of poisoning effects is needed. More generally, it would be interesting to understand the consequences of the interplay between even and odd charge states: until now, there is no spectroscopy experiment studying the odd levels, due to the frequencies involved. Indeed, the irradiation of mesoscopic devices at very high frequency (let us say higher than 40 GHz) is difficult to achieve in a cryogenic environment. We will see however that such an experiment can be implemented, using a HF generator directly coupled on-chip to the SCPT.

IV   The sample

The coupling scheme is very similar to the previous one, used to detect the HF emission/absorption properties of a Josephson junction: it relies on a capacitive coupling between the SCPT and a SQUID (see figure 6.5-a). The environment is delimited at high-frequency by the shunt capacitances C_s, and the coupling is determined by the polarization resistances (platinum wires).
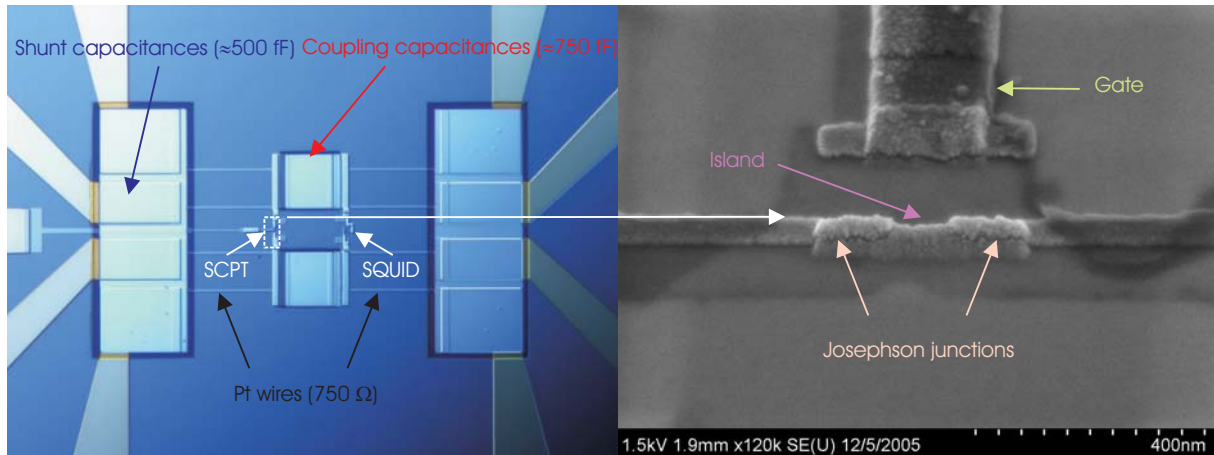

Figure 6.5: (a) - Optical microscopy picture of the sample: coupling scheme between the SCPT and the SQUID. (b) - Electronic microscopy picture of the single-Cooper pair transistor: two Josephson junctions delimit the superconducting island, which electrostatic potential can be tuned with the nearby gate.

Chapter 7

DC transport properties of the SCPT

I Introduction

In this chapter, the transport properties of a SCPT will be briefly reviewed: the data presented are related to the sample which will be studied in the AC regime, in the next chapters. Reviewing DC measurements will be a good opportunity to summarize the information that can be extracted from transport experiments: it will motivate the need to perform a spectroscopy experiment at higher frequency, and to study the HF emission of the transistor.

II $I(V)$ characteristic

As can be noticed, the $I(V)$ characteristic of a SCPT is strongly modified by the gate (see figure 7.1): the Josephson branch is $2e$-periodic, whereas the so-called Josephson-quasiparticle cycle is e-periodic. It will be shown later on, that the gate dependence of the subgap conductivity is also worth to explore.
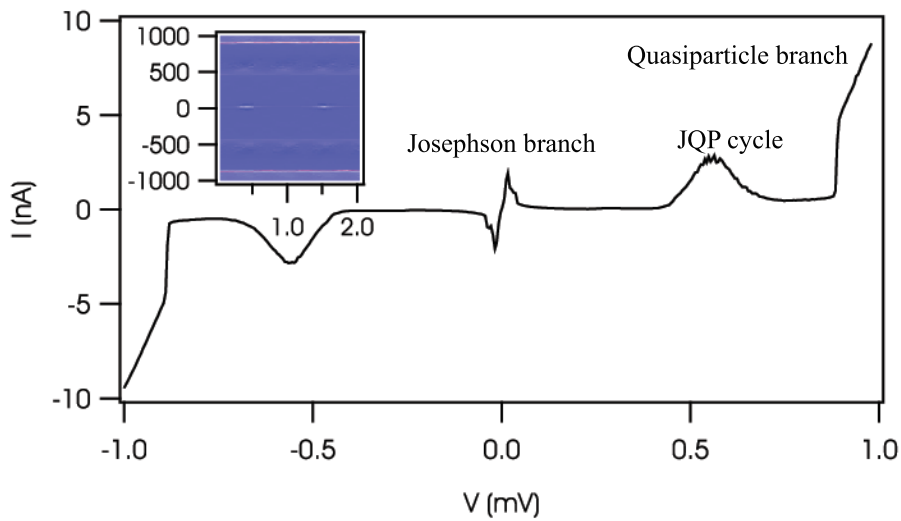
Figure 7.1: $I(V)$ characteristic of the SCPT studied in the following experiments. Inset: $I(V)$ characteristic of the SCPT, plotted *vs.* different gate voltages.

III   Josephson branch

As previously mentioned, the Josephson branch is $2e$-periodic: this was expected, given that $E_c < \Delta$. Indeed, if one takes into account odd states, this condition is required to ensure $2e$-periodicity.

IV   Resonant Cooper-pair tunneling (RCPT)

When biased in the subgap region, the $I(V)$ characteristic of the SCPT exhibits intriguing features. Two regimes can be distinguished: a low-bias regime, where these features are $2e$-periodic, and a e-periodic regime at higher voltages: these two different periodicities exhibited by the subgap conductance can be clearly seen on figure 7.2. The data are shown on figure 7.2 up to $V_B \approx 2\Delta + E_c$, *ie.* up to the Josephson-quasiparticle (JQP) cycle: above the JQP cycle, the subgap conductance is unambiguously e-periodic.
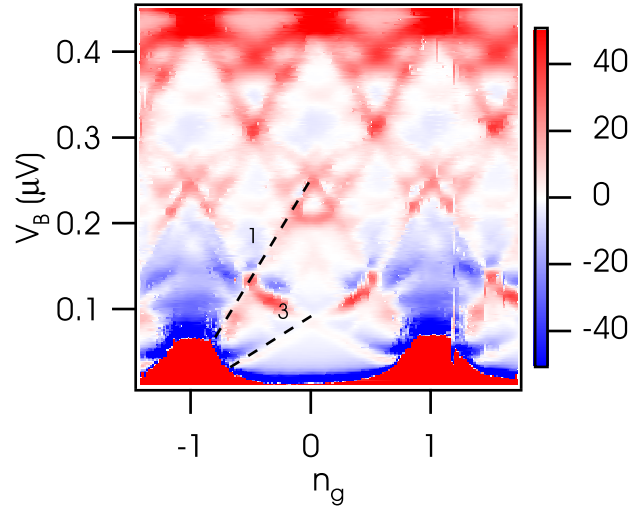
Figure 7.2: Subgap conductance of the transistor between 0 and 450 μeV: one can clearly distinguish two sets of 2e-periodic resonances, which correspond to RCPT of order '1' and '3'.

This low-bias regime being 2e-periodic, one can guess that only Cooper pairs are involved in the transport processes considered: this regime is usually referred as resonant Cooper pair tunneling (RCPT) [32]. It has been extensively studied in DC [33][34][30], but the AC regime deserves some investigation. Using a SIS junction as a high-frequency detector, capacitively coupled to the SCPT, similarly to what is shown in the first part of this thesis, we have been able to detect the HF photons emitted when the transistor is voltage biased in the RCPT regime. Let us introduce some notations that will be helpful to explain these data: until now, we have mainly used the basis of states $|n, \delta\rangle$ to describe the transistor. This was justified because due to strong charging effects in our samples, the charge on the island n, and thus the phase difference δ across the SCPT are good quantum numbers. However, when voltage biased, one has to include an electrostatic term $-2k\,e\mathrm{V_B}$ to the hamiltonian (where k corresponds to the number of Cooper pairs which have flown through the SCPT, and $\mathrm{V_B}$ is the voltage bias through the transistor): doing so, it is easier to switch to the $|n, k\rangle$ basis. This formalism will be useful to describe the AC emission of the voltage biased SCPT. The hamiltonian of the transistor reads

$$\mathcal{H} = \mathcal{H}_0 - 2\,k\,e\mathrm{V}$$

This can be understood intuitively: when k Cooper pairs tunnel through both junctions, the total energy is lowered by $k \times 2\,e\mathrm{V}$. Thus applying a finite voltage, states with different charge states can be put in resonance if the following condition is realized

$$\mathrm{E}_{|0,k\rangle} = \mathrm{E}_{|2,k+(2+i)\rangle} \quad \text{where } i \text{ is an odd integer}$$

If this condition is fulfilled, these two states are strongly coupled by the Josephson coupling. These resonances can be indexed by i: they are schematically represented for $i = 1, 3$ on figure 7.3. Their gate voltage dependence can be roughly estimated: in order to do so, let us neglect the Josephson coupling, and consider only the electrostatic term. It comes
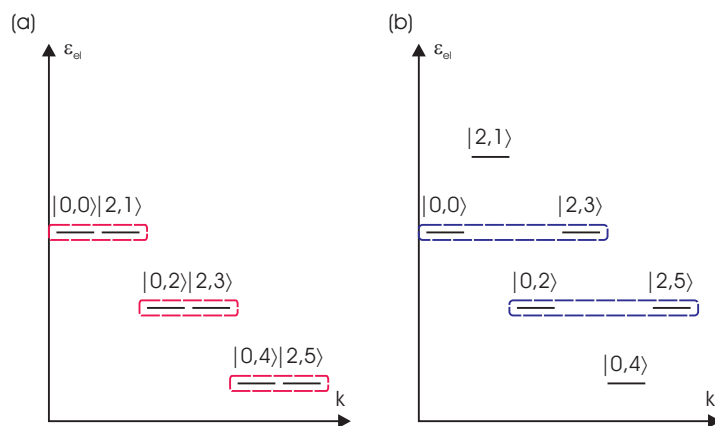
$$e\mathrm{V} = \frac{\mathrm{E_c}}{i}$$

Figure 7.3: Electrostatic energy levels represented in the basis of states $|n, k\rangle$: resonances of order 1 and 3 are represented respectively on the left and right.

With this formalism, the DC Jospehson effect can be understood as a transition between states $|0, k\rangle$ and $|0, k + 2\rangle$ (see figure 7.4).
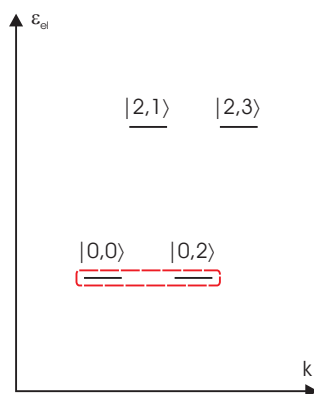

Figure 7.4: States $|n, k\rangle$ involved in the DC Josephson effect.

In the next chapter, it will be shown that the frequency content of the voltage biased SCPT can be explained using this new set of states.

Chapter 8

High-frequency emission

I   Phase dynamics of a voltage biased SCPT

In this chapter, the high-frequency emission spectrum of a voltage biased SCPT will be considered: as previously mentioned, the current bias of a SCPT is a difficult task (an ideal current bias requiring a current source with infinite output impedance, a goal which is hard to achieve at high-frequency).

1   Josephson effect as an emission/absorption process

We have seen previously that the AC Josephson effect in a Josephson junction could be understood as a combination of emitted/absorbed photons at frequency $2e\mathrm{V_B}/h$ (see figure 8.1), associated to the inelastic tunneling of Cooper pairs when the junction is voltage biased: this kind of duality between emission/absorption is related to the fact that one deals with a coherent process. On another hand, we have also seen that the SCPT presents a supercurrent (DC Josephson effect) which amplitude can be tuned by the gate: the SCPT behaves as a Josephson junction which can be tuned by the gate (see figure 8.1). So one might ask whether the SCPT presents an AC Josephson effect when voltage biased: if it is so, is there a way to modulate its amplitude, similarly to what is the case in DC? In the following section, we will focus on the issue of the frequency content of the emission spectrum of a SCPT voltage bias regime: here 'low-bias' means that we will restrict ourselves to a range of voltage bias such that the $I(V)$ characteristic is $2e$-periodic.
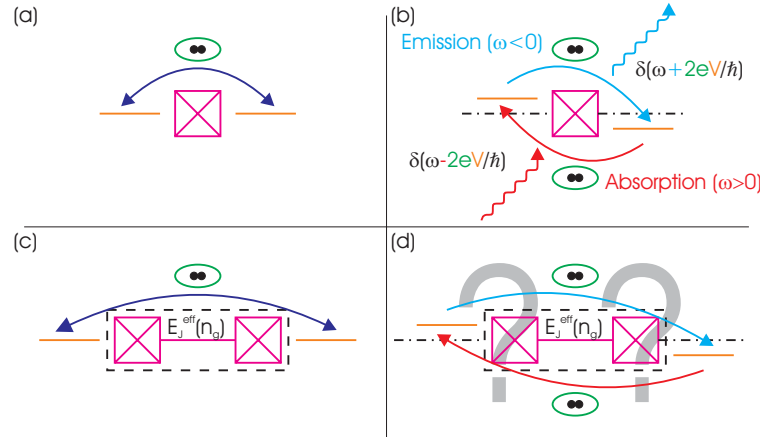
Figure 8.1: Description of the DC & AC Josephson effect in terms of emission/absorption processes of photons.

As already discussed in the case of the Josephson junction, voltage bias imposes the evolution of the phase δ (whereas current bias imposes the evolution of the quasicharge k), according to the Josephson relation

$$\frac{\mathrm{d}\delta}{\mathrm{d}t} = \frac{2e\,\mathrm{V}}{\hbar}$$

The amplitude, as well as the frequency content of the Josephson emission are determined by the other Josephson relation

$$\mathrm{I}_k(n_\mathrm{g}, \delta) = \frac{2e}{\hbar}\, \frac{\partial \mathrm{E}_k}{\partial \delta}(n_\mathrm{g}, \delta)$$

In the case of the Josephson junction, the current-phase relation is harmonic and its amplitude is determined by the Josephson coupling

$$\mathrm{I}_\mathrm{S}(t) = \mathrm{I}_0\,\sin\left(\frac{2e\mathrm{V}_\mathrm{B}t}{\hbar}\right) \quad \text{where} \quad \mathrm{I}_0 = \frac{2e}{\hbar}\,\mathrm{E}_\mathrm{J}$$

It is worth to notice that the harmonicity of the current-phase relation is linked with the low transparency of the junction: strictly speaking, the Josephson relation of any barrier of arbitrary nonzero transparency ($\mathrm{T} > 0$) is anharmonic. However in the tunnel regime, the harmonic regime is fulfilled. One also has to take into account thermal and environmental effects (due to non ideal voltage bias, ie. finite $\mathrm{Z}(\omega)$) which broaden the Josephson emission of the junction. We will ignore these two extrinsic causes of anharmonicity during the following discussion, and will consider a perfectly voltage biased SCPT. However, due to the modulation of the ratio between charging energy and Josephson coupling by the gate, it appears that the frequency content can also be tuned (cd. figure 8.2). Indeed, on can distinguish two opposite situations:

- $\mathbf{n_g = 0}$: the ratio between the effective charging energy $(n - n_\mathrm{g})^2\,\mathrm{E}_\mathrm{c}$ and the Josephson coupling E_J is maximum. Consequently, both charge states $|0\rangle$ and $|2\rangle$ are well separated, and Josephson coupling plays a minor role: this was the reason why the amplitude of the supercurrent in DC transport was so small, and in this case we find from numerical calculation (diagonalization of the hamiltonian of the SCPT) that the energy-phase relation of the transistor is almost harmonic (see figure 8.2).

- **$n_g = 1$**: the effective charging energy $(n - n_g)^2 E_c$ is equal to zero. Thus, charge states $|0\rangle$ and $|2\rangle$ are degenerate: the Josephson coupling lifts this degeneracy, and leads to the existence of two coherent superposition of states. The amplitude of the supercurrent is maximal, and a numerical determination of the energy-phase relation reveals a strong anharmonicity [70].
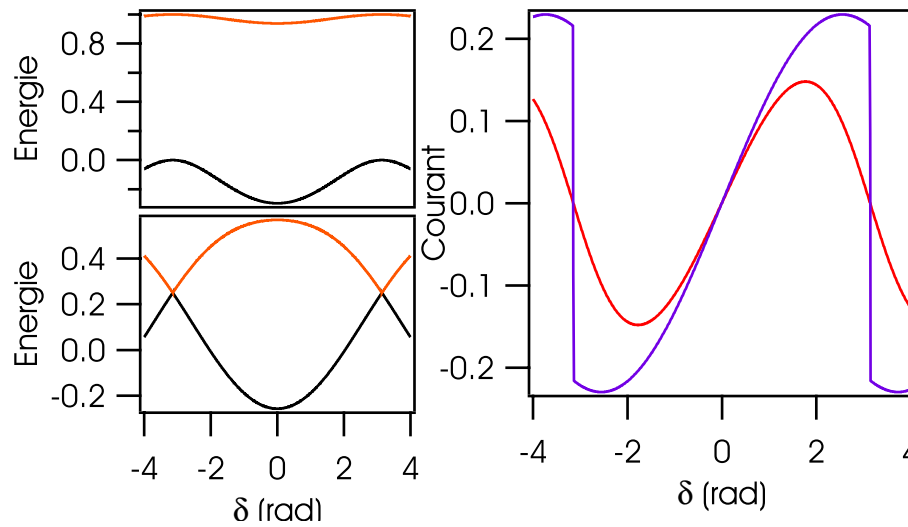

Figure 8.2: (a) - Energy phase relation (first two levels) for $n_g = 0$ (top) and $n_g = 1$ (bottom). (b) - Current phase relation for $n_g = 0, 1$: notice the strong anharmonicity for $n_g = 1$.

The AC Josephson effect can be related with the evolution of a fictitious particle, which dynamics on the fundamental level is imposed by the DC voltage bias, a strongly anharmonic frequency content at high frequency is expected around $n_g = 1$. Is that the case?

II Detection scheme

The determination of the HF emission spectrum of the SCPT relies on a detection scheme similar to the one already used to determine the HF emission spectrum of a Josephson junction (see figure 8.3): the environment of the detector is very similar (same fabrication process). We can reasonably assume that the transimpedance determined previously from the AC Josephson effect of a Josephson junction will be the same. We will only investigate the emission properties of the SCPT: attempts to detect the absorption of its HF spectrum have been unsuccesful due to a lack of sensitivity.
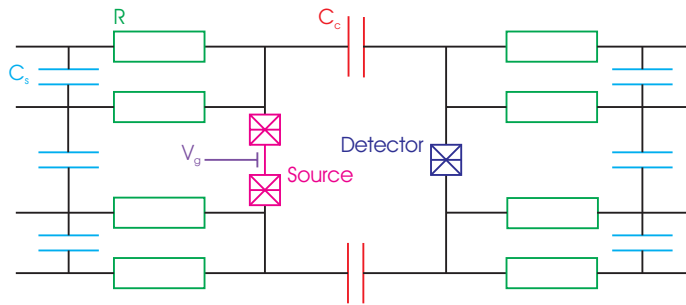
Figure 8.3: Detection scheme for the determination of the HF emission spectrum of the SCPT.

III   AC Josephson effect in a SCPT

1   Experimental results

We employed a similar procedure to detect the HF emission at low-bias for the SCPT, as the one used for the AC Josephson effect of a Josephson junction. The source (SCPT) was voltage biased: we apply a slight modulation to this bias, and detect the associated variation of the PAT current through the detector (SIS junction) with a lockin technique, which is also voltage biased (subgap regime). We use the SQUID geometry to tune the Josphson coupling of the detector to its minimum value (turning it into a SIS junction). The modulation technique employed has been crucial in this experiment, given the small amplitude of the effective Josephson coupling of the SCPT around $n_g = 0$: the sensitivity of the detection in DC was too restricting. We still record the effective amplitude of the modulation on the source, and reconstruct the quantity $\partial I_{PAT}/\partial V_S$. The data obtained are shown on figure 8.4.
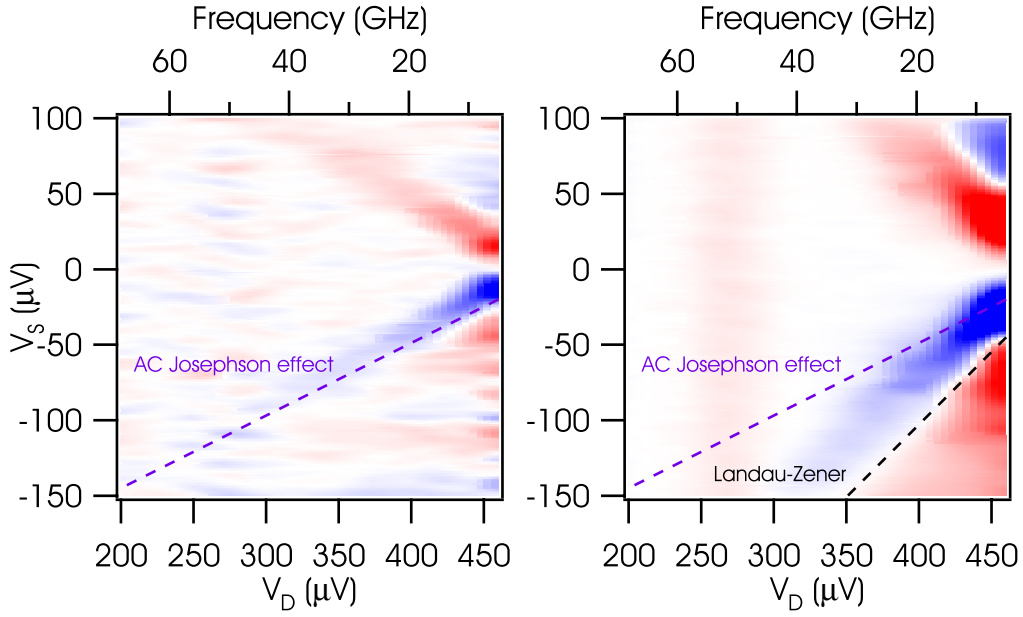
Figure 8.4: Derivative of the PAT current with respect to the voltage bias on the source $\partial I_{PAT}/\partial V_S$ for different DC voltage bias applied on the SCPT, for $n_g = 0$ (left) and $n_g = 1$ (right).

One can first notice that in both cases, the HF emission of the transistor is harmonic: only one peak is detected both at $n_g = 0$ and $n_g = 1$. We do not observe the anharmonicity expected from the energy-phase relation. The other striking feature is the frequency dependence of these two singularities: whereas at $n_g = 0$ it follows the usual Josephson relation $\omega_J = 2eV_S/\hbar$, at $n_g = 1$ it obeys $\omega = eV_S/\hbar$. Finally, instead of a set of harmonics, we observe one subharmonic: something is missing in the description of the dynamics of the phase in our device.

2   Landau-Zener effect

Actually, one can notice that it remains a degeneracy point between the fundamental level and the first excited state, when $(n_g = 1[2], \delta = \pi[2\pi])$ (if we assume the junctions are perfectly symmetric). It has been shown previously that a small gap Γ is opened when an asymmetry d is taken into account: such a situation is known to lead to transitions between these two levels at the degeneracy points, when the position of the fictitious particle is swept in a non-adiabatic manner (it can be swept relatively to n_g or δ), with a probability [31]

$$P_{LZ} = \exp\left(\frac{-\pi\,\Gamma^2}{2\,E_J\,eV_S}\right)$$

This is the so called Landau-Zener effect: the distinction between adiabatic/diabatic regimes depends on the size of the gap at the 'degeneracy point' (Γ), the amplitude of the considered energy levels (E_J) and the velocity of the fictitious particle ($2eV_S/\hbar$). A similar effect has been observed by means of self-induced Shapiro steps [30].

IV   HF emission spectrum associated to the RCPT

We have already reviewed the experimental signatures of the resonant Cooper pair tunneling processes (RCPT) on the DC transport properties of the SCPT: similarly to the DC Josephson effect, these features observable in DC bear the signature of elastic tunneling of Cooper pairs between degenerate charge states. However, such tunneling processes should also lead to emission of HF photons, due to inelastic tunneling of Cooper pairs. This would constitute an extension of the AC Josephson effect, and deserve to be explored.

1   Experimental signatures of RCPT on the HF emission spectrum

We employ the same detection scheme as the one used before to detect the AC Josephson effect, but we extend our investigation to higher voltage bias: this measurement was conducted for different gate voltages. The modulation technique was again essential in this experiment due to the low power generated by the inelastic processes associated to the RCPT. The data are presented on figure 8.5.
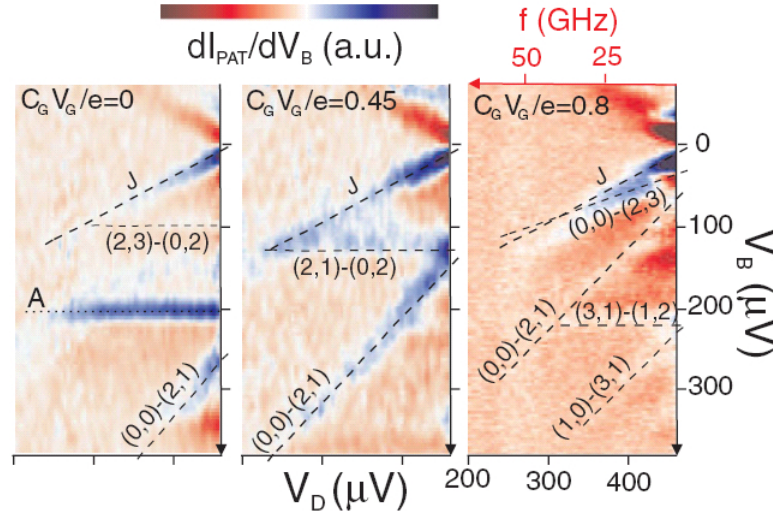

Figure 8.5: Derivative of the PAT current with respect to the voltage bias on the source $\partial I_{\text{PAT}}/\partial V_S$ for different DC voltage bias applied on the SCPT, for $n_g = 0$ (left), $n_g = 0.45$ (center) and $n_g = 0.8$ (right).

One can distinguish the features associated with the AC Josephson effect, described previously: however, contrarily to the case of the Josephson junction, other singularities in the emission noise spectrum of the SCPT can be seen. They can be understood as transitions resulting from the resonant Cooper pair tunneling (RCPT). Let us consider the two resonances observed in DC transport:

- **Resonance 1:** When the transistor is voltage biased such as states $|0,0\rangle$ and $|2,1\rangle$ are degenerate, this resonant state leads to resonances in DC transport. In the mean time, a transition can occur between resonant states $[|0,0\rangle - |2,1\rangle]$ and $[|0,2\rangle - |2,3\rangle]$ which leads to HF emission of photons of energy $2eV_B$ (see figure 8.6, $V_B = 145~\mu V$ and higher). If the voltage is increased above this value, the resonance between states $|0,0\rangle$ and $|2,1\rangle$ is destroyed: however, due to the Josephson coupling, there is a resonant transfer of Cooper pairs between states $|0,0\rangle$ and $|2,1\rangle$, and similarly

between states $|2,1\rangle$ and $|2,0\rangle$ which leads to the HF emission of photons. These features appear in the experimental data (see figure 8.5).

- **Resonance 3:** At lower voltage, states $|0,0\rangle$ and $|2,3\rangle$ can be put in resonance which leads to the resonance 3 observed in DC transport: similarly to the case of resonance 1, transition between resonant state $[|0,0\rangle - |2,3\rangle]$ and $[|0,2\rangle - |2,5\rangle]$ generates HF emission of photons (see figure 8.6, $V_B = 45~\mu V$). At higher voltage, there is HF emission of photons due to the resonant transfer of Cooper pairs between states $|0,0\rangle$ and $|2,3\rangle$ (see figure 8.5, $n_g = 0.8$).
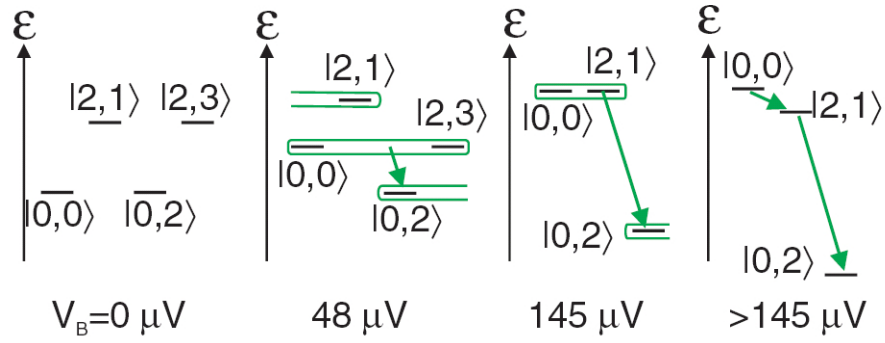

Figure 8.6: Inelastic transitions associated with the RCPT.

Chapter 9

Very high-frequency spectroscopy of the transistor

I Introduction

A large number of experiments have been performed in order to probe the complex internal energy scales of devices based on small Josephson junctions (SCPT, single-Cooper pair box), resulting from the interplay of Josephson and charging energies, but also superconducting gap (due to poisoning effects). Most of these measurements were motivated by the need to confirm the possibility to realize coherent two-level systems (qubits) starting from ultra-small capacitances Josephson junctions. This partly explains why these studies were restricted to the first two energy levels. Another explanation is the difficulty to generate very high-frequency photons in a cryogenic environment. However, it seems very interesting to perform such an experiment, in order to have a better comprehension of the charge transfer processes involved in the SCPT.

This interest relies on the existence of odd states: indeed, transitions to higher energy even states ($|4\rangle$, $|6\rangle$ ...) are unlikely to happen because they require higher order couplings. But even states are known to have a strong influence on the equilibrium properties of these devices, although the reason for that remains unclear. The issue is though that E_J and E_c can be chosen by a proper design of the junctions, the superconducting gap Δ which is the relevant energy scale concerning the poisoning effects, corresponds to very high-frequencies. Typically, for aluminum, one finds $\Delta \approx 250$ μeV ≈ 60 GHz. A good alternative to avoid the issue of generating such HF photons is to use an on-chip generator, directly coupled to the device under test: to ensure a good coupling at such frequencies, capacitive coupling between the device and the HF source is required.

II Energy levels of the SCPT

In order to determine which energy levels can be probed in this study, we have performed a numerical diagonalization of the Hamiltonian of the SCPT.
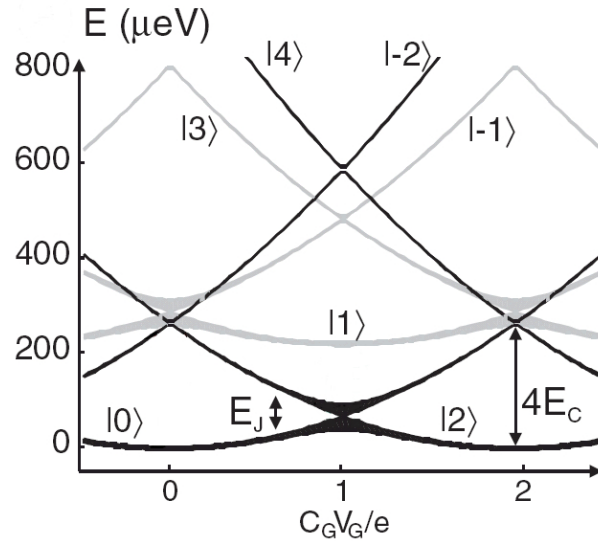
Figure 9.1: Energy levels of the SCPT: the even levels (only Cooper pairs on the island) are represented in black, whereras the odd levels (one quasiparticle on the island, *ie.* poisoned states) are represented in grey.

III   Detection scheme

To perform the spectroscopy of the transistor, one can use the detection scheme previously described in the first part, in a slightly different way: the difference in this case, is that the role played by the Josephson junction is reversed. One does not use it as a SIS junction, measuring the PAT current: now, its Josephson coupling is tuned to its maximum value in order to use it as a high-frequency generator (similarly to what was done to determine the transimpedance in the first part). Through the AC Josephson effect of this source, photons with frequencies up to $4\Delta/h$ can be generated (*ie.* 200 GHz in the case of aluminum).
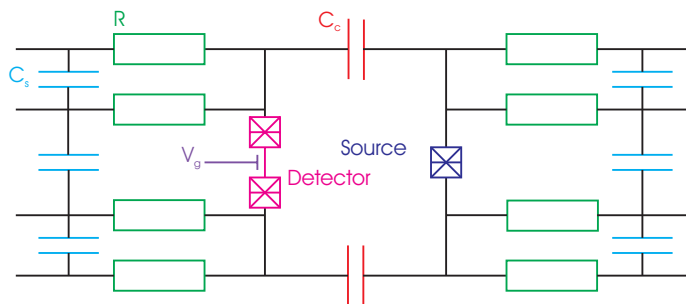

Figure 9.2: Detection scheme for the HF spectroscopy of the SCPT

IV Effect of the HF irradiation on the switching current of the SCPT

We have first performed a measurement of the switching current of the SCPT, *vs.* the frequency of irradiation by the SQUID (see figure 9.3). The measurement is performed as followed: the transistor is current biased through a 100 MΩ resistance. The value of the current bias is increased, and the voltage across the device is measured. Once the SCPT switches to its quasiparticle branch (detected by the voltage measurement), the value of the current is recorded: this procedure is repeated 10^3 times, and the switching current is defined as the most probable value of this distribution. The measurement of the switching current of the transistor is more difficult than for a Josephson junction, given the presence of the JQP cycle which makes the retrapping process more complex.
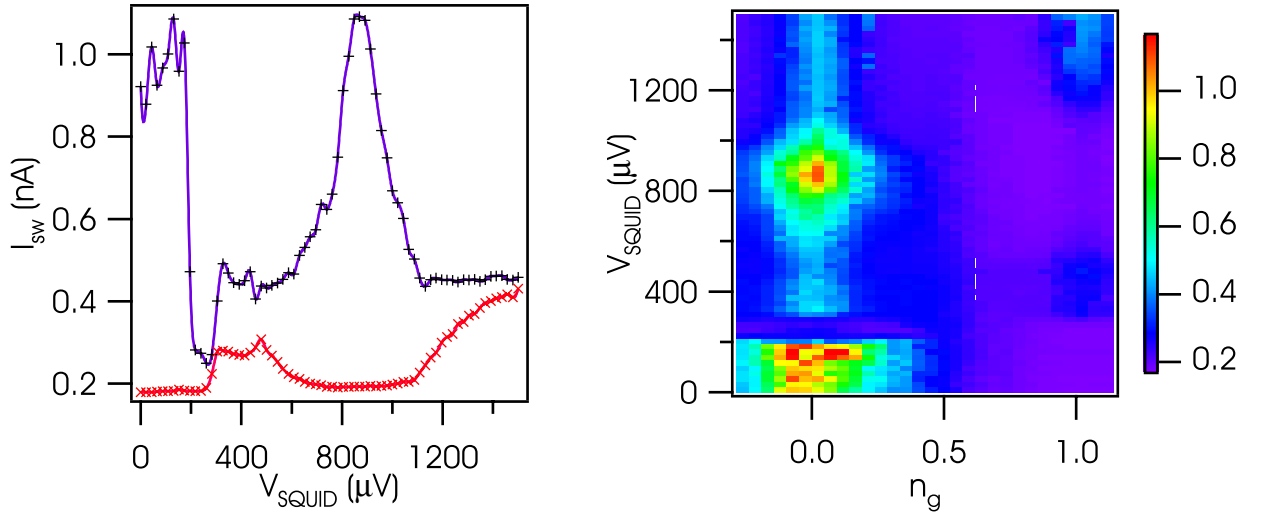

Figure 9.3: Influence of the HF irradiation on the switching current of the SCPT at T = 90 mK. (a) - Effect of the HF irradiation by the Josephson junction at ($n_{\mathrm{g}} = 0$ and $n_{\mathrm{g}} = 1$). Two regimes can be distinguished: when $e\mathrm{V}_{\mathrm{SQUID}} < 2\Delta$, the junction emits a monochromatic irradiation at $2e\mathrm{V}_{\mathrm{SQUID}}/h$ (AC Josephson effect), and when $e\mathrm{V}_{\mathrm{SQUID}} > 2\Delta$ the junction emits photons in the frequency range $[0 : 2e\mathrm{V}_{\mathrm{SQUID}}/h]$. (b) - Switching current of the SCPT *vs.* different gate voltages, and the frequency of the HF irradiation by the Josephson junction in the AC Josephson effect regime.

First of all, it can be noticed that HF irradiation have a strong impact on the switching current, for relatively low power of irradiation (17 fW): these preliminary data indicate that irradiation strongly modify the transport properties of the transistor. However, this measurement scheme is too slow: indeed, the transistor is quite resistive, and our connecting cables have a non-negligible self-capacitance. This introduces a RC time which limited to perform the switching current measurement at a rate below 100 Hz. It is thus difficult to get a good statistic.

V   A reflectometry-like experiment

1   Effect of the HF irradiation on the Josephson branch

Let us look at the effect of the HF irradiation by the nearby SQUID (AC Josephson effect regime), on the Josephson branch of the SCPT (see figure 9.4).
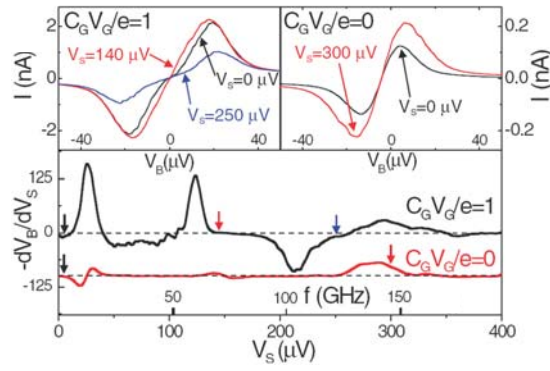

Figure 9.4: Effect of the HF irradiation on the Josephson branch of the SCPT, at T = 90 mK. (a) - Josephson branch of the SCPT at $n_g = 1$ for different conditions of irradiation: 0 GHz, 33.8 GHz and 60.4 GHz. (b) - Josephson branch of the SCPT at $n_g = 0$: 0 GHz, and 72.5 GHz. (c) - $-dV_B/dV_S$ *vs.* frequency irradiation by the Josephson junction for ($n_g = 0$ and $n_g = 1$).

As seen previously, the amplitude of the Josephson branch is highly sensitive to the HF irradiation, and more interestingly, its slope at zero bias follows a similar behavior: when the critical current is increased, the slope dI/dV_B is also increased, and conversely when the critical current is decreased, so does the slope. The slope of the Josephson branch (close to zero bias) of the SCPT appears to be the good quantity to measure, in order to detect variations of the effective Josephson coupling of the transistor under HF irradiation. To improve the sensitivity of the measurement, we used a modulation technique: we applied a DC + ac voltage bias V_S across the Josephson junction (source), and detected the variations of the voltage bias across the SCPT V_B which was slightly current biased 80 μA, with a lock-in detection scheme. The presented data are thus the following adimensionned quantity $-dV_B/dV_S$ (see figure 9.4 for $n_g = 0$ and $n_g = 1$): it is seen that the effective Josephson coupling of the transistor can either be increased or decreased. In order to unequivocally relate these variations to the internal energy scales of the SCPT, we have recorded $-dV_B/dV_S$ for different gate voltages (see figure 9.5).
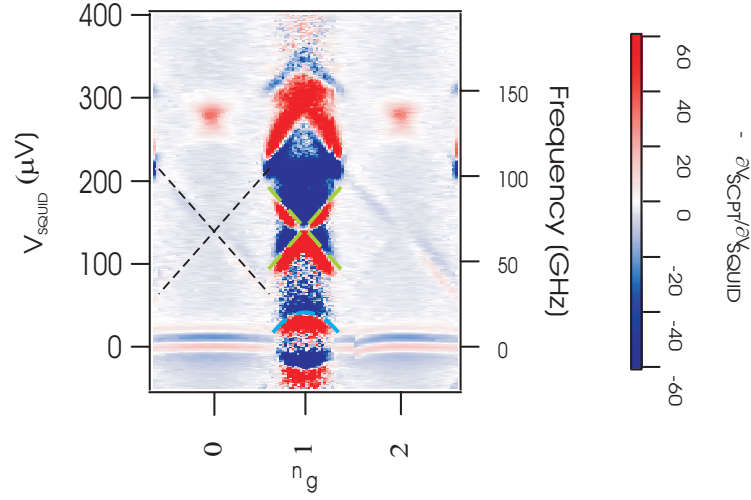
Figure 9.5: Variation of the slope of the Josephson branch *vs.* frequency irradiation and reduced gate voltage n_g, at T = 90 mK.

Different transitions between energy levels of the SCPT can be identified, which lead to the observed features in these data:

- $|n = 0\rangle \rightarrow |n = 2\rangle$: Under HF irradiation, a Cooper pair is extracted from the leads, and sent onto the island (see figure 9.6). This costs an energy $E_{|n=2\rangle} - E_{|n=0\rangle}$. These two energy levels have a similar effective Josephson coupling (seen from simulation), and the modification of the slope of the Josephson branch is thus not very significant.
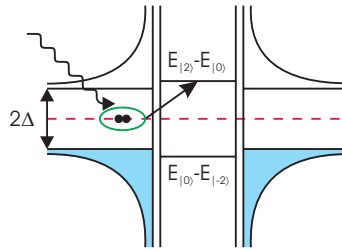

Figure 9.6: Transition induced when the SCPT is irradiated at $\hbar\omega = E_{|n=2\rangle} - E_{|n=0\rangle}$.

- $|n = 0\rangle \rightarrow |n = 1\rangle$: This transition implies the transfer of a quasiparticle on the island: this requires an amount of energy Δ to extract a quasiparticle from the leads, and $E_{|n=1\rangle} - E_{|n=0\rangle}$ to send it onto the island (see figure 9.7).
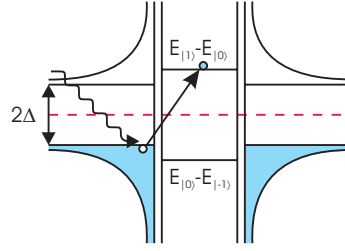
Figure 9.7: Transition induced when the SCPT is irradiated at $\hbar\omega = \Delta + \left(E_{|n=1\rangle} - E_{|n=0\rangle}\right)$.

- **Around $n_{\mathbf{g}} = 1$, $|n=1\rangle \to |n=3\rangle$:** Let us assume that the island is in a poisonned state $|n=1\rangle$: a photon of energy $\left(E_{|n=3\rangle} - E_{|n=1\rangle}\right)$ can induce the transfer of a Cooper pair from the leads onto the island. Then, a quasiparticle can escape from the island to the leads: this relaxation process can take place because our system is designed such as $E_{|n=3\rangle} > \Delta$, which allows the system to relax to charge state $|n=2\rangle$ by the escape of a quasiparticle to the leads.
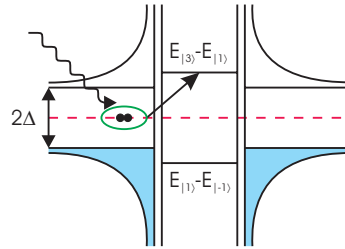

Figure 9.8: Transition induced when the SCPT is irradiated at $\hbar\omega = E_{|n=3\rangle} - E_{|n=1\rangle}$.

- **Around $n_{\mathbf{g}} = 1$, $|n=1\rangle \to |n=0\rangle$:** Assuming again that the island is in a poisoned state, if it is irradiated at frequency $\hbar\omega = \Delta - (E_{|n=1\rangle} - E_{|n=0\rangle})$, then the quasiparticle which is trapped on the island can be extracted to the leads.
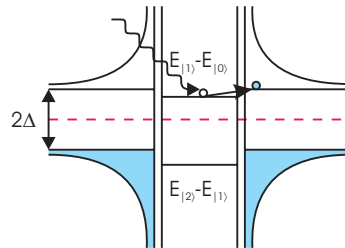

Figure 9.9: Transition induced when the SCPT is irradiated at $\hbar\omega = \Delta - (E_{|n=1\rangle} - E_{|n=0\rangle})$, if $\Delta > (E_{|n=1\rangle} - E_{|n=0\rangle})$.

One can draw the predicted transitions from the numeric diagonalization of the hamiltonian of the SCPT (see figure **??**): the simulations are in good quantitative agreement with the experimental data.
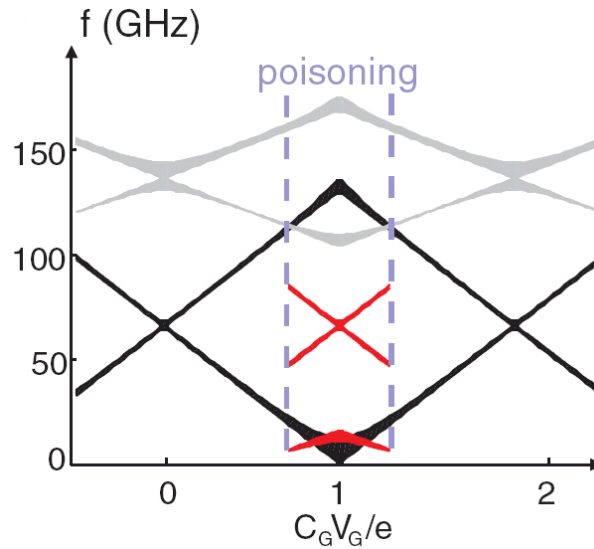
Figure 9.10: Predicted transitions under HF irradiation.

This experiment allows to understand the different charge transfer mechanisms involved in the SCPT, especially those associated with the poisoning effects, which remain a major concern in the development of qubits based on superconducting circuits. However, these effects could be useful in the field of HF photons detection: indeed, the transport properties of the transistor are highly sensitive to small irradiation power, which could be useful to developp bolometers.

ac Josephson Effect and Resonant Cooper Pair Tunneling Emission of a Single Cooper Pair Transistor

P.-M. Billangeon,[1] F. Pierre,[2] H. Bouchiat,[1] and R. Deblock[1]

[1]*Laboratoire de Physique des Solides, University Paris-Sud, CNRS, UMR 8502, F-91405 Orsay Cedex, France*
[2]*Laboratoire de Photonique et Nanostructures, CNRS, UPR 20, F-91460 Marcoussis, France*
(Received 7 October 2006; published 21 May 2007)

We measure the high-frequency emission of a single Cooper pair transistor (SCPT) in the regime where transport is only due to tunneling of Cooper pairs. This is achieved by coupling on chip the SCPT to a superconductor-insulator-superconductor junction and by measuring the photon assisted tunneling current of quasiparticles across the junction. This technique allows a direct detection of the ac Josephson effect of the SCPT and provides evidence of Landau-Zener transitions for proper gate voltage. The emission in the regime of resonant Cooper pair tunneling is also investigated. It is interpreted in terms of transitions between charge states coupled by the Josephson effect.

One of the most striking consequence of the macroscopic quantum coherence of the superconducting state is the Josephson effect which takes place when two superconductors are connected via a nonsuperconducting material (insulator or metal). It leads to a supercurrent at zero bias and an ac current when the junction is voltage biased [1,2]. In this work we investigate experimentally how the ac Josephson emission is modified when the Josephson effect competes with charging effects. To do so, we consider a single Cooper pair transistor (SCPT) constituted by two small junctions separated by a superconducting island, which energy can be tuned by a nearby electrostatic gate [3]. Because of the interplay between Josephson coupling and charging effects the SCPT exhibits peculiar electronic transport properties extensively studied over the past 15 years [3–8]. However, ac Josephson effect was less investigated. To characterize it, one can irradiate the SCPT with high frequencies (HFs) and observe Shapiro steps, which result from the locking of the superconducting phase dynamics on the frequency of the irradiating signal [2,8]. However, these steps may be hard to distinguish from other features of the SCPT. We use another technique to measure directly the ac Josephson effect: we couple the SCPT on chip to a HF detector, a superconductor-insulator-superconductor (SIS) junction, and measure the photo-assisted tunneling (PAT) quasiparticle current due to the emission of the SCPT [9,10].

The device probed in this experiment at 90 mK is a SCPT (normal state resistance 48.5 kΩ) coupled capacitively to a small SIS junction (estimated capacitance 1 fF, normal state resistance $R_T = 25$ kΩ). Both structures are made in aluminum (superconducting gap $\Delta = 210$ μeV) and embedded in an on chip environment constituted by resistances (8 Pt wires, $R = 750$ Ω, length $= 40$ μm, width $= 750$ nm, thickness $= 15$ nm) and capacitances (estimated value $C_C \approx 750$ fF, size: 23×25 μm^2, insulator: 65 nm of Al$_2$O$_3$) designed to provide a good HF coupling between the two devices [Fig. 1(a)]. The SIS

junction has a SQUID geometry in order to minimize its critical current with a magnetic flux.

We first present transport measurements performed on the SCPT. On Fig. 1(b) the $I(V_B)$ characteristic for low bias voltage of the SCPT at two gate voltages is shown. At both values, the SCPT shows a Josephson branch which extends to finite voltages as commonly seen for SCPT [11–13] (and Josephson junction [14–17]) embedded in a dissipative environment. The gate dependence of the Josephson branch is 2e periodic, as expected from the Hamiltonian

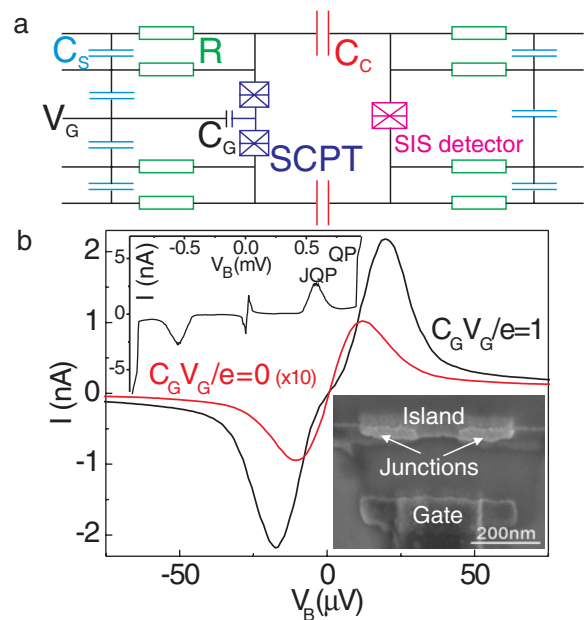FIG. 1 (color online). (a) Schematic picture of the SCPT coupled to a Josephson junction and the on chip circuit ($R = 750$ Ω, $C_C \approx 750$ fF). (b) Josephson branch of the SCPT at $C_G V_G/e = 1$ and 0 (multiplied by 10). Upper inset: $I(V)$ characteristic of the SCPT at high bias showing the Josephson-quasiparticle peak (JQP) and the quasiparticle (QP) tunneling. Lower inset: SEM picture of the SCPT.

of the SCPT:

$$H = \sum_n [E_C(n - C_G V_G/e)^2 |n\rangle\langle n|$$
$$- E_J \cos(\delta/2)(|n\rangle\langle n + 2| + |n + 2\rangle\langle n|)] + H_S$$

with $E_C = e^2/2C_\Sigma$ the charging energy (C_Σ is the total capacitance of the island), E_J the Josephson energy of each junction, δ the superconducting phase difference between the reservoirs, and $|n\rangle$ the state with n electrons on the island. H_S describes a superconducting metal by the BCS theory and favors paired electrons on the island [18], leading to the $2e$ periodicity, if the superconducting gap is bigger than E_C [8]. The transport measurement of the SCPT allows to determine its charging energy ($E_C = 65 \ \mu$eV) and Josephson energy ($E_J = 28 \ \mu$eV).

We now turn to the detection of the ac Josephson effect. For a dc voltage biased junction it results from the evolution of the superconducting phase difference δ across the junction according to the Josephson relation $d\delta/dt = 2eV_B/\hbar$, with V_B the dc voltage bias. Because of the periodic current-phase relation of the junction, this leads to an oscillating current. Since the SCPT can be considered at low voltage as a Josephson junction with a gate-dependent critical current, it should exhibit a gate-dependent ac Josephson effect. To detect it, the PAT current through the SIS junction is measured at $C_G V_G/e = 0$ and 1, versus bias voltage V_B and detector voltage V_D [Fig. 2(a), two lower panels]. To improve sensitivity we modulate V_B and monitor the modulated part of the PAT current $\partial I_{\text{PAT}}(V_D)/\partial V_B$ with a lock-in technique. The same type of measurement is shown for a small Josephson junction [Fig. 2(a), upper panel] [10]. When biased at V_D the detector is sensitive to photons of energy higher than $eV_D - 2\Delta$. This relation between V_D and the energy of detected photons allows a frequency resolved detection. The signature of the ac Josephson effect is then a peak, followed by a dip, on $\partial I_{\text{PAT}}(V_D)/\partial V_B$ at a detector voltage V_D corresponding to the Josephson frequency ν_J: $eV_D - 2\Delta = h\nu_J$. Since ν_J depends linearly on the source voltage ($h\nu_J = 2eV_B$ for a Josephson junction), the position of the peak in $\partial I_{\text{PAT}}(V_D)/\partial V_B$ versus V_D varies linearly with V_B, with a slope dependent on the relation between the source voltage and the Josephson frequency. We find that this slope is the same for a Josephson junction and for the SCPT at $C_G V_G/e = 0$, and corresponds to the relation expected from the Josephson relation (dashed line of Fig. 2). However, for $C_G V_G/e = 1$ this slope is divided by a factor 2, as if $h\nu_J = eV_B$. We attribute this factor 2 to the proximity of ground and first excited states which favors Landau-Zener (LZ) transitions. Indeed for $C_G V_G/e = 1$ the ground state and the first excited state are nearly degenerate at $\delta = \pi$ modulo 2π [Fig. 2(c)]. During the phase evolution of the SCPT, the system can there either stay in the ground state [J arrow of Fig. 2(c)] or go into the excited state (LZ arrow) [19]. If this latter
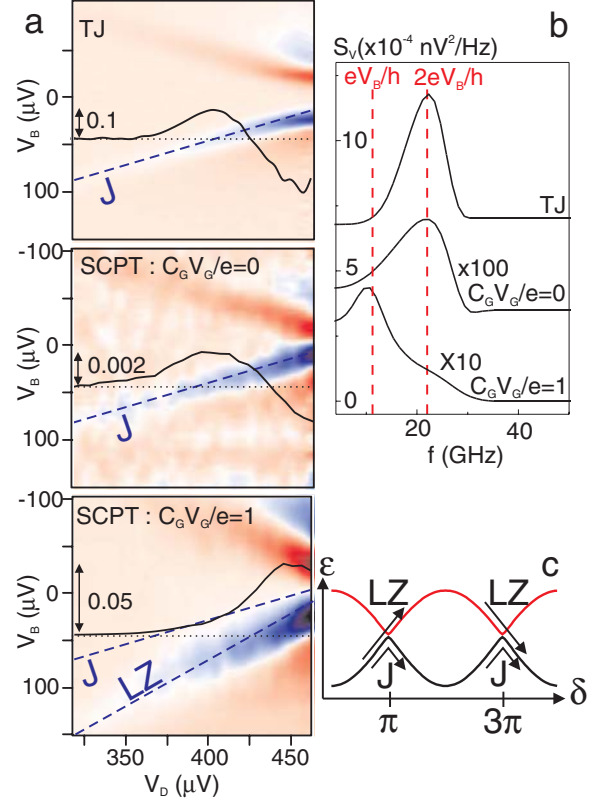

FIG. 2 (color online).   (a) Derivative of the PAT current of the detector vs V_B of the SCPT (dI_{PAT}/dV_B) (or a Josephson junction for the upper panel, noted TJ) for $C_G V_G/e = 0$ and 1 (lower panel). The dashed line J (LZ) indicates the slope of the Josephson (Landau-Zener) effect. The solid curves are dI_{PAT}/dV_B at $V_B = 45 \ \mu$V, with the scale in pA/μV indicated by the arrow on the curve and the zero line shown by the dotted line. (b) Voltage power spectrum of the ac Josephson effect extracted from the curves shown on A for a Josephson junction (TJ) and for the SCPT at $C_G V_G/e = 0$ and 1. The curves are shifted for clarity. (c) Sketch of the phase dependence of the two lowest energy levels of the SCPT at $C_G V_G/e = 1$ and illustration of the Landau-Zener (LZ) and Josephson (J) effect.

transition always happens, the effective periodicity of the energy-phase relation, and thus current-phase relation, is doubled [8], leading to the observed doubling of the Josephson period. This requires three conditions: first a high probability for LZ transition [19], second a relaxation time longer than the period of the Josephson effect, and third a relaxation time shorter than the time needed to equalize the population of the ground and first excited state during the phase evolution. This implies relaxation time of the order of few nanoseconds, in agreement with relaxation induced by the electromagnetic environment [21]. Note that poisoning effect cannot lead to the doubling of the Josephson period close to $C_G V_G/e = 1$. Without LZ effect, close to $C_G V_G/e = 1$, one should expect a strongly nonharmonic current-phase relation. In our case, this is hidden by the LZ effect, which restores a sinusoidal current-phase relation.

Using a numerical deconvolution method [9], we extract from the data taken at $V_B = 45 \ \mu$V the voltage power spectrum $S_V(\omega, V_B)$ [Fig. 2(b)] across the detector leading to the measured PAT current [Fig. 2(a)]. $S_V(\omega, V_B)$ exhibits peaks at the expected frequency. For $C_G V_G / e = 1$ we find a peak at eV_B/h, attributed to the LZ transitions, but also an extension of the spectrum around $2eV_B/h$. This might be due to incomplete LZ effect. Because of the rather broad IV characteristic of the detector, those spectra have to be taken cautiously at low frequencies and for a precise determination of the width of the Josephson emission. We find a rather large emission width around 8 GHz (corresponding to 30 μV), which is consistent with the width of the Josephson branch measured in dc [Fig. 1(b)]. This seems to indicate that the electromagnetic environment acts similarly on the dc and ac Josephson effect. To analyze the data, we assume that the area of the Josephson peak is given by the voltage fluctuation induced by the source and thus proportional to $Z^2 I_C^2$, with Z the transimpedance of the circuit (ratio of the ac voltage at the detector divided by the ac current of the source) and I_C the critical current of the source. Z was measured for the same environment [10]. We find that the critical current at $C_G V_G / e = 0$ is 1.9 nA, compared with the theoretical value 1.45 nA [22] and 6.5 nA at $C_G V_G / e = 1$, compared with an expected value of 6.8 nA. To conclude this part, our direct detection of the emission of the SCPT demonstrates a gate-dependent ac Josephson effect, not only in amplitude but also in frequency due to Landau-Zener transitions.

Besides the dc Josephson peak, the differential conductance of a SCPT exhibits peaks at finite bias [23,24]. Hereafter we focus on the region where the source voltage V_B of the SCPT is smaller than $2\Delta + E_C$, with only tunneling of Cooper pair (CP). For appropriate values of V_B and V_G, one observes a sharp increase of the dc current associated to transitions between the CP states of the system leading to peaks of differential conductance $\partial I/\partial V_B$ [Fig. 3(a)]. The bias voltage has two effects on the SCPT emission: it induces an evolution of the superconducting phase and modifies the energy of the charge states. To describe this last effect it is convenient to consider states with n electrons on the island and k electrons having passed through the SCPT, noted $|n, k\rangle$ [8]. The energy of the state $|n, k\rangle$ in the presence of an applied voltage V_B is changed by $-keV_B$. It is then possible to draw the diagram of energy levels at different bias voltage for a given gate voltage [Fig. 3(b) for $C_G V_G / e = 0.45$] and deduce the expected transitions and resonance. In this formalism, the ac Josephson effect is a transition induced by the Josephson coupling between levels like $|0, 0\rangle$ and $|0, 2\rangle$. When V_B is such that the energy of state $|0, 0\rangle$ is resonant with another state [e.g., in Fig. 3(b), $|2, 3\rangle$ at $V_B = 48 \ \mu$V (resonance "3") or $|2, 1\rangle$ at 145 μV (resonance "1")] high order Josephson terms lead to an increase of differential conductance $\partial I/\partial V_B$ [line 1 and 3 on Fig. 3(a)]. This resonant Cooper pair tunneling (RCPT) is
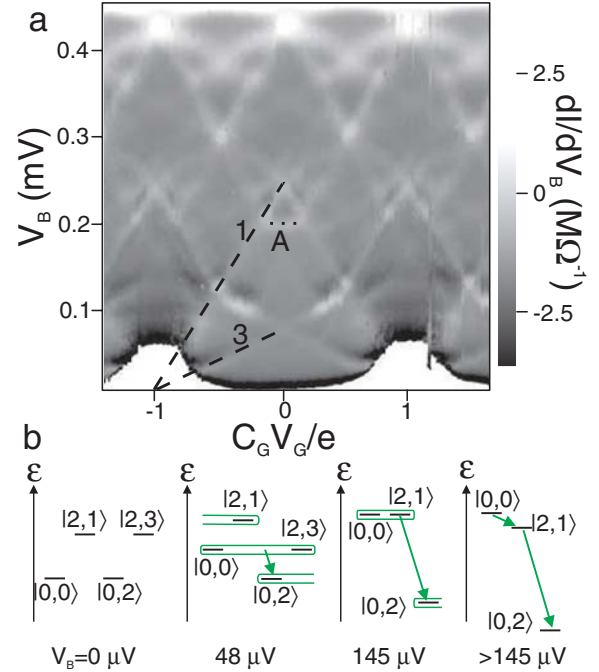

FIG. 3 (color online). (a) Differential conductance of the SCPT. The resonances 1 and 3 (see text) are indicated on the plot. (b) Energy levels of the SCPT at different bias voltage. The arrows indicate transitions between states resulting from the coupling by the Josephson effect of charge states. The green rectangles represent degenerate states coupled by the Josephson term.

$2e$ periodic, as expected from the Hamiltonian of the system, except at high voltage ($V_B > 150 \ \mu$V) where poisoning (i.e., presence of nonpaired electrons on the SCPT) restores an e periodicity.

Since RCPT implies transitions between charge states induced by the Josephson coupling, it may lead to HF emission [25]. To characterize this emission, we perform the same type of measurement as for the ac Josephson effect on a wider range of bias and gate voltage (Fig. 4). Beside the already mentioned ac Josephson effect ("J" dashed line) the SCPT emission at a given source voltage presents peaks at certain frequencies leading to features on the PAT current for particular values of detector bias. We relate them to transitions between quantum states of the system. The energies of these transitions are calculated using the formalism presented before. RCPT happens when V_B is high enough to allow the tunneling of CP, as illustrated on Fig. 3(b). When such a tunneling between states $|n, k\rangle$ and $|n, k + 2q\rangle$, involving an intermediate state $|n', k'\rangle$, is permitted two emission processes happen sequentially. First the emission of a photon of energy $(k' - k)e(V_B - V_0)$ corresponding to the difference in energy between $|n, k\rangle$ and $|n', k'\rangle$, with V_0 the onset voltage where the transition $|n, k\rangle \rightarrow |n', k'\rangle$ happens [e.g., transition $|0, 0\rangle - |2, 1\rangle$ indicated by the dashed line $(0, 0) - (2, 1)$ on Fig. 4]. Second, when $V_B > V_0$, there is the emission of a photon corresponding to the transition from $|n', k'\rangle$ to
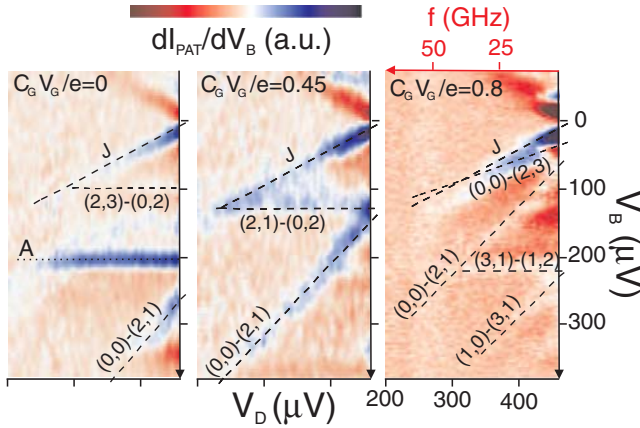
FIG. 4 (color online).   Derivative of the PAT current of the detector vs bias voltage V_B of the SCPT for different gate voltage, indicated on each plot. The dashed lines indicate the transitions predicted by the theory of RCPT (see text). The dashed line noted J correspond to ac Josephson effect. The color scale is not the same for all plots.

$|n, k + 2q\rangle$, which energy is $2qeV_B - (k' - k)e(V_B - V_0)$. Since we measure the signal derivative of the PAT current versus V_B, this transition appears essentially as a step versus V_B at $V_B = V_0$, with an extension in frequency up to $2qeV_B/h$ [e.g., the horizontal line $(2, 1) - (0, 2)$ on Fig. 4]. Close to $C_G V_G/e = 1$ all the RCPT resonances collapse into the Josephson peak [Fig. 3(a)]. It is then more complicated to separate the different phenomena at small voltage. Thus for $C_G V_G/e = 0.8$ the ac Josephson effect (line J) is mixed with a RCPT resonance [line $(0, 0) - (2, 3)$]. This prevents us to measure accurately the transition to Landau-Zener effect versus gate voltage.

Measurements of high-frequency emission can also provide information on processes not expected from the RCPT theory. As measured on the differential conductance of the SCPT, poisoning leads to an e periodicity at sufficiently high voltage. We then have to consider the charge states with an odd number of electrons on the island. This is why for $C_G V_G/e = 0.8$, we have signature of transitions between states $|1, 0\rangle$ and $|3, 1\rangle$ [line $(1, 0) - (3, 1)$] and between $|3, 1\rangle$ and $|1, 2\rangle$ [line $(3, 1) - (1, 2)$]. Another process is the feature A [Fig. 3(a)] at $V_B = 205~\mu$V. It exhibits a HF emission at 50 GHz (Figure 4, $C_G V_G/e = 0$). An explanation for this can be that, due to poisoning at $V_B = 205~\mu$V, the energy levels with one quasiparticle can be populated. For $C_G V_G/e = 0$ the charge state $|1\rangle$ and $|-1\rangle$ are degenerate and coupled by the Josephson effect. This leads to LZ transitions and HF emission at $eV_B/h = 50$ GHz, which is indeed the typical frequency of the feature A. This LZ effect for the poisoned SCPT takes place on a region of width 0.3 around $C_G V_G/e = 0$.

In conclusion, we have performed a direct detection of the HF emission of a SCPT by coupling it on chip to a SIS detector. This demonstrates an ac Josephson effect which is gate dependent in amplitude but also in frequency, due to Landau-Zener effect. We have also detected the emission in the RCPT regime, and interpreted the observed peaks as signatures of transitions between charge states coupled by the Josephson effect.

[1] M. Tinkham, *Introduction to Superconductivity* (McGraw-Hill, New York, 1996), 2nd ed.
[2] A. Barone and G. Paterno, *Physics and Applications of the Josephson Effect* (Wiley-Interscience, New York, 1982).
[3] D. V. Averin and K. K. Likharev, in *Mesoscopic Phenomena in Solids*, edited by B. L. Altshuler *et al.* (Elsevier, Amsterdam, 1991).
[4] T. A. Fulton *et al.*, Phys. Rev. Lett. **63**, 1307 (1989).
[5] D. V. Averin and V. Ya. Aleshkin, JETP Lett. **50**, 367 (1989).
[6] L. J. Geerligs, V. F. Anderegg, J. Romijn, and J. E. Mooij, Phys. Rev. Lett. **65**, 377 (1990).
[7] P. Joyez *et al.*, Phys. Rev. Lett. **72**, 2458 (1994).
[8] P. Joyez, Ph.D. thesis, Paris 6 University, 1995.
[9] R. Deblock, E. Onac, L. Gurevich, and L. P. Kouwenhoven, Science **301**, 203 (2003).
[10] P.-M. Billangeon, F. Pierre, H. Bouchiat, and R. Deblock, Phys. Rev. Lett. **96**, 136804 (2006).
[11] J. B. Kycia *et al.*, Phys. Rev. Lett. **87**, 017002 (2001).
[12] W. Lu, A. J. Rimberg, and K. D. Maranowski, Appl. Phys. Lett. **81**, 4976 (2002).
[13] S. V. Lotkhov, S. A. Bogoslovsky, A. B. Zorin, and J. Niemeyer, Phys. Rev. Lett. **91**, 197002 (2003).
[14] D. V. Averin, Yu. V. Nazarov, and A. A. Odintsov, Physica (Amsterdam) **165–166B**, 945 (1990).
[15] L. S. Kuzmin *et al.*, Phys. Rev. Lett. **67**, 1161 (1991).
[16] G.-L. Ingold and Yu. V. Nazarov, in *Single-Charge Tunneling*, edited by H. Grabert and M. H. Devoret (Plenum, New York, 1992).
[17] G.-L. Ingold and H. Grabert, Phys. Rev. Lett. **83**, 3721 (1999).
[18] M. T. Tuominen, J. M. Hergenrother, T. S. Tighe, and M. Tinkham, Phys. Rev. Lett. **69**, 1997 (1992).
[19] From measurements on different junctions, we estimate the asymmetry of tunnel junctions of the SCPT to be less than 10%. This leads to a calculated gap in energy at $C_G V_G/e = 1$ and $\delta = \pi$ of less than $\epsilon = 2.8~\mu$eV. The probability of Zener transition $P_Z = \exp(-\pi\epsilon^2/2E_J eV_B)$ [20] is then higher than 0.95 at $V_B = 10~\mu$V and 0.99 at $45~\mu$V.
[20] K. Mullen, Y. Gefen, and E. Ben Jacob, Physica (Amsterdam) **152B**, 172 (1988).
[21] G. Ithier *et al.*, Phys. Rev. B **72**, 134519 (2005).
[22] This is deduced from the calculated energy levels and the current-energy relation $I(\delta) = 2e/\hbar \partial E(\delta)/\partial\delta$.
[23] A. Maassen van den Brink, G. Schön, and L. J. Geerligs, Phys. Rev. Lett. **67**, 3030 (1991).
[24] D. B. Haviland *et al.*, Phys. Rev. Lett. **73**, 1541 (1994).
[25] O. Naaman and J. Aumentado, arXiv:cond-mat/0609491 [Phys. Rev. Lett. (to be published)].

PHYSICAL REVIEW LETTERS

Very High Frequency Spectroscopy and Tuning of a Single-Cooper-Pair Transistor with an On-Chip Generator

P.-M. Billangeon,[1] F. Pierre,[2] H. Bouchiat,[1] and R. Deblock[1]

[1]*Laboratoire de Physique des Solides, Université Paris-Sud, CNRS, UMR 8502, F-91405 Orsay Cedex, France*
[2]*Laboratoire de Photonique et Nanostructures, CNRS, UPR 20, F-91460 Marcoussis, France*

A single-Cooper-pair transistor (SCPT) is coupled capacitively to a voltage biased Josephson junction, used as a high-frequency generator. Thanks to the high energy of photons generated by the Josephson junction, transitions between energy levels, not limited to the first two levels, were induced and the effect of this irradiation on the dc Josephson current of the SCPT was measured. The phase and gate bias dependence of energy levels of the SCPT at high energy is probed. Because the energies of photons can be higher than the superconducting gap we can induce not only transfer of Cooper pairs but also transfer of quasiparticles through the island of the SCPT, thus controlling the poisoning of the SCPT. This can both decrease and increase the average Josephson energy of the SCPT: its supercurrent is then controlled by high-frequency irradiation.

Circuits based on small Josephson junctions can behave like macroscopic quantum systems [1–4]. This is, in particular, the case for the single-Cooper-pair transistor (SCPT), a superconducting metallic island connected *via* tunnel junctions to two superconducting reservoirs. The electrostatic state of the island is controlled by a nearby gate. Because of the interplay of charging and Josephson effect, this system can be considered, at low voltage, as a Josephson junction which Josephson energy, and thus critical current, can be tuned by a gate voltage. Because of its fundamental interest as an electrometer and as a building block for quantum computing, the SCPT has been extensively studied over the last 15 years. To resolve its gate voltage and superconducting phase dependent energy levels, essentially two techniques were used. The first is spectroscopy by using microwave irradiation on the gate, often limited to transitions between the first two energy levels. The second technique is transport spectroscopy: current is measured at different bias voltages V_B and gate voltages V_G to probes energy levels within eV_B of the ground state. The current results from all the tunneling processes allowed at energy eV_B, leading to an interesting but complicated characteristic $I(V_B, V_G)$.

In this Letter we investigate a SCPT irradiated by high-frequency (HF) photons generated by a Josephson junction. This allows us to work at frequencies much higher than usual spectroscopy experiments. We study how the average Josephson coupling of the SCPT is affected by HF irradiation. Because this technique permits to probe transitions involving only a single-Cooper-pair (CP) or a single quasiparticle (QP) it gives very direct information on the high-energy spectrum of the SCPT, in particular, on the tunneling of one QP to or from the island, i.e., the poisoning of the SCPT, an important issue in the context of quantum computing with states involving only CPs.

The device probed is a SCPT (normal state resistance 48.5 kΩ) coupled capacitively to a small Josephson junc-

tion (estimated capacitance 1 fF, normal state resistance 25 kΩ). Both structures are made of aluminum (superconducting gap $\Delta = 210$ μeV) and embedded in an on-chip environment consisting of resistances (8 Pt wires, $R = 750$ Ω, length $= 40$ μm, width $= 750$ nm, thickness $= 15$ nm) and capacitances (estimated value $C_C \approx 750$ fF, size: 23×25 μm^2, insulator: 65 nm of Al$_2$O$_3$) designed to provide a good high-frequency coupling between the two devices [Fig. 1(a)] [5,6]. The sample is measured in a dilution refrigerator of base temperature 90 mK.

We first present transport measurements on the SCPT. Figure 1 shows the $I(V_B)$ characteristic for low voltage of the SCPT at two values of the gate voltage. The SCPT exhibits a dissipative Josephson branch which extends to finite voltages [7] and with a finite slope dI/dV_B at low bias voltage. This is commonly seen on SCPTs [8–10] (and Josephson junction [11–14]) when they are embedded in a dissipative environment. The effect of the environment is more important if the Josephson coupling is small. Hence the slope dI/dV_B of the Josephson branch is, for a given environment, an increasing function of the Josephson coupling. Hereafter we call supercurrent the highest value of the current on the Josephson branch. The supercurrent is $2e$ periodic, very small for $C_G V_G/e = 0$ (modulo 2), and maximum for $C_G V_G/e = 1$ (modulo 2). The change in the slope of the Josephson branch at low bias and $C_G V_G = e$ is attributed to Zener effect [15]. The $2e$ periodicity is expected from the gate dependence of the energy levels of the SCPT [4], which has the Hamiltonian:

$$H = \sum_n \left\{ E_C \left(n - \frac{C_G V_G}{e} \right)^2 |n\rangle\langle n| - E_J \cos\left(\frac{\delta}{2}\right)(|n\rangle\langle n+2| + |n+2\rangle\langle n|) \right\} + H_S$$

with $E_C = e^2/2C_\Sigma$ the charging energy (C_Σ the total capacitance of the island), E_J the Josephson energy of
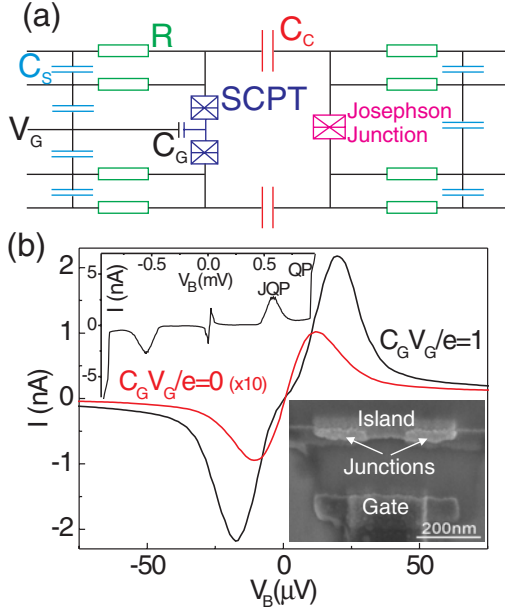
126802-1

FIG. 1 (color online). (a) Sketch of the SCPT coupled to a Josephson junction and the on-chip circuit ($R = 750\ \Omega$, $C_C \approx 750$ fF). (b) Josephson branch of the SCPT at $C_G V_G/e = 1$ and $C_G V_G/e = 0$ (multiplied by 10). Upper inset: $I(V)$ characteristic of the SCPT at high bias showing the JQP peak and the QP tunneling. Lower inset: SEM picture of the SCPT.

each junction, δ the superconducting phase difference between reservoirs, and $|n\rangle$ the state with n electrons on the island. H_S describes a superconducting metal by the BCS theory and makes it energetically favorable to have an even number of electrons on the island, leading to an odd-even free energy difference, which value is close to Δ at low temperature [16]. The ground state of the system, if $\Delta > E_C$, consists only of paired electrons. At higher voltage V_B, tunneling of a Cooper pair together with QP (Josephson-QP peak) and tunneling of QP (QP step) are possible (inset of Fig. 1). The $I(V_B, V_G)$ curve of the SCPT yields its charging energy ($E_C = 65\ \mu$eV) and the Josephson coupling of one junction ($E_J = 28\ \mu$eV).

We use a voltage biased SQUID, constituted by two Josephson junctions in parallel, named hereafter the source, as a high-frequency generator to irradiate the SCPT. When the SQUID bias V_S is nonzero but below $2\Delta/e$, an alternating Cooper pair current related to the ac Josephson effect runs through the SQUID. This current writes $I(t) = I_C(\Phi)\sin(\omega_J t)$ with $\omega_J/2\pi = 2eV_S/h$ the Josephson frequency, determined by the source voltage V_S. The critical current $I_C(\Phi)$ is modulated by a magnetic flux Φ through the SQUID and its maximum value $\pi\Delta/(2eR_T)$ is determined by the source's normal state resistance R_T [17]. The microwave photons generated by the junction are coupled to the SCPT *via* the on-chip circuit. This offers a tunable frequency together with an efficient and nearly frequency independent coupling in the range 10–200 GHz, but with a very small power generated (estimated value 17.5 fW) and a not perfectly monochro-

matic signal due to the emission bandwidth of the ac Josephson effect [18], in particular in the dissipative environment of our setup [15].

Below we study the effect of this irradiation on the SCPT, at maximum source power. On Fig. 2(a), upper panels, we show the modification of the Josephson branch at $C_G V_G/e = 1$ and $C_G V_G/e = 0$ for different source voltages V_S, i.e., different Josephson frequencies. For $C_G V_G/e = 0$, where the supercurrent is the smallest, HF irradiation at 145 GHz ($V_S = 300\ \mu$V) leads to an increase of both the supercurrent and the slope dI/dV_B. For $C_G V_G/e = 1$ HF irradiation leads to a global *increase* of both the supercurrent and dI/dV_B at 68 GHz ($V_S = 140\ \mu$V), even though the supercurrent is maximum at the chosen gate value. At higher frequency (121 GHz,
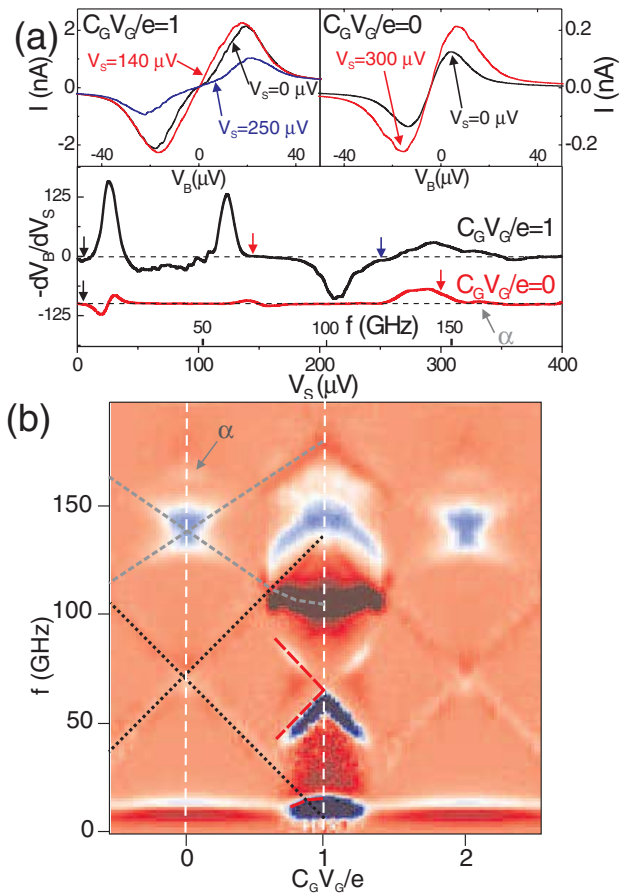

FIG. 2 (color online). (a) Upper panels: Josephson branch of the SCPT at $C_G V_G/e = 1$ (left panel) and $C_G V_G/e = 0$ (right panel) and different voltage V_S of the source, i.e., different Josephson frequencies. Lower panel: derivative of the voltage across the SCPT when current biased at $I = 80$ pA vs V_S (see text) under HF irradiation for $C_G V_G/e = 1$ and $C_G V_G/e = 0$. The arrows correspond to voltage V_S shown in the upper panels. The curves are shifted for clarity, the dashed line indicates no signal. (b) Variation of V_B in logarithmic scale at small current (see text) under HF irradiation and for different values of gate voltage. The two vertical dashed lines correspond to the curves shown on (a), lower panel. The colored line on the left part is a guide to the eye.

$V_S = 250 \; \mu\text{V}$), the Josephson branch of the SCPT is strongly reduced. The slope of the Josephson branch and the supercurrent exhibit the same qualitative dependence versus irradiation, which we relate to an induced change of the average Josephson energy of the SCPT. More precisely, we call "phase dependence" the amplitude of the super-conducting phase dependence of a given energy level: $\delta E_J = \max[E(\delta)] - \min[E(\delta)]$. By analogy with a single Josephson junction, this quantity can be seen as the Josephson energy of the level under consideration. If, due to irradiation, both the ground state of the SCPT, with a phase dependence δE_{Ji}, and an excited level, with a phase dependence δE_{Jf}, are populated with respective probability P_i and P_f the average phase dependence $\delta E_J^{\text{eff}} = P_i \delta E_{Ji} + P_f \delta E_{Jf}$ will determine the slope of the Josephson branch and the supercurrent detected in the experiment.

In the following we focus on the slope dI/dV_B of the Josephson branch, which is easier to measure, and is closely related to δE_J^{eff} [19], since, for a given electromagnetic environment, dI/dV_B is an increasing function of δE_J^{eff}. To measure dI/dV_B, the SCPT is current biased with a small fixed dc current ($I = 80 \; \text{pA}$), and the voltage V_B across the SCPT is monitored. To increase sensitivity, we modulate the source voltage V_S, and detect with a lock-in technique the modulated voltage of the SCPT, which is proportional to dV_B/dV_S. Figure 2(a), lower panel, shows for $C_G V_G/e = 1$ a strong increase of δE_J^{eff} for frequencies around 12 GHz and 60 GHz, leading to a decrease of V_B versus V_S. This is followed by a reduction of δE_J^{eff} for frequencies above 100 GHz. For $C_G V_G/e = 0$, HF irradiation leads to a higher δE_J^{eff} for frequencies close to 70 GHz. Above 125 GHz δE_J^{eff} increases. Figure 2(b) shows the same data (dV_B/dV_S versus Josephson frequency) as a function of V_G [20]. To interpret these results we numerically solve the Hamiltonian of the system, with the parameters deduced from the transport experiment. To account for the even-odd asymmetry a free energy Δ is added to the energy of the odd charge states. This yields the energy levels of the SCPT as a function of V_G and super-conducting phase δ. In Fig. 3(a) the levels are plotted as a function of V_G. We include the δ dependence through a width, which represents the phase dependence δE_J of the considered level. The absorption of a photon induces transitions between levels, followed by relaxation to the ground state, with two types of processes: (i) the absorption of one photon of energy $\hbar\omega$ allows the transfer of one Cooper pair from or to the island [transition b and a of Fig. 3(c) at $C_G V_G/e = 0$], leading to a transition from the initial energy level E_i to the final energy level E_f, with $E_f - E_i = \hbar\omega$. The expected signal is then a peak (increase of δE_J^{eff}) or a dip (decrease of δE_J^{eff}). (ii) Processes which involve the transfer of one quasiparticle from the island (transition c and d of Fig. 3(c) at $C_G V_G/e = 0$). The energy balance is then $\hbar\omega \geq (E_f - E_i + \Delta)$ to allow the injection or extraction of a QP to the reservoirs [Fig. 3(b)]. The expected signal is then steplike, and its derivative is a
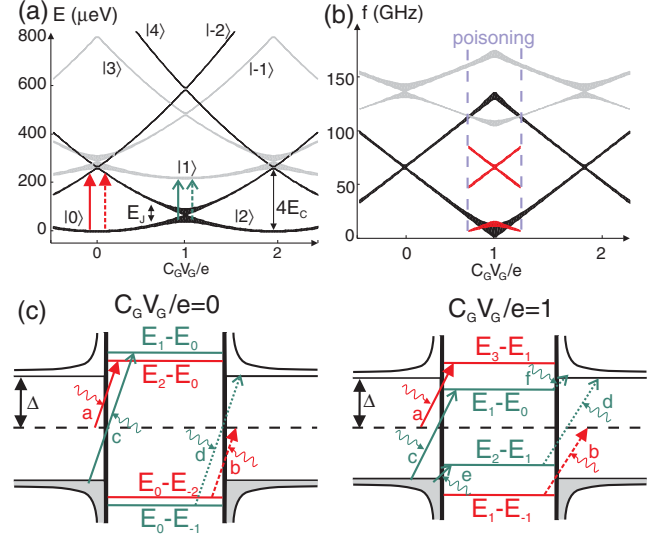

FIG. 3 (color online). (a) Calculated spectrum of the SCPT with parameters $E_C = 65 \; \mu\text{V}$ and $E_J = 28 \; \mu\text{V}$. The colored arrows represent transitions induced by HF irradiation, which involve the transfer of a CP to the island (red arrow) or from the island (red dashed arrow), or the transfer of a QP to the island (green arrow) or from the island (green dashed arrow). (b) Predicted gate dependence of the frequencies at which a change in the averaged phase dependence (see text) of the SCPT is expected, involving CP (black), QP (gray) tunneling or presence of an unpaired electron on the island (red). Poisoning is indicated on the figure. (c) Sketch of the QP density of states in the contacts and the energy of charge states in the SCPT at two gate values. The arrows illustrate the different photo-assisted tunneling processes possible.

peak. With these basic rules we can deduce the frequencies at which a change in the slope of the Josephson branch, due to a transition to a level with a different phase dependence δE_J, is expected. If the system is always in the lowest energy state, we get the black lines (involving transfer of CP) and gray lines (involving transfer of QP) of Fig. 3(b). This reproduces correctly the data except near $C_G V_G/e = 1$, where the sharpest features are not predicted. To do so, we assume that, near $C_G V_G/e = 1$, the system can also be in the state with one QP on the island (state $|1\rangle$) and thus consider transitions starting from this state (transition a, b, e, and f of Fig. 3(c) at $C_G V_G/e = 1$). The calculation then reproduces accurately the frequencies and qualitatively the phase dependence of energy levels induced by the Josephson coupling. The agreement for the phase dependence is only qualitative due to intrinsic bandwidth of emission of our HF source and/or widening introduced by the photon-assisted tunneling.

We find that the calculated spectrum of the SCPT is consistent with the data up to 200 GHz. Moreover, despite the $2e$ periodicity versus gate of the Josephson branch, the SCPT is still affected by poisoning [21–24], i.e., the presence of a QP on the island for $C_G V_G \approx e$. In our case, the poisoning is revealed by HF irradiation and happens for $C_G V_G/e$ between 0.7 and 1.3. Because the phase depen-

dence of state $|1\rangle$ at $C_G V_G/e = 1$ is very small, poisoning leads to a reduction of δE_J^{eff}. HF irradiation at proper frequencies allows a quicker escape of QP, leading to an increase of δE_J^{eff}. The presence of QP on the island is a common problem of SCPT, and more generally circuits based on small Josephson junctions, and is a strong limitation for the coherence of these systems. We show that irradiation at sufficiently high frequencies can accelerate the escape of these QP and thus reduce the effect of poisoning. On the contrary, by using frequencies higher than 2Δ we can force poisoning. In this regime, the SCPT is extremely sensitive to photons and can have interesting bolometric application [25].

We can access the dynamics of poisoning in the SCPT. To do so, we assume a quantum efficiency (number of electrons transfer on the SCPT for a given number of incident photons) for photon-assisted tunneling similar to the one measured in another experiment with two Josephson junctions coupled capacitively in the same environment as the present sample [5]. We relate the measured change of supercurrent under irradiation to the probability for the system to be in an excited state with a QP on the SCPT, which is directly related to the time spent by the QP on the SCPT. We thus deduce a QP lifetime of 0.5 μs at $C_G V_G/e = 0$ under irradiation at 145 GHz [Fig. 2(a), right upper panel] and 0.8 μs at $C_G V_G/e = 1$ under irradiation at 121 GHz [Fig. 2(a), left upper panel]. Those values are smaller than the ones measured for regular poisoning [23,24]. This difference is attributed to the nonequilibrium situation due to HF irradiation.

So far, only transfer of one CP or one QP was considered. Actually, the sequential tunneling of one QP and then one CP, followed by relaxation to the ground state, is also possible. This may be the case at point α [Fig. 2(b)] where the frequency (160 GHz) is high enough to allow tunneling of one QP on the island when absorbing a photon (transition from state $|0\rangle$ to state $|1\rangle$). If, before this QP leaves the island, another photon is absorbed, the SCPT can go to the charge state $|3\rangle$, with a lower δE_J than $|1\rangle$, leading to a reduction of the averaged phase dependence, observed in the experiment. This effect exists only for a high enough flux of photons and indeed disappears at lower power (not shown).

In conclusion, by using a Josephson junction as a tunable HF generator and by coupling it capacitively to a SCPT we perform spectroscopy on this SCPT up to 200 GHz. Up to high energy the experimental spectrum of the SCPT is consistent with the calculated energy levels with only two parameters, the charging energy and the Josephson coupling. Moreover, thanks to the high energy of photons involved in our experiment, we can reveal and reduce the poisoning of the SCPT by HF irradiation. We also demonstrate that we can induce the transfer of quasiparticle onto the SCPT, i.e., induce poisoning, and investigate the dynamics of this nonequilibrium poisoning. Our experiment shows that HF irradiation can lead not only to a decrease but also an increase of the average Josephson energy, and thus supercurrent.

[1] T. A. Fulton *et al.*, Phys. Rev. Lett. **63**, 1307 (1989).
[2] J. M. Martinis, M. H. Devoret, and J. Clarke, Phys. Rev. B **35**, 4682 (1987).
[3] P. Joyez *et al.*, Phys. Rev. Lett. **72**, 2458 (1994).
[4] P. Joyez, Ph.D. thesis, Paris 6 University, 1995.
[5] P.-M. Billangeon, F. Pierre, H. Bouchiat, and R. Deblock, Phys. Rev. Lett. **96**, 136804 (2006).
[6] R. Deblock, E. Onac, L. Gurevich, and L. P. Kouwenhoven, Science **301**, 203 (2003).
[7] We observe the same behavior on the Josephson junction, which has the same electromagnetic environment as the SCPT.
[8] J. B. Kycia *et al.*, Phys. Rev. Lett. **87**, 017002 (2001).
[9] W. Lu, A. J. Rimberg, and K. D. Maranowski, Appl. Phys. Lett. **81**, 4976 (2002).
[10] S. V. Lotkhov, S. A. Bogoslovsky, A. B. Zorin, and J. Niemeyer, Phys. Rev. Lett. **91**, 197002 (2003).
[11] D. V. Averin, Yu. V. Nazarov, and A. A. Odintsov, Physica (Amsterdam) **165–166B**, 945 (1990).
[12] L. S. Kuzmin *et al.*, Phys. Rev. Lett. **67**, 1161 (1991).
[13] G.-L. Ingold and Yu. V. Nazarov, in *Single Charge Tunneling*, edited by H. Grabert and M. H. Devoret (Plenum, New York, 1992).
[14] G.-L. Ingold and H. Grabert, Phys. Rev. Lett. **83**, 3721 (1999).
[15] P.-M. Billangeon, F. Pierre, H. Bouchiat, and R. Deblock, cond-mat/0609755.
[16] M. T. Tuominen, J. M. Hergenrother, T. S. Tighe, and M. Tinkham, Phys. Rev. Lett. **69**, 1997 (1992).
[17] M. Tinkham, *Introduction to Superconductivity* (McGraw-Hill, New York, 1996), 2nd ed.
[18] A. J. Dahm *et al.*, Phys. Rev. Lett. **22**, 1416 (1969).
[19] Note that our simple model does not take into account the interplay of irradiation effect and Zener effect around $C_G V_G/e = 1$.
[20] Note that the nearly gate independent feature seen at $V_S = 20 \mu$V ($f = 10$ GHz) is attributed to the change of impedance of the SCPT environment when the source is biased on the Josephson branch.
[21] J. Aumentado, M. K. Keller, J. M. Martinis, and M. H. Devoret, Phys. Rev. Lett. **92**, 066802 (2004).
[22] J. Männik and J. E. Lukens, Phys. Rev. Lett. **92**, 057004 (2004).
[23] O. Naaman and J. Aumentado, Phys. Rev. B **73**, 172504 (2006).
[24] A. J. Ferguson, N. A. Court, F. E. Hudson, and R. G. Clark, Phys. Rev. Lett. **97**, 106603 (2006).
[25] J. M. Hergenrother, J. G. Lu, M. T. Tuominen, D. C. Ralph, and M. Tinkham, Phys. Rev. B **51**, 9407 (1995); Physica (Amsterdam) **203B**, 327 (1994).